Control of Air Exchange and Particle Deposition within the Buddhist Cave Temples at Yungang, China

Thesis by

Christos S. Christoforou

In Partial Fulfillment of the Requirements

for the Degree of

Doctor of Philosophy

California Institute of Technology

Pasadena, California

1995

(Submitted May 8, 1995)

Acknowledgements

I would like to acknowledge the contribution of several people here at Caltech, without whose help this thesis would not have been possible. First is my advisor, Glen Cass, who spent many an hour with and without me working on various aspects of this study. His guidance and patience made much of this thesis possible.

Special thanks are also due to Lynn Salmon, who worked closely with me before, during, and after the experiments in China, and whose help was perhaps more transparent but no less valuable. Financial support for this work and critical technical assistance was provided by the Getty Conservation Institute and their consultants, and I especially thank Neville Agnew, Jim Druzik, Po-Ming Lin, Shin Maekawa, Dushan Stulik, and Roland Tseng for their help. The smooth operation of the experiments at Yungang would not have been possible without the cooperation of two host organizations in China. The help of the State Bureau of Cultural Relics in Beijing is greatly appreciated, including participation by Huang Kezhong, Zhu Changling, Sheng Weiwei, Li Xiu Qing, and Li Hua Yuan. The assistance of the staff of the Yungang Grottoes is gratefully acknowledged and I would like to thank Xie Ting Fan, Yuan Jin Hu, Huang Ji Zhong, and Zhi Xia Bing, among others, for their help. Special thanks are also due our translators Bo Guo Liang of the Shanxi Institute of Geological Science and Zhong Ying Ying from Taiyuan University.

I extend also my thanks to Ken McCue who has yet to send me away without first answering my questions, be they related to computers, math, or even politics and sports (even though his contribution in the latter category is of questionable value). Past and present members in our research group

were also always friendly and helpful to me, and their assistance is gratefully acknowledged. Previous work done by Bill Nazaroff was instrumental in accomplishing the particle deposition modeling part of this work.

I am grateful to friends outside school who have stood by me no matter what. Luckily I have been blessed with many friends- too many to individually mention, but I would be remiss if I did not mention one of my best friends, Marios, who has helped me considerably, both in Texas and in California.

I have also been lucky because I have family that has always loved and supported me. My father, Stelios and my mother Alexandra have always believed in me, and have been a tremendous influence in my life.

Last, but by no means least, my wife Erika and our little baby Alexandros Rex, who have changed my life in many wonderful ways- thank you.

Abstract

The Yungang Grottoes are a collection of man-made Buddhist Cave Temples in the northern part of Shanxi Province in the People's Republic of China. These cave temples were carved into the face of a cliff in the 5th century AD and contain more than 50,000 Buddhist sculptures, some of which retain their historical coloring. The sculptures in the caves are soiled at a rapid rate by the deposition of airborne particles, generated in part by activities in one of China's largest coal mining regions. During the month of April, 1991, an extensive environmental monitoring experiment was conducted there, and additional measurements were made through the following year. The overall purpose of that work was to characterize the exposure of the grottoes to air pollutants in a manner that will establish a basis for the future protection of the grottoes from air pollution damage.

First, measurements were made in order to quantify the particulate air pollution levels at Yungang, and to gather data necessary for verification of models that predict the fate of airborne particles as they deposit onto surfaces inside the caves. Average mass deposition rates to horizontal surfaces of 13.42 $\mu g\ m^{-2}\ s^{-1}$ outdoors and 5.23 $\mu g\ m^{-2}\ s^{-1}$ inside Cave 6 were measured over a one year period in 1991-92. These rates are comparable to the rates inferred by examination of historically accumulated deposits within the caves. The surface area coverage by coarse particles is dominated by particles larger than about 10-20 μm in diameter, while the mass flux is dominated by even larger particles greater than 20-30 μm in diameter. Comparison of the deposition rate in Cave 6, which retains a wooden temple structure in front of the cave entrances, to that in Cave 9 which is open to the outdoors shows that the wooden shelter does provide some protection. During April 1991, the deposition rate to horizontal surfaces in Cave 6 was 4.5 $\mu g\ m^{-2}\ s^{-1}$

compared to 13.4 $\mu g\ m^{-2}\ s^{-1}$ in Cave 9 and 21.5 $\mu g\ m^{-2}\ s^{-1}$ outdoors.

Also during April, 1991, temperatures and air exchange rates were measured at Caves 6 and 9 at Yungang in order to establish baseline parameters necessary for modeling the air flow that carries air pollutant particles into and out of the caves. Air flow through the caves was found to be governed by a natural convection flow pattern that is driven by the difference between the temperature of the outdoor air and the temperature of the interior walls of the caves. During the day, warm outdoor air enters the upper entrances to the caves, is cooled by the cave walls and flows out through the ground level exits from the caves, while during the night the situation is reversed. The average air velocity at the entrance of Cave 9 during the course of the experiment was 0.274 $m\ s^{-1}$, amounting to an air exchange rate of 121 $m^3\ min^{-1}$, which achieves one complete air change within Cave 9 in only 4.3 minutes on average. Cave 6 is larger than Cave 9, and air flow through Cave 6 is restricted by the presence of the wooden temple structure that is built over the entrances to Cave 6, yielding times to achieve a complete air exchange within Cave 6 that are typically 4 times longer than at Cave 9 under the April conditions studied. A theoretical model has been developed that takes as input cave wall and outdoor air temperatures and then predicts indoor air temperatures as well as air velocities at the entrance to the caves. The model can be used to predict air flows through the caves in the presence of increased resistance to air flow such as may occur following the future installation of filtration systems for particle removal at the caves.

Next, computer-based models have been constructed that simulate the particle deposition processes within the caves. The evolution of the airborne particle concentration and size distribution is tracked as outdoor air is drawn into the caves by a natural convection flow that is driven by the temperature

difference between the outdoor air and the interior walls of the caves. Particle deposition rates are computed from the boundary layer flows along the surfaces within the caves. Predicted aerosol size distributions and particle deposition fluxes within Caves 6 and 9 at Yungang are compared to experimental observations made during the period April 15-16, 1991. It is found that horizontal surfaces within Caves 6 and 9 at Yungang would become completely covered by a full monolayer of deposited particles in only 0.3-0.5 years under the April 15-16 conditions studied here, and will be soiled even more rapidly under annual average conditions.

Finally, alternative approaches to the control of the particle deposition problem within the Yungang Grottoes are examined using the computer models described earlier. Two general approaches are possible: (1) control of particle concentrations in the outdoor air through reduction of particle generation at local sources, and (2) removal of particles from the air entering the caves by filtration or similar technical means. Both mechanical filtration and passive filtration systems are examined. It was found that mechanical filtration using high efficiency filters will reduce the mass of particles deposited onto upward facing surfaces within the caves by more than 99% provided that the infiltration of unfiltered air into the caves is eliminated. Passive filtration, where the existing natural convection flow is utilized instead of mechanical fans to drive air through low pressure drop filters, was also examined. It was found that about a 97% reduction of the total mass of particles deposited on horizontal surfaces in the caves can be achieved by passive filtration if filters are placed in the surface of newly reconstructed shelters in front of the caves that have been designed specifically for that purpose.

Table of Contents

Chapter 1

Chapter 2

Chapter 3

List of tables

List of figures

Chapter 1. Air pollution damage to historical monuments

1.1 Introduction

Ancient monuments today not only have to weather the natural elements but also must withstand anthropogenic air pollutants as well. Sulfur dioxide, mainly emitted to the atmosphere during fossil fuel combustion, is known not only to affect human, animal, and plant life but also may damage stonework and metal (Brimblecombe et al., 1989). In the case of stone deterioration, SO_2 often attacks marble and limestone, producing a gypsum (calcium sulfate) crust that is easily eroded, causing a loss of the stone surface. While the buildings on the Acropolis in Athens, Greece, for example, have been at the mercy of the weather for over 2300 years, recent studies have shown that sulfates and nitrates, among other man-made chemical agents, are principally responsible for the corrosion of the marble at the Parthenon (Sikiotis and Delopoulou, 1992).

Another problem that plagues both works of art and building surfaces is soiling due to the deposition of airborne particles. This problem is not new by any means. The poet Horace mentions the blackening of buildings in ancient Rome (Brimblecombe, 1987). Another famous example is that of the Sistine Chapel at the Vatican. The wall paintings inside became covered by layers of soot and other deposits thus greatly affecting the visual qualities of the frescoes until their recent cleaning was completed. It has been shown that humans can perceive that a white surface is becoming soiled when as little as 0.2% of that surface has been covered by black particles (Hancock et al., 1976). Thus the optical properties and appearance of surfaces are easily affected by even small amounts of deposited particulate matter. Extreme cases also exist, as will be studied here, where air pollution and particle

deposition rates are so high that works of art are literally buried under a thick blanket of deposited dark-colored dust.

1.2 The Yungang Grottoes

One archaeological site that suffers from a very high rate of airborne particle deposition is the collection of more than 20 Buddhist cave temples at Yungang in northern China, located about 16 km west of the industrial city of Datong, in Shanxi province. The Yungang ("Cloud Hill") Grottoes are a collection of man-made caves excavated into the side of a steep sandstone cliff beginning around the middle of the 5th century A.D. under the patronage of the emperors of the Northern Wei Dynasty. In 398 AD, Emperor Daowu of the Northern Wei Dynasty established his capital at Ping Cheng near the present city of Datong, and for more than 100 years this region became a center of political, cultural, and religious life (Liu, 1989). Beginning under the supervision of the Buddhist monk Tanyao, 21 large devotional caves, 32 smaller caves, and upwards of 1100 niches were excavated into the cliffs at Yungang during the period of time when the Northern Wei capital was nearby.

The larger caves are similar in architecture. A passageway dug into the cliff face at ground level opens into a large man-made cavern excavated behind the cliff face. These rooms within the cliff are typically rectangular, between 10 to 15 m long on each side and approximately 12.5 m high. At the rear of some caverns, and at the center of others there is a pillar that stretches from the cave floor nearly to the ceiling. This central column typically is carved into a huge statue of the Buddha, but there are examples of pillars that take the form of a pagoda. The interior walls of these chambers are decorated with more than 51,000 bas-reliefs and statues ranging from several centimeters in

height to more than 10 m in height, that depict Buddhist deities and scenes from the life of the Buddha. Some of these stone carvings still retain their historical coloring (Cox 1957; Sickman and Soper 1968; Knauer 1983).

The larger caves usually have an entry at ground level and another opening through the cliff face to the outdoors at about the third floor level. During antiquity these entrances to the larger caves were sheltered by wooden temple structures one room deep and several stories high that were built against the outside front of the cliff face. Repairs to the cave temples were made during the Liao and Ching Dynasties, but by the early 1900's visitors report that the caves had fallen into a state of neglect (Cox, 1957). At present, only Caves 5 and 6 still retain the wooden temple structures in front of their entrances. Today agencies of the Chinese government are actively trying to protect the grottoes. The Yungang Grottoes Institute has been established to care for the caves; the area immediately adjacent to the grottoes has been turned into a park and the caves are open to visits by the public.

1.3 The problem at Yungang and its relationship to indoor air quality research

The caves at Yungang and the carvings inside were cleaned in 1986 and documentary photographs were taken. Today however there is visible soiling due to the deposition of airborne particles onto the sculptures, especially on upward-facing horizontal surfaces. During the present study the thickness of the particle deposits was measured to be at some places as deep as 0.8 cm at sites that were photographed in a cleaned condition in 1986 (Christoforou et al., 1994). An approach must be formulated that will protect the sculptures inside these caves from being permanently damaged by this continuing assault by dark-colored abrasive particles deposited from the atmosphere.

In order to understand how to control the particle deposition and soiling problem at the caves, a series of investigations needs to be undertaken, not unlike those necessary for understanding other more conventional indoor air quality problems. First, the sources of outdoor particles need to be identified, and the outdoor airborne particle size distribution and chemical composition must be established. Once the outdoor particle characteristics have been determined, the mechanisms by which these particles enter the indoor space must be understood. Introduction of airborne particles into modern buildings has been studied extensively, and computer-based models exist that can track outdoor air pollutants as they are distributed through buildings by air conditioning systems. These models can simulate particle removal by the filters present in the building ventilation systems, advection between rooms, infiltration of untreated air into the building, exhaust flows from the building, emissions from indoor sources, coagulation among particles in the indoor air, and particle deposition onto surfaces (Nazaroff and Cass, 1989).

In the case of a structure such as the Yungang Grottoes, a more difficult modeling problem is encountered. Air exchange rates between the outdoors and the interior of the caves at Yungang are not controlled by a mechanical ventilation system. Instead, it will be shown in this research that air circulation through those caves is driven by a natural convection flow that varies by time of day according to changes in outdoor temperatures and cave wall temperatures. In order to perform engineering calculations relevant to particle control within these caves, mathematical models first must be built that can predict the air flows that carry pollutants into and out of the caves based on the volume of the caves, their height, the surface area of walls, ceilings, and floors, the geometry of the entrances through which air must flow, and also thermal conditions such as cave wall temperatures and out-

door air temperatures. Once the air exchange rates are understood, then models can be built that predict the indoor airborne particle size distribution and chemical composition given data on outdoor pollutant levels. Next, models for airborne particle deposition onto surfaces can be linked to the air exchange models and indoor particle mechanics models in order to predict particle deposition fluxes onto the statues inside the caves.

If such a computer-based representation of the advection and fate of airborne particles can be constructed then that model can next be used to study how to control such particle deposition problems, either through selective elimination of certain particle sources or through removal of particles from the air entering the grottoes by filtration or other means. Before such models can be used with confidence to design control systems, they must be thoroughly tested against field experimental data. Given that the Yungang Grottoes exist in a fairly remote location, acquisition of such experimental data initially poses a major barrier to understanding how to solve the problem at hand.

The problem at Yungang has its own unique characteristics and many of its features were not well understood at the start of the present research. Such features are listed below:

(a) At the outset of this investigation, reports existed that outdoor air pollutant levels at Yungang are very high, but those reports are not backed-up by a thorough characterization of the outdoor air pollution problem at the Grottoes.

(b) The airborne particles at Yungang are probably much larger in size than urban soots that have been studied previously for their potential to soil museum collections in the United States. This means that measurement methods for characterizing large particle size distribu-

tions and deposition rates are needed before experiments at Yungang can be undertaken.

(c) The Yungang Grottoes are open to the atmosphere and air exchange is not forced by fans or any other mechanical means. It is not obvious in advance how or why that air exchange occurs.

(d) It is not obvious in advance which air pollution sources dominate air quality at Yungang.

(e) It is not obvious how to control the particle deposition problem at Yungang in an engineering sense, given that an elaborate particle removal system based on conventional air conditioning system technologies may not be adaptable to a cave temple.

1.4 Objectives of the research

The objectives of this research are first to quantitatively characterize the airborne particle and particle deposition problems at the Yungang Grottoes. Secondly, an understanding of the fluid mechanics of the air motion through such cave temples is sought, as it is that air motion that brings airborne particles into the grottoes. Next, mathematical modeling methods are sought that can provide a flexible physical description of the cause and effect relationships that govern particle deposition and soiling at Yungang. Finally, an understanding of how to control particle deposition within the context of historically important cave temples is desired.

1.5 Approach

The present work begins with the preparation and execution of a series of field experiments, conducted on-site at Yungang, designed to meet the need for baseline data on physical conditions at the Grottoes. A method first is

developed for measuring coarse particle size distributions, both for airborne and for deposited particles. That method must be both precise and suitable for application at a remote site like Yungang. Methods chosen for characterization of airborne particle properties then are applied to study air quality inside and outside of Caves 6 and 9 at Yungang during intensive experiments conducted in April-May of 1991, and at a less intensive rate for the following one-year period. Concurrently with the particle characterization experiments, meteorological measurements are carried out: outdoor air temperatures as well as indoor air and cave wall temperatures are recorded by instrumenting the caves with thermistors, and air velocities at the entrance to the caves likewise are logged. A computer-based model next is built that predicts the air exchange rates into and out of the caves. This model takes as input outdoor air temperatures as well as cave wall temperatures and predicts indoor air temperatures as well as air flows through the entrances to the caves. A particle deposition model for the caves is built based on modification of existing models that describe particle deposition phenomena in commercial buildings. The particle deposition model is linked to the air exchange model so that particles can be tracked from the outdoors into the caves and then onto the various surfaces inside the caves. Data gathered during the experiments at Yungang are used to evaluate the accuracy of these models.

Once the behavior of the caves is understood given both outdoor air quality and the fluid mechanical processes active within the caves, the computer-based models developed are used to study how various control measures could be employed to affect both air exchange and particle deposition rates inside the caves. Control measures are evaluated that include supression of outdoor particle sources and filtration of particles from the outdoor air that

enters the grottoes. Particular attention is paid to developing principles that underly the passive filtration of particles: use of the strong natural convection flow generated by indoor/outdoor temperature differences at the caves to drive air through filters without the use of mechanical fans.

1.6 References

Brimblecombe, P., Hammer, C., Rodhe, H., Ryaboshapko, A., and Boutron, C.F. (1989) Human influence on the sulphur cycle, in *Evolution of the global biogeochemical sulphur cycle* (Eds. Brimblecombe, P. and Lein, A.Y.) John Wiley, Chichester, England.

Brimblecombe, P. (1987) *The big smoke*, Methuen, London.

Christoforou, C. S., Salmon, L. G., and Cass, G. R. (1994) Deposition of atmospheric particles within the Buddhist cave temples at Yungang, China. *Atmos. Environ.*, **28**, 2081–2091.

Cox, L. B. (1957) *The Buddhist Cave-Temples of Yün-Kang & Lung-Men.* The Australian National University, Canberra, Australia.

Hancock R. P., Esmen, N. A., and Furber, C. P. (1976) Visual response to dustiness. *J. Air Pollut. Control Assoc.* **26**, 54-57.

Knauer, E. R. (1983) The fifth century A.D. Buddhist cave temples at Yün-Kang, North China. *Expedition*, Summer, 27-47.

Liu, L. L. (1989) *Chinese Architecture*, Academy Editions, London.

Nazaroff, W. W., and Cass, G. R. (1989) Mathematical modeling of indoor aerosol dynamics. *Environ. Sci. Technol.* **23**, 157-166.

Sickman, L., and Soper, A. (1968) *The art and architecture of China*, Yale University Press, Pelican History of Art, New Haven and London.

Sikiotis, D., and Delopoulpou, P. (1992) The corrosion of pentelic marble by the dry deposition of sulfates and nitrates. *Sci. Tot. Environ.* **120**, 213-224.

Chapter 2. Deposition of atmospheric particles within the Buddhist cave temples at Yungang

2.1 Introduction

Ancient monuments exposed to the environment are subject to physical, chemical, and biological degradation over the years. This can be caused by weathering by the elements over time, including factors such as erosion by rainfall, the daily cycling of temperature and relative humidity that produces stresses in stone objects, and by freeze/thaw cycles, for example. Air pollution and wind borne dust likewise can degrade stone sculpture. Airborne particles that deposit onto stone monuments will absorb and scatter light that would otherwise be reflected to an observer and therefore will affect the object's visual qualities (Nazaroff and Cass, 1991). Over time, deposited particles can become incorporated into the surface of the gypsum crusts that form on some types of stone, thereby permanently altering the surface.

The collection of more than 20 Buddhist cave temples at Yungang in northern China suffers from a very high rate of airborne particle deposition. The caves and the carvings inside were cleaned in 1986 and documentary photographs were taken (Great Treasury of Chinese Fine Arts, 1986). Today however there is visible soiling due to deposition of airborne particles onto the sculptures, especially on upward-facing horizontal surfaces. During the present study the thickness of some of the particle deposits was measured to be as deep as 0.8 cm at sites that were photographed in a cleaned condition in 1986. The relationship between the ambient particulate air pollution problem and the deposition flux within the caves needs to be established. Knowing the sources that generate particle emissions to the atmosphere as well as their size distribution, control strategies may be devised and imple-

mented which in turn will enable the control of the deposition flux of particles onto surfaces in the caves.

During the month of April 1991, an extensive environmental monitoring experiment was conducted at the Yungang Grottoes. The overall purpose of this work was to characterize the exposure of the grottoes to air pollutants in a manner that will establish a basis for the future protection of the grottoes from air pollution damage. This chapter is primarily concerned with determining the airborne particle size distribution and measuring particle deposition fluxes to both vertical and horizontal surfaces within the caves. This knowledge will facilitate engineering calculations of particle filtration characteristics, which is needed for control system design.

2.2 Experimental methods

2.2.1 Sample collection

Two caves were chosen for analysis, Caves 6 and 9. As shown in Figures 2.1 and 2.2, their architecture is similar: an elliptic interior shape with a large central pillar, a large entrance at ground level with a smaller opening into the cliff at about the third floor level. Cave 6, unlike Cave 9, still retains a wooden temple structure in front of the surfaces of which consist largely of narrow wooden doors with wooden latticework backed by paper windows. Samples were taken inside Cave 6, inside Cave 9, and outdoors under the overhanging cliff in front of Cave 9, at locations shown in Figures 2.1 and 2.2.

Both long-term and short-term experiments were carried out. During the spring of 1991 (the first sampling period), eight 24-hour periods were sampled, beginning at midnight of April 12, 14, 17, 20, 23, 26, 29, and May 1. The results from this sampling program will be used to characterize the

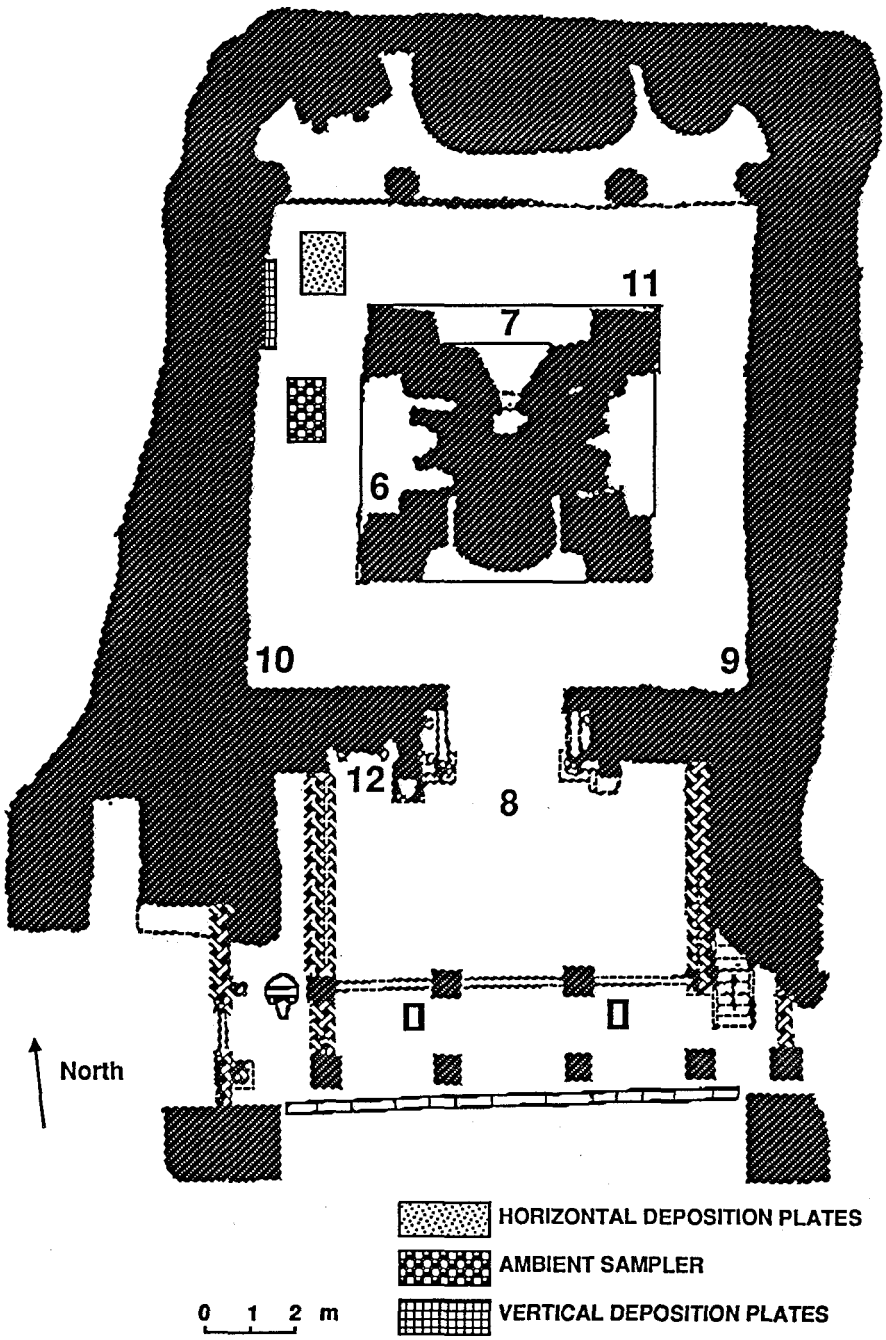

Figure 2.1 Horizontal section of Cave 6 showing ambient sampler and deposition plates location. The numbers show the location of the measurements of accumulated deposits from the period 1986-1991 (See Table 2.4).

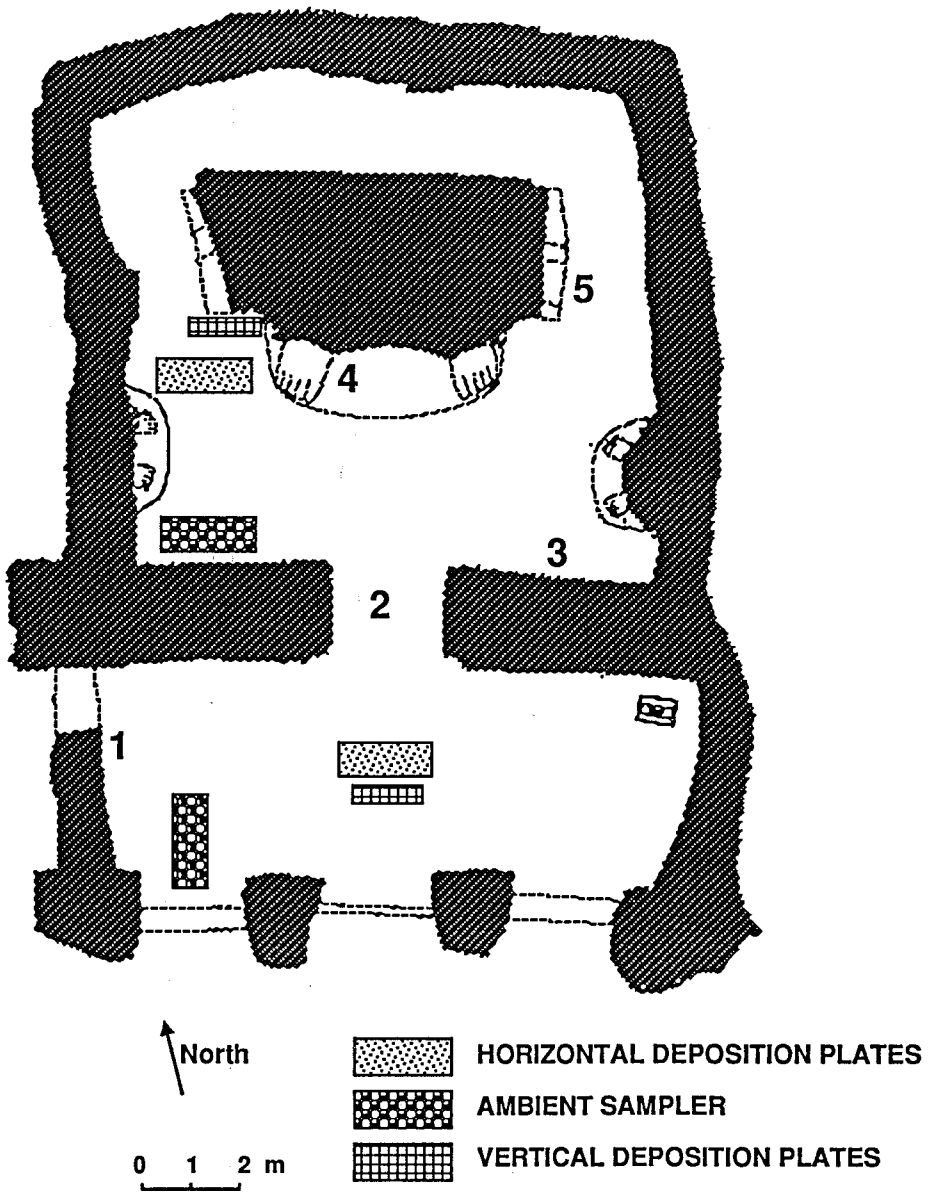

Figure 2.2 Horizontal section of Cave 9 showing ambient sampler and deposition plates location. The numbers show the location of the measurements of accumulated deposits from the period 1986-1991 (See Table 2.4).

concentration and size distribution of airborne coarse particles as well as deposition patterns of atmospheric coarse particles over the course of a spring month. A second set of two experiments lasted 44 hours each with samples taken over consecutive 4-hour intensive sampling periods. These two intensive periods began at 2:00 a.m. on April 15, and at 2:00 a.m. on April 24. The results from the first of these intensive periods will be used at a later point to provide model validation data to a theoretical model that predicts particle deposition patterns within the caves given the outdoor atmospheric particle concentrations.

In order to better understand particle concentration and deposition patterns and how they are affected by seasonal variations, the sampling program was continued. Samples of 24-hour duration were taken at 6-day intervals during one month of each remaining quarter of the year (July 1991; October 1991; January 1992). During these three sampling periods deposition measurements were made at two of the three locations sampled during the spring of 1991: inside Cave 6 and outdoors. Sampling for the characterization of the airborne particle concentration and size distribution at the two sites also was continued.

During the spring sampling period the deposition flux to both horizontal and vertical surfaces was measured at each of the three locations. The objective of these experiments was to measure the flux to surfaces of coarse particles greater than $2\mu m$ diameter. Coarse particle deposition to horizontal surfaces occurs at a relatively rapid rate by inertial deposition mechanisms and by gravitational sedimentation. Deposition to vertical surfaces is much slower because gravitational sedimentation acts parallel to the collection surface. In the case of vertical collection surfaces, particle deposition could be significantly affected by turbulent deposition from the convective

boundary layer along the cave wall. For the smallest particles of interest to us, thermophoretic motion of the particles driven by temperature differences between the cave walls and the air in the caves could be important (Nazaroff and Cass, 1989a). For that reason, care was taken to bring the vertical deposition plates within the caves to the temperature of the cave walls. The vertical collection plates were fastened on a large aluminum plate which was then held against the cave wall by metal pins such that these plates were in thermal contact with the cave walls. The wall sampled inside Cave 9 was smooth while the wall in Cave 6 was uneven and care was taken to orient the plates such that they were truly vertical as measured by a spirit level. The thermal environment of the horizontal deposition plates is not as important because particle sedimentation dominates the deposition flux in this case. The horizontal deposition plates were placed on top of large wooden platforms at a height of about 1 m above ground level. The vertical outdoor deposition surfaces were fastened to an aluminum plate that was then attached to the side of the wooden support that also held the outdoor horizontal collection plates.

As mentioned previously, the cave walls contain both areas with smooth surfaces and areas with rough surfaces. The rough surfaces in turn vary greatly from sand grain-scale roughness elements to areas of decayed rock with irregularities of the scale of centimeters. It is not practical to measure deposition to the rough surfaces using surrogate surfaces as many roughness scales are involved. Instead, direct observations of historical dust deposits that have accumulated on the actual rough surfaces should be made in those cases. For the case of the smooth surfaces inside the caves, deposition measurements using surrogate surfaces are practical and were made during the present sampling campaign. Two surrogate surfaces were used for the collection of parti-

cles: glass slides (75 mm by 25 mm by 1 mm thick) and Millipore filters (47 mm in diameter, 0.22 μm pore size, membrane filter GSWP047 00). In the case of horizontal plates located inside the caves where sedimentation toward the plates is the dominant collection mechanism and where high air velocities that might otherwise resuspend deposited particles are not present, particles collected on these surrogate surfaces will reasonably represent collection on most actual horizontal surfaces. For the case of vertically-oriented surfaces inside the caves and those surfaces exposed to outdoor wind conditions, these smooth surfaces should adequately simulate actual smooth surfaces, but may collect and retain fewer particles than would be the case for rougher surfaces.

Separate horizontal collection plates were exposed for each of the 24-hour periods listed previously, while a single set of vertical deposition plates was continuously exposed for the entire 19-day spring experiment because of the great difference in deposition rates between horizontal and vertical surfaces (Ligocki et al., 1990). Duplicate samples were taken. One of each pair of glass slides was transported back to the laboratory in Pasadena, CA, covered with a thin microscope cover slide (24 mm by 50 mm by 0.15 mm thick) to prevent particles from becoming detached from the surface, while the second slide of each pair was carried carefully but without a cover slip. Only those samples that were protected by a glass cover slip were used in subsequent analyses. All Millipore filter samples were transported back to the laboratory sandwiched between two glass slides (75 mm by 50 mm by 1 mm thick for the lower plate and 50 mm by 43 mm by 0.15 mm thick for the upper plate). Both glass slides and Millipore filters were transported while secured to the bottom of square covered plastic Petri dishes (100 mm by 100 mm) that were sealed at the edges with Teflon tape. Duplicate samples (only glass slides were used) were collected during the summer, fall, and winter sampling

periods and those were sent by courier and air express to the laboratory in Pasadena.

The ambient aerosol samples were taken over 24-hour periods by drawing air at a rate of 1 $L\ min^{-1}$ through a 47 mm diameter Millipore filter (0.22 μm pore size, membrane filter GSWP047 00) secured in an open-faced filter holder, thus ensuring collection of both large and small particles. The 0.22 μm pore size filter was chosen because the pores are small enough to preclude any loss of larger particles inside the pores. Also, because the pores are small they are invisible under the light microscope (at the magnification used) and therefore do not interfere with particle counting and sizing. The ambient filters were transported back to the laboratory sandwiched between two glass plates and were analyzed using optical microscopy. Samples also were taken to determine particle chemical composition in two size ranges, fine ($d_p \leq 2.1\ \mu m$) and coarse ($d_p > 2.1\ \mu m$). These results are described Salmon et al., (1994). Ambient aerosol mass concentration was also determined gravimetrically by pre-weighing and post-weighing of aerosol samples collected on 47 mm diameter Teflon filters (See Salmon et al., (1994)). Results of that atmospheric sampling program showed that over 74% of the outdoor airborne particle mass at Yungang is in the coarse particle fraction, and for that reason the present chapter focuses on coarse particle deposition.

2.2.2 Optical microscopy analysis

The method used for obtaining the particle size distributions and number counts consists of a light microscope that is connected to a Macintosh IIci computer by a video camera and a special frame-grabbing board (Quick-Capture, part No. DT2255, Data Translation, Inc., Marlboro, MA). The deposition sample is placed under the microscope and with the aid of a pub-

lic domain analysis program called IMAGE* a digital picture of the sample is grabbed and stored on the computer for subsequent analysis. A total of 60 video frames are captured per glass slide examined, 30 at 170× magnification (used to size and count particles less than about 18 μm) and 30 at 85× magnification (used to size and count particles greater than about 18 μm). Each frame in turn must have its background gray-level subtracted, sharpness enhanced, and the lowest gray-level which indicates the presence of a particle must be chosen. The frame is then made strictly black and white (no grays), where black indicates that a particle is present and white indicates space between particles. The program IMAGE then scans the entire frame counting and recording the number of picture elements (pixels) contained within each black area. The list of particles is sorted from smallest to largest, the number of particles of each size is found, for each size (in pixels) a diameter is approximated by assuming that the cross-sectional area is circular, and then the corresponding spherical volume is calculated. The particles are gathered into consecutive size bins in order to plot particle size and mass distributions. The total mass of all the particles measured in the small and large particle size range is divided by the surface area of the glass slide corresponding to one frame of the appropriate size multiplied by the number of such frames processed and by the elapsed time over which the glass slide was exposed to produce a particle mass flux to the slide in units of $\mu g\ m^{-2}\ s^{-1}$. Calculations showed that counting 600 particles per sample gave size distributions that deviated in number counts in the largest size intervals studied by as much as 27% from the true size distribution, while counting 1500 particles per sample resulted in size distributions in the largest

* The author is Wayne Rasband and the newest version of the program is available via anonymous ftp from alw.nih.gov

size intervals studied that deviated by less than 8% from the true value. A total of 2000 particles were counted, whenever possible, on each glass slide. Particles were then grouped into eleven equal (on a logarithmic scale) size intervals spanning the size range from 2.0 μm to 147.9 μm particle diameter.

The absolute size accuracy of the automated micro-video method was examined in the laboratory. Glass microspheres of different nominal sizes were deposited onto glass slides which were subsequently analyzed using the micro-video method. The same frames also were analyzed "manually": Polaroid photographs were taken through the microscope of the same particles as well as an embedded length scale and the image of the spheres was measured using a vernier caliper. The results of these experiments are shown in Table 2.1. It was found that the difference in the diameters between the two methods was always less than 5%.

The reproducibility of the results of the automated micro-video method also was tested. For this purpose, two horizontal glass slides (A and B) were exposed simultaneously, outdoors, for the same period of time. Then, 40 frames were captured from each specimen, and analyzed (results A1 and B1). The same video frames were processed a second time through IMAGE to determine if there were important effects of the system operator's intervention in the counting process that occurs when translating from gray scale to black and white images (results A2 and B2). Finally, a new set of 40 video frames was captured from each plate, making sure that the locations were different from the first set of pictures, and these frames were analyzed as well (results A3 and B3). As shown in Figure 2.3, there is close agreement in all six cases.

The ambient coarse particle concentration and size distribution also was measured using automated light microscopy. Each ambient sample collected by filtration onto a Millipore filter was sandwiched between a bottom glass

Table 2.1 Comparison of automated micro-video measurements of the diameters of glass microspheres vs measurements made from Polaroid photographs

Nominal diameter (μm)	micro-video high magn. (μm)	micro-video low magn. (μm)	Polaroid high magn. (μm)	Polaroid low magn. (μm)
40	42.7	42.9	40.6	41.0
40	41.5	41.4	39.6	39.8
40	40.5	40.4	39.3	39.0
20	23.7	22.8	24.1	22.9
20	22.9	21.9	22.5	21.8
20	23.1	21.6	23.1	22.2
11	13.4	-	13.7	-
11	13.6	-	13.8	-

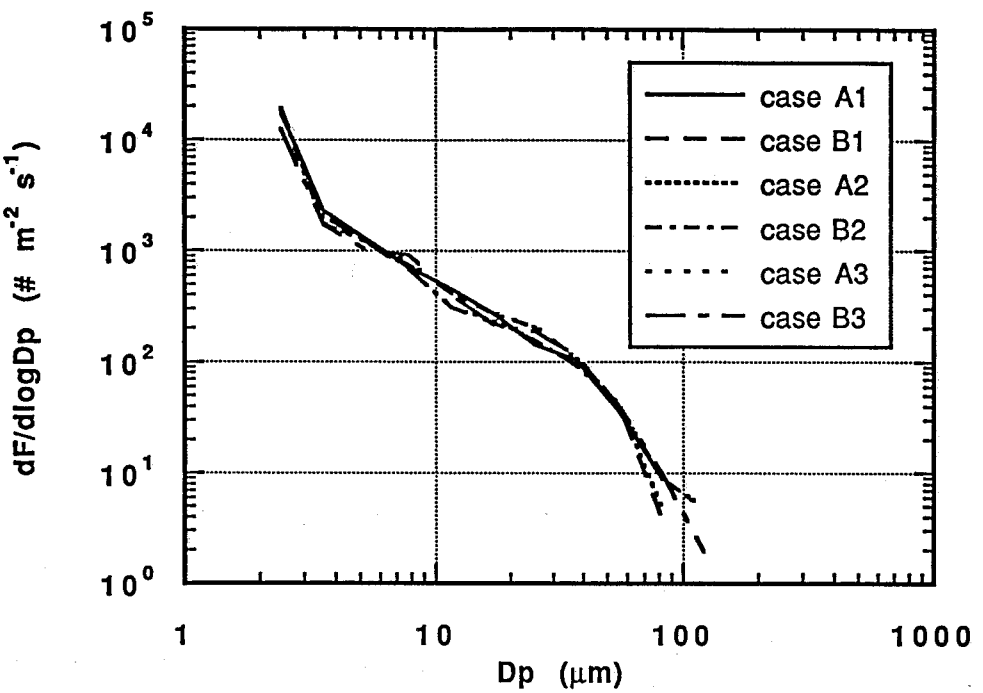

Figure 2.3 Reproducibility of the micro-video measurement of the number flux, F, of coarse particulate matter deposited onto two duplicate horizontal slides A and B: case 1 initial imaging and counting; case 2 reprocessing of initial video frames; case 3 second set of video frames taken at different locations on the slides.

plate (75 mm by 50 mm by 1 mm thick) and a top cover glass plate (43 mm by 50 mm by 0.15 mm thick) to keep it flat. It was then placed under the microscope and particle number counts and size were analyzed just as for the deposition plates. Knowing the total exposed surface area of the filter and volume of air passed through, the airborne coarse particle size distribution can be obtained. Knowledge of the size distribution permits the calculation of the particulate mass per unit volume of air if a particle density is assumed.

2.3 Results and discussion

The method of particle size analysis by automated light microscopy has been used by others (Heidenreich, 1987; John et al., 1991), and investigations performed in support of the present study have shown that glass slides are well suited for computer-aided optical microscopy analysis. For that reason the deposition results presented in this chapter are based on data obtained from glass slides.

Figure 2.4a shows the average flux of deposited coarse particulate matter onto horizontal surfaces. It represents the average of each of the eight 24-hour sampling events during the spring 1991 experiments. For particle sizes $d_p > 21\ \mu m$, the particle deposition rate outside is higher than in Cave 9, which in turn is higher than inside Cave 6. For particles with $d_p < 21\ \mu m$ however, the particle flux inside Cave 6 and outdoors is about the same. The deposition flux of the smaller ($d_p < 21\ \mu m$) coarse particles inside Cave 9 is higher than at either of the other two locations and that might be due to the fact that the floor in Cave 9 is covered with very soft dirt, unlike Cave 6 which has a tile floor, and the outdoors, where the soil is more heavily packed. Occasional entry into Cave 9, where the control module for our electronic

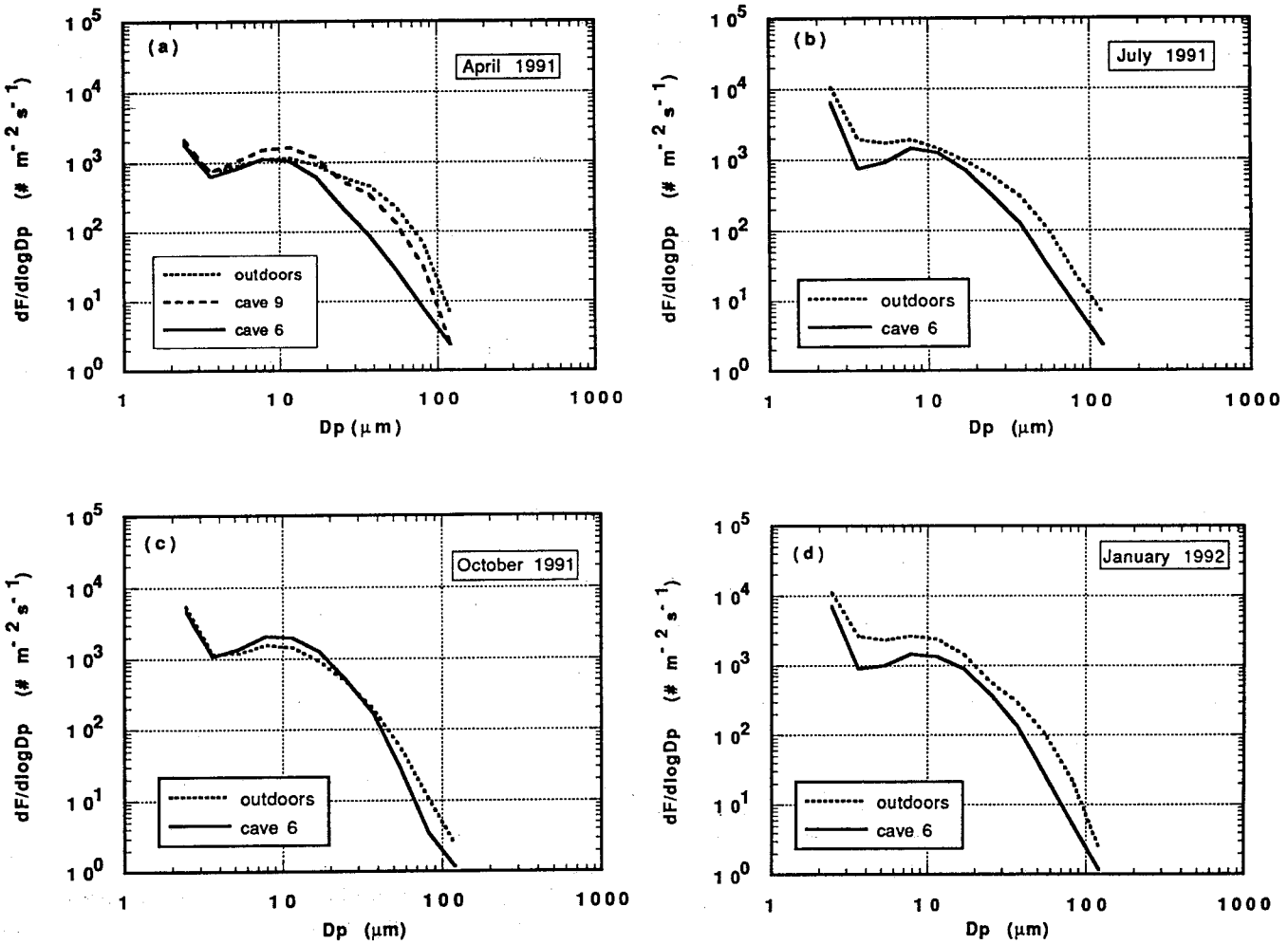

Figure 2.4 Average number flux, F, of coarse particulate matter deposited onto horizontal surfaces at Yungang as a function of particle diameter, d_p.

equipment as well as several instruments was located may have generated enough dust to have biased the results slightly. It should be noted here that the two largest particle size bins studied were very sparsely populated because the residence time in the atmosphere for particles of that size is very small.

In Figures 2.4b-d, monthly average particle fluxes outdoors and within Cave 6 are documented for the remaining three seasons of the year. Again, particle deposition rates inside Cave 6 are significantly below those outdoors in all cases except for particles in the $5 - 30$ μm size range during October.

Figure 2.5 shows the size distribution of coarse airborne particles at each of the three locations during the spring sampling period. Results shown there are the average over all eight 24-hour sampling events during the spring 1991 sampling period. It can be seen that for particles that are larger than 21 μm in diameter, the outdoor concentration is higher than that inside Cave 9, which in turn is higher than that inside Cave 6. That is expected since Cave 6 has the wooden temple front that acts as a partial barrier to the transfer of the coarser particles from the outdoor air to the inside of the cave. As far as the smaller particles are concerned ($d_p < 21$ μm), Figure 2.5 suggests no definite trend between the outdoor and indoor sites. That the concentration outdoors is smaller in most size intervals than that inside the caves might be due to the fact that the visitors to the caves may be a source of dust resuspension.

Table 2.2 shows the average projected surface area distribution of particles depositing onto horizontal surfaces over all four seasons of the year studied. The projected surface area flux is proportional to the rate at which the surfaces become covered with visible dust. It has been shown that the threshold for human perception that a white surface is becoming soiled by

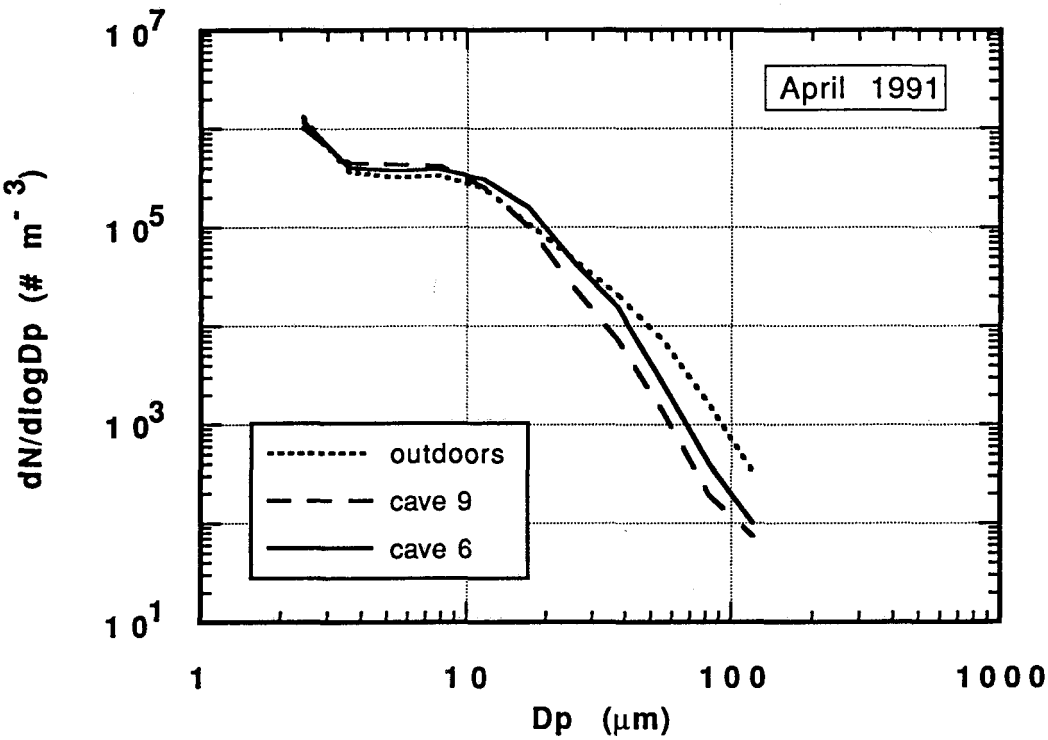

Figure 2.5 Average number distribution of coarse airborne particulate matter at Yungang, April 1991, as a function of particle diameter, d_p.

Table 2.2 Projected surface area flux of coarse particulate matter onto horizontal surfaces at Yungang

	April 1991			July 1991	
size (μm)	Outdoors ($\mu m^2\ m^{-2}\ s^{-1}$)	Cave 9 ($\mu m^2\ m^{-2}\ s^{-1}$)	Cave 6 ($\mu m^2\ m^{-2}\ s^{-1}$)	Outdoors ($\mu m^2\ m^{-2}\ s^{-1}$)	Cave 6 ($\mu m^2\ m^{-2}\ s^{-1}$)
2.02-2.99	1500	1700	1400	8400	5100
3.00-4.42	1300	1300	1100	3400	1300
4.43-6.54	3400	3900	3000	6600	3500
6.55-9.67	8900	12200	9200	15900	12100
9.68-14.3	20900	29300	18700	26200	22700
14.3-21.2	35500	45300	24200	38400	28700
21.2-31.3	51700	45500	19100	49900	27000
31.3-46.3	84800	64100	16400	57100	23600
46.3-68.4	91400	54100	11600	42400	12500
68.5-101.2	60300	27800	6800	20200	7400
101.3-149.7	13200	4600	4700	12300	4500
Total	372900	289800	116200	280800	148400

	October 1991		January 1992	
size (μm)	Outdoors ($\mu m^2\ m^{-2}\ s^{-1}$)	Cave 6 ($\mu m^2\ m^{-2}\ s^{-1}$)	Outdoors ($\mu m^2\ m^{-2}\ s^{-1}$)	Cave 6 ($\mu m^2\ m^{-2}\ s^{-1}$)
2.02-2.99	4300	3700	8700	5600
3.00-4.42	2000	1800	4500	1600
4.43-6.54	4500	5200	8700	3800
6.55-9.67	12700	16800	21700	12000
9.68-14.3	25500	35100	43100	24200
14.3-21.2	35900	48700	56800	35400
21.2-31.3	39800	42000	49800	33400
31.3-46.3	36700	32000	55800	25600
46.3-68.4	23000	11700	43800	11400
68.5-101.2	9900	3100	20300	5100
101.3-149.7	4500	2600	4900	2200
Total	198800	202700	318100	160300

dark colored particles occurs once approximately 0.2% of the area of a surface has become covered (Hancock et al., 1976). With brown or gray colored particles, a somewhat higher coverage probably would be required before the deposits would become visible. From the data in Table 2.2, at the deposition coverage rate of $2.9 \times 10^5 \mu m^2\ m^{-2}\ s^{-1}$ observed during the spring within Cave 9, horizontal surfaces would reach 0.2% coverage needed for detectable soiling in about 6.9×10^3 s or 1.9 hours (on average), for example. This is completely consistent with our own observations that the glass plates and Millipore filters used in these experiments are noticeably dirty at the end of a day. The surface area coverage tables show that most of the coverage by coarse particles is due to particles in the size range 14 - 101 μm particle diameter even though smaller particles are more numerous.

The average mass flux to horizontal surfaces is shown in Figures 2.6a - d. The mass flux was found by integrating the area under the deposited coarse particle number distribution curve, i.e., taking all particles in each size interval to be spheres having a diameter of the same size as the log midpoint of each interval, and finally assuming a density of 2.2 g cm^{-3} for the particles. That particle density value was obtained by measuring the density of a bulk deposit of particles removed from Cave 6. Results from all four seasons of the year are shown. The mass flux to horizontal surfaces inside Cave 6 remains in the range 4.5 to 6.2 $\mu g\ m^{-2}\ s^{-1}$ regardless of the time of the year. Outdoors the mass flux is about the same for summer and winter, but higher during the spring. The lowest mass fluxes outdoors were found during the fall. The springtime peak in outdoor deposition rates is influenced by regional dust storms that occur at that time of year.

Table 2.3 shows the total mass flux of coarse particulate matter onto horizontal surfaces. The total mass flux of particulate matter deposited onto

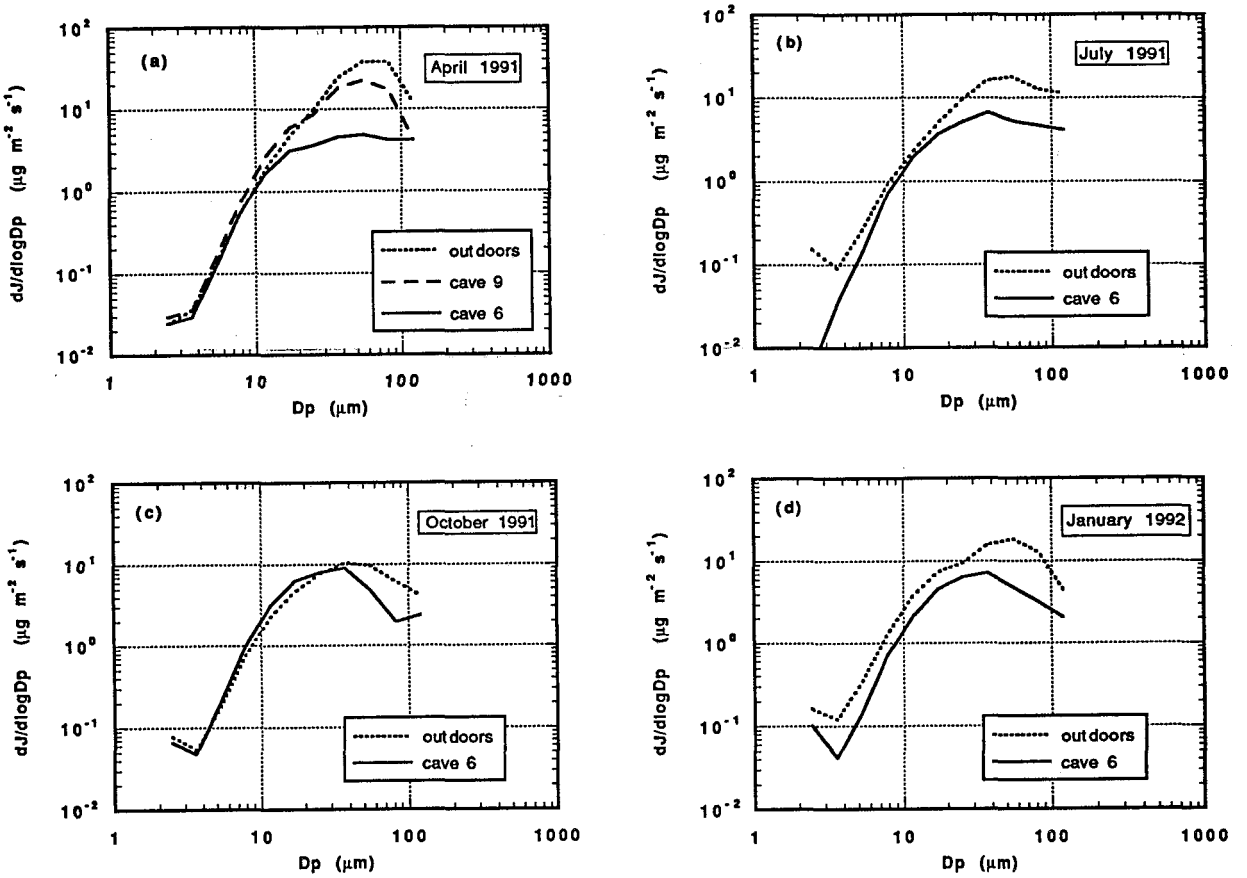

Figure 2.6 Average mass flux, J, of coarse particulate matter onto horizontal surfaces at Yungang as a function of particle diameter, d_p.

Table 2.3 Total mass flux onto horizontal surfaces at Yungang

Location	Date	Mass flux[a] $\mu g\ m^{-2}\ s^{-1}$
Outdoors	April 1991	21.50
Inside Cave 9	April 1991	13.40
Inside Cave 6	April 1991	4.54
Outdoors	July 1991	12.70
Inside Cave 6	July 1991	5.43
Outdoors	October 1991	7.16
Inside Cave 6	October 1991	5.84
Outdoors	January 1992	12.30
Inside Cave 6	January 1992	5.12
Outdoors	Annual Average	13.42
Inside Cave 6	Annual Average	5.23

a. Based on a density of ρ=2.2 g cm^{-3}

horizontal surfaces in Cave 6 is about one-third of that deposited in Cave 9 which in turn is about half the outdoor mass flux.

During the course of the experiment, accumulated deposits were collected from the actual horizontal surfaces of the statues inside Caves 6 and 9 as listed in Table 2.4 from samples taken at the locations shown in Figures 2.1 and 2.2. It was known that those deposits had been accumulating for five years because samples were collected at locations that were documented to have been cleaned last in 1986 when selected statues were cleaned during photodocumentation of the grottoes. When the mass deposition rates measured over our year-long experiment are extrapolated to cover the entire period 1986-1991, it is seen that the results of our experiments using surrogate deposition surfaces are comparable to the reality of the deposits on the sculptures (see Table 2.5).

The particle deposition velocity, which is defined as the ratio of the particle deposition flux ($\# \ m^{-2} \ s^{-1}$) to the airborne particle number concentration ($\# \ m^{-3}$), is a measure of the fluid mechanical processes that govern particle deposition rates (Ligocki et al., 1990). Theoretical predictions can be made for the deposition velocity under specified air flow conditions (Nazaroff and Cass, 1989ab). Deposition velocity measurements for coarse particles onto a variety of horizontal surfaces have been reviewed by several authors (e.g., see Nicholson, 1988; Sehmel, 1980). Measured results in general do not agree well with theoretically predicted values. During the present study, deposition velocities were computed as a function of particle size by taking the ratio of the particle number flux to the surface to the ambient concentration for each of the particle size intervals defined previously at the three experiment locations. Deposition velocity measurements for April 14, 1991 at Yungang are shown in Figure 2.7a. The trend is that of increasing deposition velocity

Table 2.4 Measurements of accumulated deposits from the period 1986-1991

Site	Location[a]	Deposit Depth (cm)	Mass Loading[b] (g m^{-2})
Outside Cave 9	1	0.76	6658
Cave 9	2	0.25	2695
Cave 9	3	0.06	16[c]
Cave 9	4	0.13	572
Cave 9	5	0.8	4981
Cave 6	6	0.13	201
Cave 6	7	0.06	113
Cave 6	8	1.0	2655[d]
Cave 6	9	0.5	156
Cave 6	10	0.4	171
Cave 6	11	0.5	298
Cave 6	12	0.1	370

a. See Figures 2.1 and 2.2 for an indication of the various locations.

b. Deposits are on horizontal surfaces cleaned in 1986, except for locations 3 and 8.

c. Deposit on a nearly vertical surface.

d. Deposit on horizontal surface that was not cleaned in 1986.

Table 2.5 Mass deposition comparison for horizontal surfaces at Yungang

Location	1986 - 1991 Actual[a] (g m^{-2})	5-year estimate from glass plate samples[b] (g m^{-2})
Inside Cave 6	113 — 370	716
Inside Cave 9	572 — 4981	2113
Under cliff overhang in front of Cave 9	6658	3390

a. Weighed deposit mass collected from a known area.

b. Calculated mass deposit using values from Figure 2.6, extrapolated to a five-year period. Particle density used is ρ=2.2 g cm^{-3}

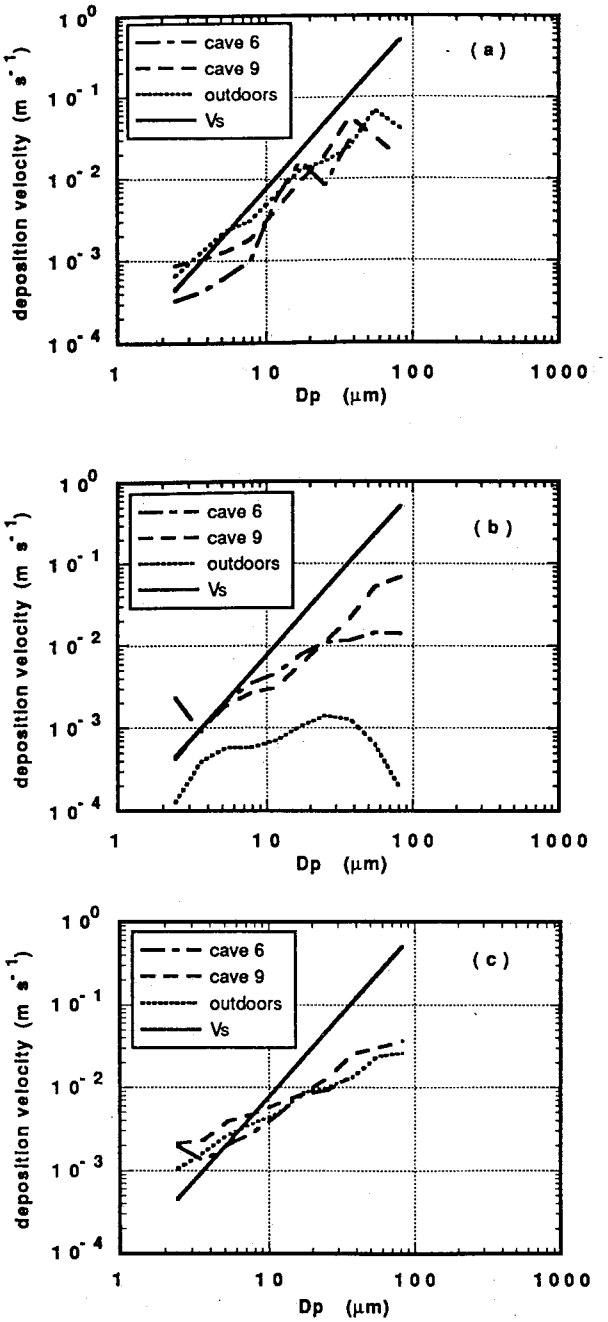

Figure 2.7 Deposition velocity onto horizontal surfaces at Yungang as a function of particle diameter d_p (dashed lines) compared to the terminal gravitational settling velocity, V_s, of equivalently sized spherical particles of density 2.2 $g\ cm^{-3}$ (solid line): (a) 14 April, 1991; (b) 1 May, 1993; (c) spring average, 1991.

with increasing particle diameter. That is as expected, because the large airborne particles settle out of the atmosphere under the influence of gravity, and the larger the particle the larger its terminal settling velocity. The deposition velocity is shown to be a little larger outdoors than it is inside the two caves but the difference in the deposition velocities in the interior of the two caves is small.

The experimentally determined deposition velocity values show reasonable agreement to theoretically calculated values of the terminal settling velocity for spherical particles of equivalent volume and density at times when outdoor wind speeds are low, such as during the day shown in Figure 2.7a. This calculation depends on the particle density, ρ, and the deposition velocity curves lie close to the terminal settling velocity curve for $\rho = 2.2\ g\ cm^{-3}$. Exact agreement between the deposition velocity for particles to horizontal surfaces in the caves and the terminal settling velocity for a sphere in still air is not expected because the air within the caves is in motion. During the day a downdraft occurs in the caves, while at night an updraft is observed, both circulation patterns being driven by a thermal siphon effect. The outdoor air in the spring is warmer than the cave walls during the day but colder at night, and natural convection driven flows reverse direction in a regular diurnal pattern.

Over the period April 29 - May 1, 1991, strong wind storms occurred at Yungang, with wind speeds at times exceeding 8 $m\ s^{-1}$, accompanied by coarse airborne particle concentrations exceeding 1200 $\mu g\ m^{-3}$ over a 24-hour averaging time on May 1. The largest deviation between the terminal settling velocity curves and the experimental values occurs in the larger size intervals during such high wind events as shown in Figure 2.7b. That result is due to scouring of the larger coarse particles by wind gusts outdoors (the

deposition plates were ungreased because we wished to mimic the ungreased statuary). When averaging over the course of a month, events like those shown in Figure 2.7b reduce the apparent net deposition velocity for larger coarse particles yielding a spring seasonal average like that of Figure 2.7c. The deposition velocity curves might also be affected by the fact that there are not many particles to be counted in the largest size intervals and therefore results are prone to a higher degree of uncertainty at the largest particle sizes.

Deposition measurements to vertical surfaces during the spring sampling period are presented in Table 2.6 and Figure 2.8ab. Data on the deposition velocity as a function of particle size to vertical surfaces are exceedingly sparse. Ligocki et al., (1990) have reported fine particle deposition velocity measurements to vertical surfaces from a study conducted inside museums. In a related but different context, Liu and Ahn (1987) have reported on particle deposition rates onto silicon wafers inside laminar flow clean rooms used during the manufacture of semiconductor devices. One of the reasons that data are seldom available for coarse particle deposition as a function of particle size onto vertical surfaces is that the flux of coarse particles towards a vertical surface is very small. As a result long sampling times are required if measurements are to be made. In the case of the present study at Yungang, the sample collection lasted for the entire duration of the spring experiment (a little less than 19 days). Even so, there were not many particles present, especially in the larger size intervals. Figure 2.9 shows the deposition velocity for particles depositing onto vertically oriented smooth surfaces. It can be seen that the deposition velocity values range from 10^{-3} to 10^{-5} $m\ s^{-1}$. The surface area coverage rate on vertical surfaces shown in Table 2.6 is two orders of magnitude lower than for coarse particle deposition to horizontal surfaces, and confirms that the soiling problem should be (and is) most evident on

Table 2.6 Average projected surface area flux of coarse particulate matter onto vertical surfaces at Yungang, April 1991

size interval (μm)	Outdoors ($\mu m^2\ m^{-2}\ s^{-1}$)	Cave 9 ($\mu m^2\ m^{-2}\ s^{-1}$)	Cave 6 ($\mu m^2\ m^{-2}\ s^{-1}$)
2.02-2.99	220	480	83
3.00-4.42	48	83	5
4.43-6.54	130	170	16
6.55-9.67	290	250	48
9.68-14.3	340	81	64
14.3-21.2	390	110	93
21.2-31.3	700	110	150
31.3-46.3	870	110	78
46.3-68.4	850	73	49
68.5-101.2	380	110	—
101.3-149.7	120	—	—
Total	4340	1580	590

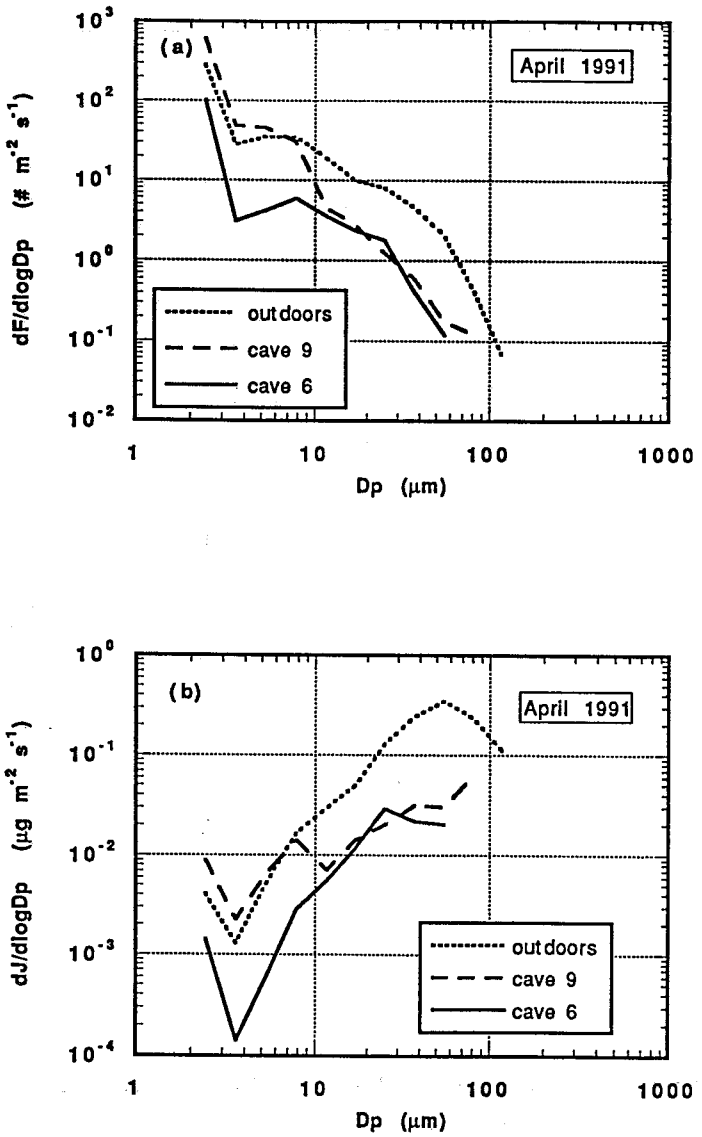

Figure 2.8 Coarse particulate matter deposited onto vertical surfaces at Yungang, April 1991, as a function of particle diameter d_p: (a) average number flux, F, and (b) average mass flux, J.

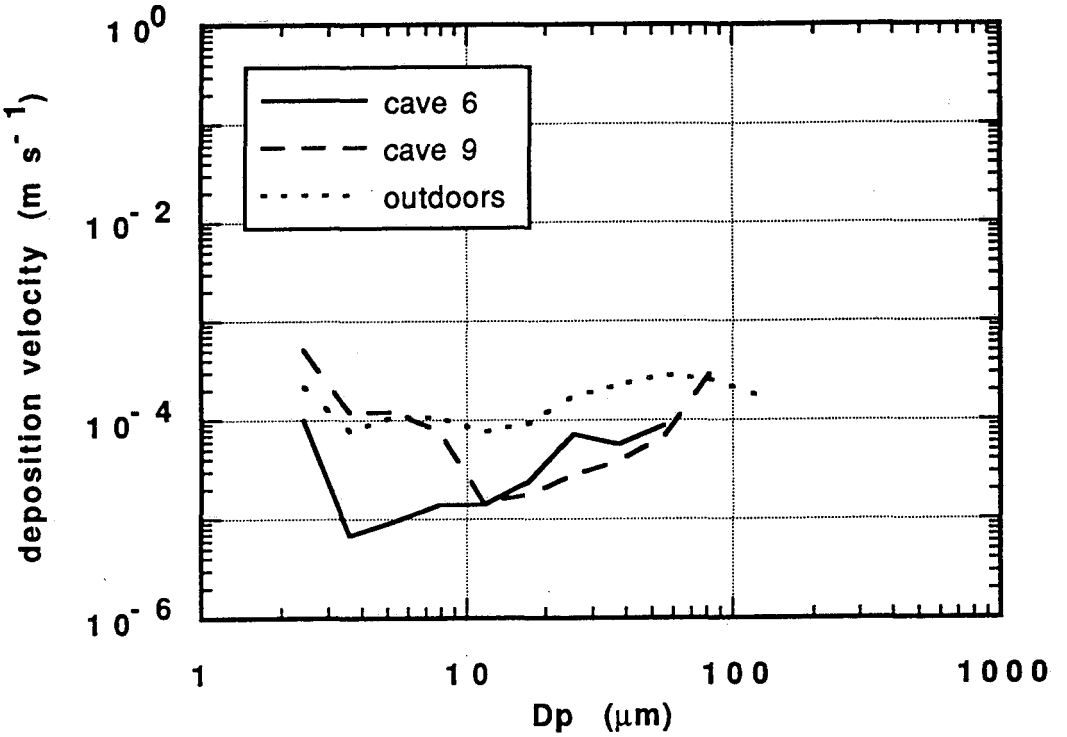

Figure 2.9 Deposition velocity onto vertical surfaces at Yungang, Spring 1991 as a function of particle diameter d_p.

upward facing surfaces inside the caves. The outdoor deposition velocity curve remains almost flat with increasing particle diameter. Ligocki et al. (1990) provide deposition velocity graphs for fine particle ($d_p \leq 2.1\ \mu m$) accumulation on smooth vertical surfaces. It is seen that the trend there is the same, i.e., particle deposition velocity remains almost constant over the range of particle diameters studied.

2.4 Conclusions

Coarse particle deposition rates onto horizontal surfaces have been measured as a function of particle size at the Yungang Grottoes. The mass fluxes were found to range from 13.42 $\mu g\ m^{-2}\ s^{-1}$ outdoors to 5.23 $\mu g\ m^{-2}\ s^{-1}$ inside Cave 6 over a one year period. These mass deposition rates are approximately the same as estimates derived by removal of historically accumulated deposits from within the caves. Size distribution measurements show that most of the deposited mass is contributed by particles larger than $20-30\ \mu m$ in diameter.

The rate of surface area coverage by coarse particles depositing on horizontal surfaces inside the caves was measured, and ranged from $2.9\text{x}10^5 \mu m^2\ m^{-2}\ s^{-1}$ inside Cave 9 to $1.2\text{x}10^5 \mu m^2\ m^{-2}\ s^{-1}$ inside Cave 6. At a surface area coverage rate of $2\text{x}10^5 \mu m^2\ m^{-2}\ s^{-1}$, 100% surface coverage by deposited particles occurs within a two month period, clearly explaining why the statues inside the caves are becoming visibly soiled at a rapid rate.

Measurements show that there is a marked decrease in the deposition of coarse particles inside Cave 6 when compared to Cave 9 and the outdoors. Also, mass deposition rates inside Cave 6 were found to be almost constant over the course of a year. That might be attributed to the wooden temple front structure that protects the entrance to Cave 6 and that acts as a partial barrier to the migration of particles from the outside. Cave 9 has

no such temple front, and clearly a greater fraction of the outdoor particles enter Cave 9. Reconstruction of temple fronts over the entrances to the remaining caves thus would be expected to slow the soiling problem somewhat. If careful thought is given to the design, even better protection than is presently provided by the shelter over Cave 6 could be achieved through installation of an air filtration system within existing or reconstructed temple front buildings (Nazaroff and Cass, 1991). The particle concentration and size distribution data reported here should facilitate the design of such a particle control system.

2.5 References

The Great Treasury of Chinese Fine Arts (1986) Peoples Fine Arts Publishing House, Shanghai People's Fine Arts Publishing House, Cultural Relic Publishing House, and China Architecture Publishing House: Beijing, China; Vol. 10.

Hancock R.P., Esmen, N.A., and Furber, C.P. (1976) Visual response to dustiness. *J. Air Pollut. Control Assoc.* **26**, 54-57.

Heidenreich, E. (1987) Particle characterization by size and shape. *J. Aerosol Sci.* **18**, 777-780.

John, W., Fritter, D.N., and Winklmayr, W. (1991) Resuspension induced by impacting particles. *J. Aerosol Sci.* **22**, 723-736.

Ligocki, M.P., Liu, H.I.H, Cass, G.R., and John, W. (1990) Measurements of particle deposition rates inside Southern California museums. *Aerosol Sci. Technol.* **13**, 85-101.

Liu, B.Y.H. and Ahn, K. (1987) Particle deposition on semiconductor wafers. *Aerosol Sci. Technol.* **6**, 215-224.

Nazaroff, W.W., and Cass, G.R. (1989a) Mass-transport aspects of pollutant removal at indoor surfaces. *Environ. Int.* **15**, 567-584.

Nazaroff, W.W., and Cass, G.R. (1989b) Mathematical modeling of indoor aerosol dynamics. *Environ. Sci. Technol.* **23**, 157-166.

Nazaroff, W.W., Ligocki, M.P., Ma, T., and Cass, G.R. (1990) Particle deposition in museums: comparison of modeling and measurement results. *Aerosol Sci. Technol.* **13**, 332-348.

Nazaroff, W.W., and Cass, G.R. (1991) Protecting museum collections from

soiling due to the deposition of airborne particles. *Atmos. Environ.* **25A**, 841-852.

Nicholson, K.W. (1988b) The dry deposition of small particles: A review of experimental measurements. *Atmos. Environ.* **22**, 2653-2666.

Salmon, L. G., Christoforou, C. S., and Cass, G. R. (1994) Airborne pollutants in the Buddhist cave temples at the Yungang Grottoes, China. *Environ. Sci. Technol.*, **28**, 805-811.

Sehmel, G.A. (1980) Particle and gas dry deposition: A review. *Atmos. Environ.* **14**, 983-1011.

Chapter 3. Air exchange within the Buddhist cave temples at Yungang

3.1 Introduction

Chapter 2 and work published elsewhere (Salmon et al., 1994, Salmon et al., 1995) describe air monitoring and particle deposition monitoring experiments conducted at the Buddhist cave temples at Yungang. The overall purpose of that work was to characterize the exposure of the grottoes to air pollutants in a manner that will establish a basis for the future protection of the grottoes from air pollution damage. The purpose of the present chapter is to describe the processes that drive air flow through these caves. That air flow acts to transport air pollutant particles into the caves from the outdoors. Hence an understanding of the air flow patterns at the Yungang Grottoes is critical to an understanding of the air pollution problems that affect these cave temples.

Today agencies of the Chinese government are actively trying to protect the grottoes, which suffer from a severe air pollution problem. The Yungang Grottoes are situated about 16 km west of the industrial city of Datong, in the middle of one of China's largest coal mining regions. Total suspended particulate (TSP) matter concentrations measured outdoors at the Grottoes during a 1-year period averaged 508 $\mu g\ m^{-3}$ (See Chapter 2). Peak 24-hr average TSP airborne particle concentrations exceeding 1200 $\mu g\ m^{-3}$ were measured during April, 1991. These airborne particles enter the caves and deposit onto the surfaces of the statues and carvings inside. Measurements show that horizontal surfaces inside Cave 9 become completely covered by a monolayer of dark-colored particles within a few months at present (Salmon et al., 1995).

Airborne particles enter the caves as air is exchanged between the outdoor

atmosphere and the caves' interior. In order to understand the particle deposition problem, it is necessary to understand how much air is moving through the caves and the various factors that determine the air flow. The mechanism by which air enters and exits such cave temples is not well documented at present. Flow of air in and out of natural caves is sometimes due to changes in atmospheric pressure which leads to a phenomenon known as cave breathing (Wigley, 1967; Moore, 1978). Other previous investigations in mine shafts (Harris and Kingery, 1973) and also in natural caves (Wigley and Brown, 1976; Quindos et al., 1987) have been undertaken that use natural convection to explain air flows in caves. Radon 222 concentration measurements have been made in order to define features of the natural circulation inside caves (Wilkening and Watkins, 1976). However little is known about air exchange in man-made caves that are similar to those studied at Yungang. In particular we seek enough information to be able to calculate how the air flow would respond to the reconstruction of the wooden temple buildings that once sheltered the entrances to the caves in antiquity and how the air flow would respond to the insertion of particle filtration material into the window panels of such temple building fronts.

3.2 Experimental methods

Two caves were chosen for analysis, Caves 6 and 9. As shown in Figure 3.1, their architecture is similar: an almost cubic room at the rear of each cave 10-15 m on each side, having a central pillar that stretches from the floor almost to the ceiling.

In Cave 6 the central pillar is fashioned in the shape of a pagoda, whereas the column in Cave 9 is carved into a monumental statue of the Buddha. The entrances to Cave 9 through the rock cliff face are open directly to

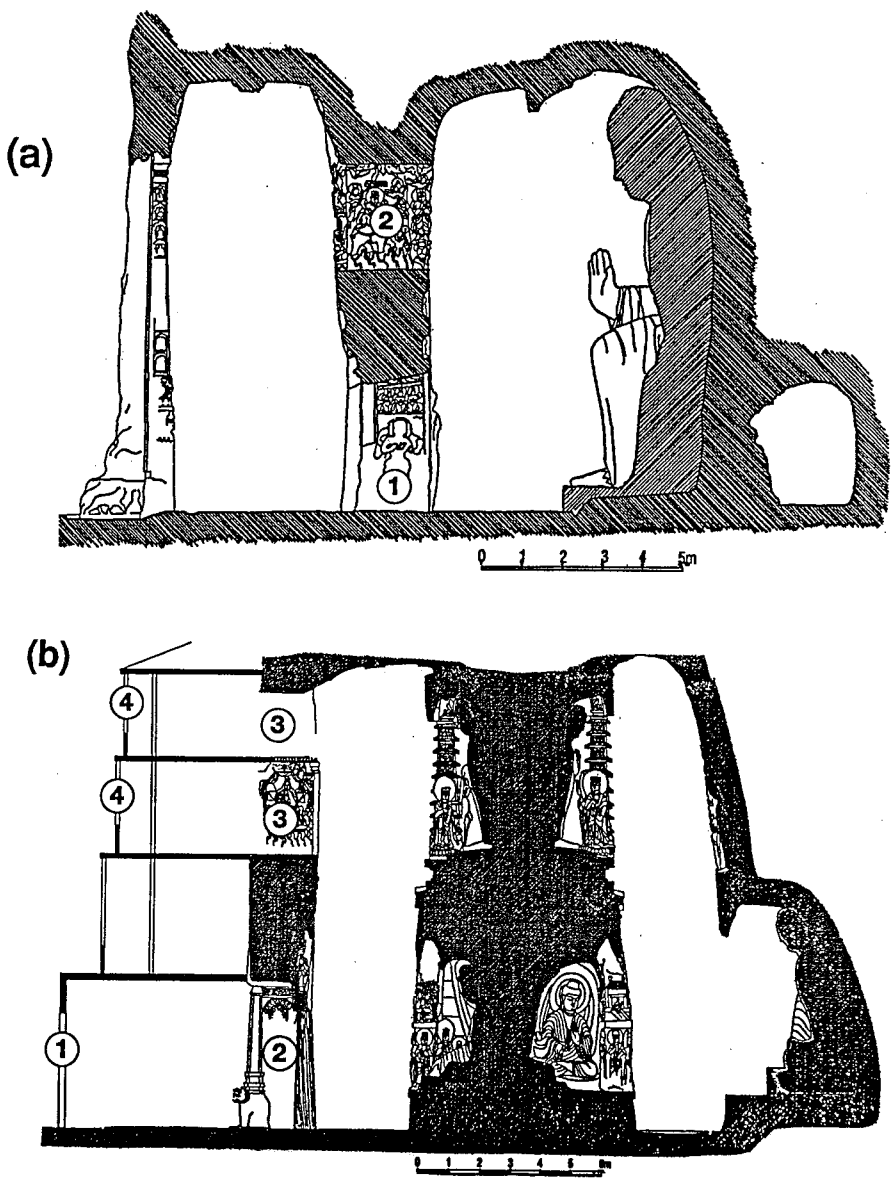

Figure 3.1 Vertical cross-section of Cave 9 (top) and Cave 6 (bottom).

the outdoors. Cave 6, unlike Cave 9, retains its traditional wooden temple building that shelters the entrances through the cliff face. The surfaces of that building consist largely of narrow wooden door panels with a wooden lattice work backed by paper windows.

Between April 12, 1991 and April 30, 1991, experiments were conducted at Yungang to measure the airflow into and out of the caves using a battery of instruments. Thermo-electronic air velocity probes, hand-held mechanical air velocity meters and perfluorocarbon tracer (PFT) techniques were used to measure the air exchange rates. Measurements also were made that relate to the driving forces that cause the air flow. These include cave wall temperatures, indoor and outdoor air temperatures and outdoor wind speed and direction.

An omnidirectional air velocity probe (TSI model 1620) was placed near the center of the ground level entrance to Cave 9 (position 1 in Figure 3.1a) and was used to record the absolute value of the air velocity through that cave entrance continuously over the course of the experiment. Periodic air velocity measurements were made at that entrance to Cave 9 using a hand-held mechanical air velocity meter (vaneometer, part no. 6610A4306, Whatman Labs, Hillsboro, OR) from which the speed and direction of the air flow into or out of the cave was noted as a function of time of day. The hand-held velocity meter also was used to measure air speed and direction through the ground floor entrance to the wooden temple building attached to Cave 6 (position 1 in Figure 3.1b) with the wooden doors open, through the ground level opening in the rock wall between the antechamber and interior chamber of Cave 6 (position 2 in Figure 3.1b) with the wooden temple front doors open and with the temple front doors closed, and through the upper level opening in the rock wall between the antechamber and the interior cham-

ber of Cave 6 (positions 3 in Figure 3.1b) during two intensive periods of observation on April 15-16 and April 24-25, 1991.

Air exchange rates were also measured during the experiment using perfluorocarbon tracer (PFT) techniques (Dietz and Cote, 1982). Sources were placed at selected locations inside the caves that emitted perfluorocarbons at a small but constant rate. Collection tubes through which the tracer will permeate were exposed and then analyzed to give the tracer concentration within the caves from which the total rate of air infiltration ($m^3\ hr^{-1}$) into the caves can be calculated. Some tracer collection tubes were left in place for the duration of the 20-day experiment to obtain long-term average air exchange rates, and others were used to measure air exchange for each four hour period during a 48 hour intensive sampling experiment that was conducted on April 15-16, 1991. Analysis of the PFT samples taken was performed by the staff at Brookhaven National Laboratory.

Cave wall temperatures and indoor air temperatures were measured by thermistor arrays that were placed at an elevation of 1.98 m above floor level inside Cave 6 and at elevations of 1.98 m, 4.70 m and 5.72 m above floor level inside Cave 9. The cave wall temperature thermistors (part no. 44202, Yellow Springs Instrument Co., Yellow Springs, OH) were secured within shallow surface cracks in the cave walls using a thermal joint compound in order to ensure thermal contact with the wall. The air temperature thermistors were held in place 5.1 cm away from the surface of the cave walls. This placement was chosen in order to sample air temperatures within the fluid boundary layer along the cave walls. Signal conditioning circuits transformed the thermistors' output into voltage values that were proportional to the temperature.

Outdoor air temperatures were recorded on paper chart recorders at the

weather station operated by the Chinese government at the Yungang Grottoes. These measurements were subsequently entered into computer data files (two data points every hour).

Natural convection boundary layer flows were expected along the interior vertical walls of the caves due to wall/air temperature differences. In order to confirm the magnitude of these flows, an omnidirectional velocity probe (TSI model 1620) was placed 1.65 m above ground level and 1 cm away from the cave walls. This probe was placed in Cave 9 during the first half of the experiment and in Cave 6 during the second half of the experiment.

Finally, wind speed and direction outdoors were recorded with the aid of an automated weather station (part no. 03001-5, Campbell Scientific Inc., Logan, UT). The purpose of the outdoor wind speed and direction measurements was to determine whether or not pressure differences induced by high speed winds normal to or parallel to the face of the cliff containing the cave entrances were obviously influencing air motion through the caves.

With three exceptions, the above measurements were logged automatically every minute between April 12, 1991 and April 30, 1991 with the aid of a Campbell Scientific CR-10 measurement and control module (Campbell Scientific Inc., Logan, UT). Temperature measurements inside Cave 6 and outdoors were recorded with the aid of a chart recorder, and the mechanical air velocity meter readings were recorded manually in laboratory notebooks.

3.3 Results and discussion

Figure 3.2 shows the air temperature outside the caves as well as the cave wall temperature and near-wall air temperature measurements made inside Cave 9 at 1.98 m above floor level.

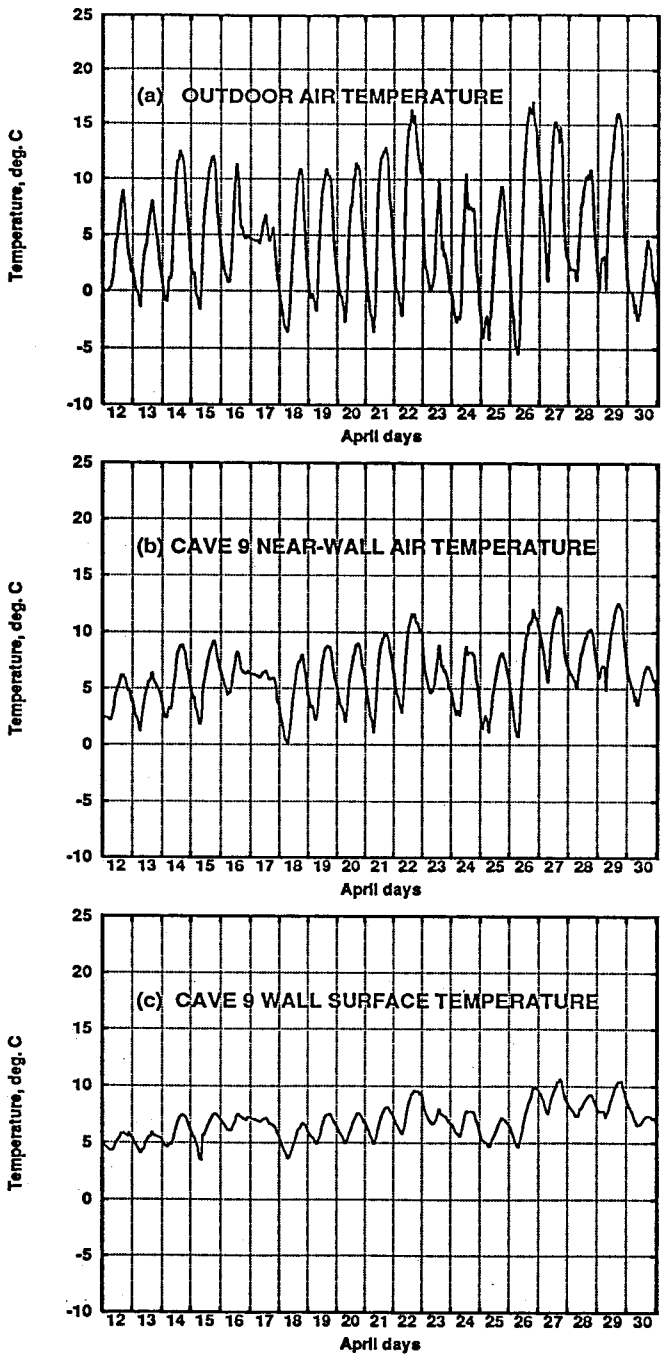

Figure 3.2 Air temperatures and cave wall temperatures at Yungang, April 12-30, 1991: (a) shows the outdoor air temperature, (b) the air temperature measured 5.1 *cm* away from the vertical rock wall in Cave 9 and (c) the Cave 9 rock wall surface temperature.

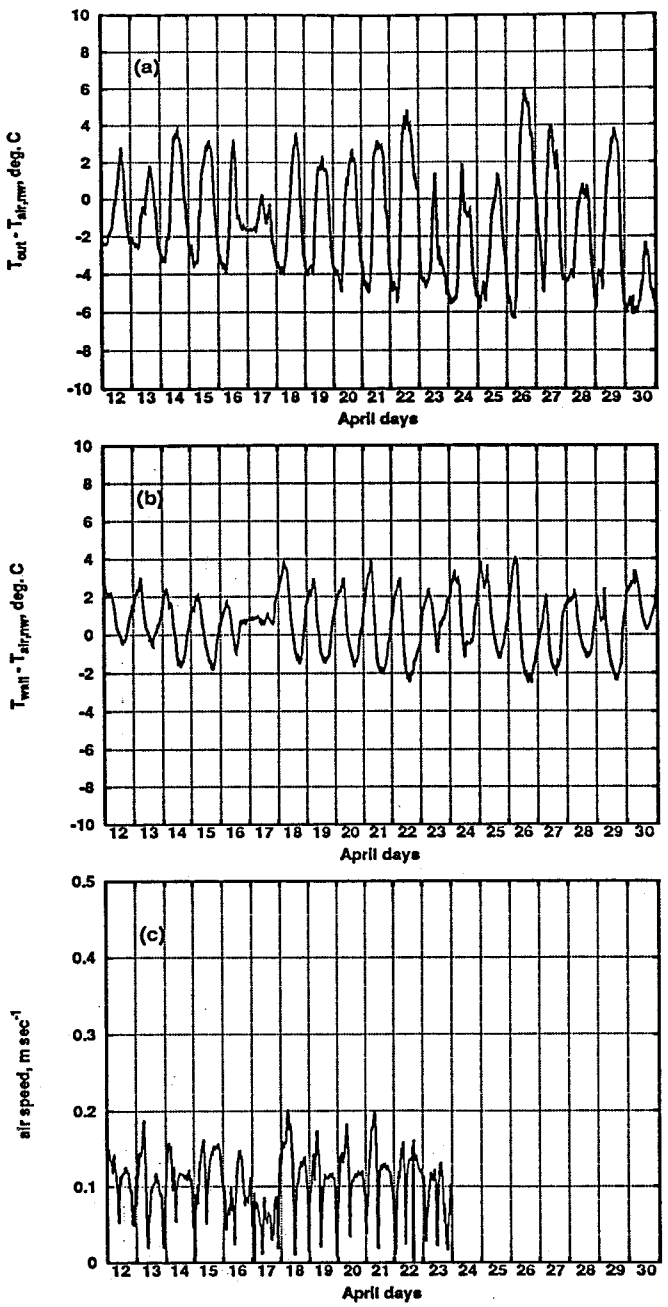

Figure 3.3 Temperature differences and air speed along the cave walls at Yungang, April, 1991: (a) temperature difference between the outdoor air, T_{out}, and the near-wall air inside Cave 9, $T_{air,nw}$, (b) wall surface temperature, T_{wall}, minus near-wall air temperature, $T_{air,nw}$, inside Cave 9, and (c) air speed in the boundary layer along the walls of Cave 9.

The indoor temperature data that were originally logged at 1 min intervals have been smoothed using a low-pass filter that removes fluctuations having a period shorter than one hour. Figure 3.3 shows the temperature differences between the outdoor air and the near-wall air inside Cave 9 and also between the near-wall air inside Cave 9 and the cave walls. The following general comments can be made about these temperature measurements:

(a) Not surprisingly, the outdoor air is warmer during the day than it is at night. Peak hourly average outdoor air temperatures during the daytime over the days of the experiment were in the range 4.7 ^oC to 16.8 ^oC, while the daily nighttime minimum hourly average temperatures outdoors were in the range -5.5 ^oC to 1.1 ^oC.

(b) The temperature of the cave walls during April is typically less than the outdoor air temperature during the day, but is typically warmer than the outdoor air temperature during the night. For example, on April 14, 1991, hourly average outdoor air temperatures ranged from a low of -0.9 ^oC at night to a high of 12.5 ^oC in the afternoon, whereas during the same day hourly average cave wall surface temperatures inside Cave 9 ranged from a low of 4.6 ^oC at night to a high of 7.1 ^oC during the afternoon.

(c) Near-wall air temperatures inside the caves lie between those of the cave wall temperatures and the outdoor air temperatures. The near-wall air in the caves is warmer than the cave walls but cooler than the outdoor air during the day and the reverse is true at night. Hourly average indoor air temperatures measured 5.1 cm away from the walls during the April 14, 1994 event discussed in item (b) above ranged from a maximum value of 8.8 ^oC during the day to a minimum value of 2.6 ^oC during the night. This means that the indoor air is denser

than the outdoor air during the day and less dense than the outdoor air during the night.

(d) Wall-air temperature differences typically pass through zero around 1050 hours in the morning and again around 2025 hours at night.

(e) The outdoor and indoor air temperatures typically are periodic with a 24 hour cycle, and this periodicity is reflected to a lesser extent in the daily cycling of the rock wall surface temperature.

(f) There is a long-term warming trend in the outdoor air over the course of the experiment that is reflected in a slow upward trend in the temperature of the cave wall surface, which suggests that seasonal cycling of the wall surface temperature occurs to some extent.

Wall and air temperature thermistors were placed at an elevation of 1.98 m above ground level in Cave 6, and again the near-wall air temperatures were measured 5.1 cm away from the cave walls. Wall temperature and near-wall air temperature cycles were observed inside Cave 6 that were were similar to those seen inside Cave 9. Even though the average near-wall air temperature inside Cave 6 was almost the same as the average near-wall air temperature inside Cave 9 at the same height above ground level, the daytime near-wall air temperature peaks inside Cave 6 were lower than those inside Cave 9 by about 1.4 ^oC, and the minimum nighttime near-wall air temperatures inside Cave 6 were warmer than the corresponding values inside Cave 9 by about 2.5 ^oC. The situation was similar for the wall surface temperatures. The average of the daily peak 1-hr average wall temperature values inside Cave 6 was 6.4 ^oC (compared to 8.3 ^oC for Cave 9), while the mean of the nighttime minimum 1-hr average wall temperatures in Cave 6 was 5.1 ^oC (compared to 4.2 ^oC for Cave 9).

Figure 3.3c shows the air speed along the wall in Cave 9 as a function of time. The flow of air along the cave walls is observed to follow a natural convection pattern. That air flow is periodic, typically with two high flow events per day. One of these high flow events typically occurs between midnight and mid-morning each day and logically corresponds to flow up the wall at a time when the walls are warmer than the air in the caves. The second period of high flow along the walls occurs during the afternoon and early evening when the cave walls are cooler than the air in the caves and logically corresponds to flow down the cool cave walls. Figure 3.3b shows the temperature difference between the cave wall and the air 5.1 *cm* away from that wall inside Cave 9. It is seen that the air flow along the wall graphed in Figure 3.3c tracks that temperature difference. Typically when the wall-air temperature difference is near zero, so is the air velocity along the wall, and when the absolute value of the temperature difference is greatest, so is the air velocity near the walls.

The air velocity at the center of the ground level entrance of Cave 9 (position 1 in Figure 3.1a) as recorded by the omnidirectional velocity probe is shown in Figure 3.4a. Figure 3.4b shows the same dataset after the data have been smoothed and with the air flow direction stated based on the records from the hand-held mechanical velocity meter. In Figure 3.4b, a positive air velocity denotes air flow from outdoors into Cave 9 through the ground level entrance (position 1 in Figure 3.1a) accompanied by flow out of the third floor level exit (position 2 in Figure 3.1a) from the cave. Negative velocity indicates flow out of the ground level entrance to the cave accompanied by flow into the upper level opening through the cave wall. The velocity is periodic during the course of the day. It goes to zero twice, first sometime typically around 0930 hours in the morning and then again around 2100 hours at night.

These changes can be explained with the aid of Figure 3.3 which shows

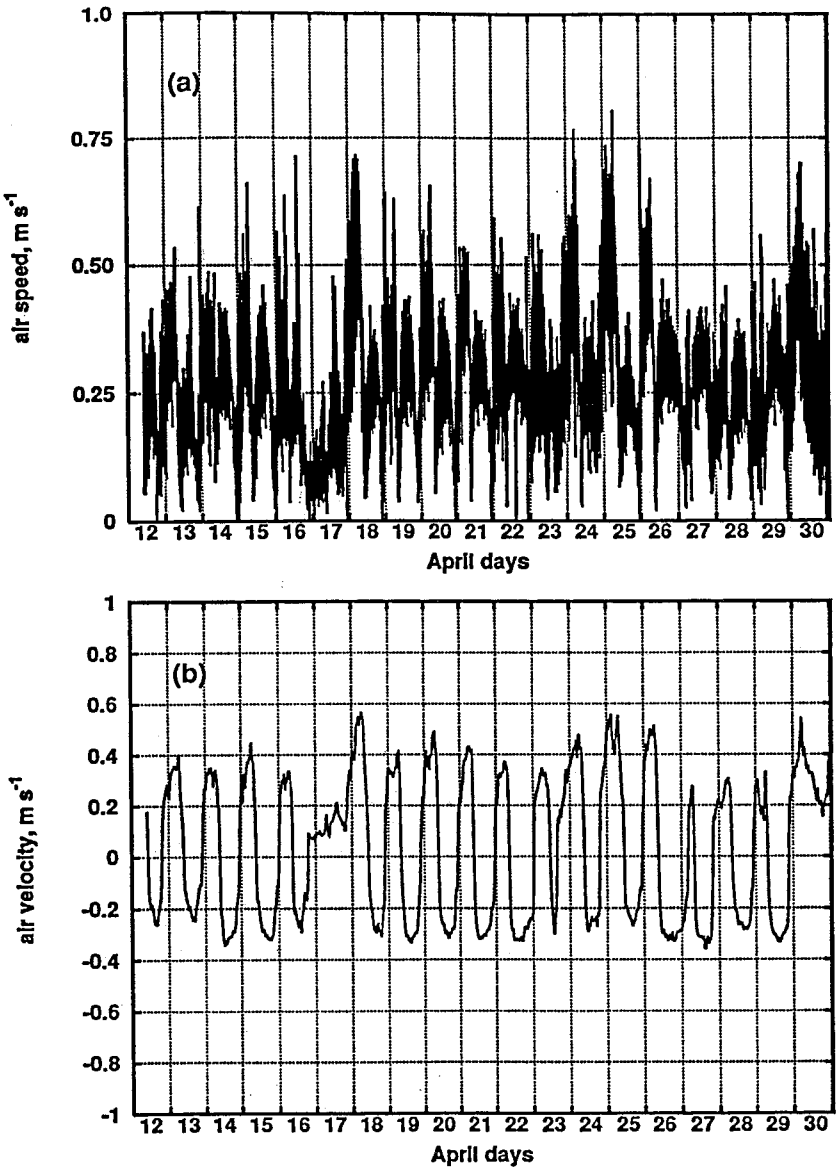

Figure 3.4 Air flows at the entrance to Cave 9 at Yungang, April, 1991: (a) air speed measured in the ground level entrance to Cave 9 (position 1 in Figure 3.1a), and (b) smoothed air velocity data from (a) above with the direction of the air flow assigned based on periodic mechanical air velocity meter readings. Positive velocity indicates flow of air into the cave at the ground level entrance.

the temperature difference between outdoor air and the near-wall air inside the cave and also between the cave wall and the near-wall air inside Cave 9. Late at night and in the early morning when the cave wall is warmer than both the outdoor air and the air in the cave, air rises along the walls; air that is warmer than that outdoors accumulates and exits the cave from the opening that exists in the rock wall at the third floor level, while cooler outdoor air enters the cave through the main ground level entrance to replace the warm air leaving at the upper level exit. As the wall/air temperature difference and the indoor/outdoor air temperature difference decreases, so does the magnitude of the air velocity in the entrance to the cave. As the outdoor air is warmed during the day, eventually the temperature of the air entering Cave 9 becomes greater than the cave wall surface temperature. Around mid-morning, the flow of air through the cave entrance reverses direction and then begins to increase. Warm outdoor air is drawn into the cave through the opening at the third floor level and then is cooled by contact with the colder cave walls; cold air accumulates and then flows out through the ground floor main entrance. This outflow at ground level continues until about 2100 hours at night, at which time the outdoor air temperature and the air temperature inside Cave 9 again become nearly equal to the wall temperature, in which case the air exchange is reduced to nearly zero. Next, air starts flowing into the cave through the ground level main entrance as the interior air temperature falls below that of the cave wall temperature, and the cycle continues. The average air speed at the center of the entrance of Cave 9 was found to be 0.274 $m\ s^{-1}$ over the course of the April 1991 experiments.

In order to compute the air volume entering or leaving Cave 9, it is necessary to know the air velocity distribution across the entrance through the rock wall

where the omnidirectional velocity probe was placed. In order to determine that velocity distribution, the hand-held mechanical velocity meter was used to make measurements each hour at a matrix of nine points across the face of the entrance over three twenty-four hour periods. The mechanical velocity meter data were then averaged to determine the volume-weighted average air velocity entering Cave 9. The results of these measurements are shown in Figure 3.5. The air velocities averaged over the nine points generally agree well with the single measurement taken at the center of the entrance at the same time. Regression of air velocity at the center of the door on the volume-weighted average air velocity through the door results in a slope of 1.06 ± 0.05, an intercept of $-0.07 \pm 0.04\ m\ s^{-1}$ and a correlation coefficient of 0.91. Therefore the air flow through the Cave 9 entrance is approximately a plug flow and the velocity measurement taken at the center of the entrance is sufficient to describe the air flow in or out of the caves.

Using the smoothed omnidirectional velocity probe measurements in the entrance of Cave 9 and the dimensions of the entrance, the average air volume flowing through Cave 9 was calculated to be 7300 $m^3\ hr^{-1}$ or 121 $m^3\ min^{-1}$ averaged over the period April 12-30, 1991. At that flow rate, one complete air exchange is achieved within Cave 9 in only 4.3 minutes on average.

Air flow rates through the caves also were measured using the perfluorocarbon tracer technique. Averaged over the entire duration of the experiment, the volume of air flowing through Caves 6 and 9 was measured to be $8620 \pm 1480\ m^3\ hr^{-1}$ and $8190 \pm 1240\ m^3\ hr^{-1}$ respectively. The result obtained for Cave 9 from the tracer experiment is clearly in reasonable agreement with the result obtained from the omnidirectional velocity probe at the entrance to Cave 9. Since Cave 6 is approximately four times larger in volume than Cave 9, the rough equality of long-term average volumetric air flow

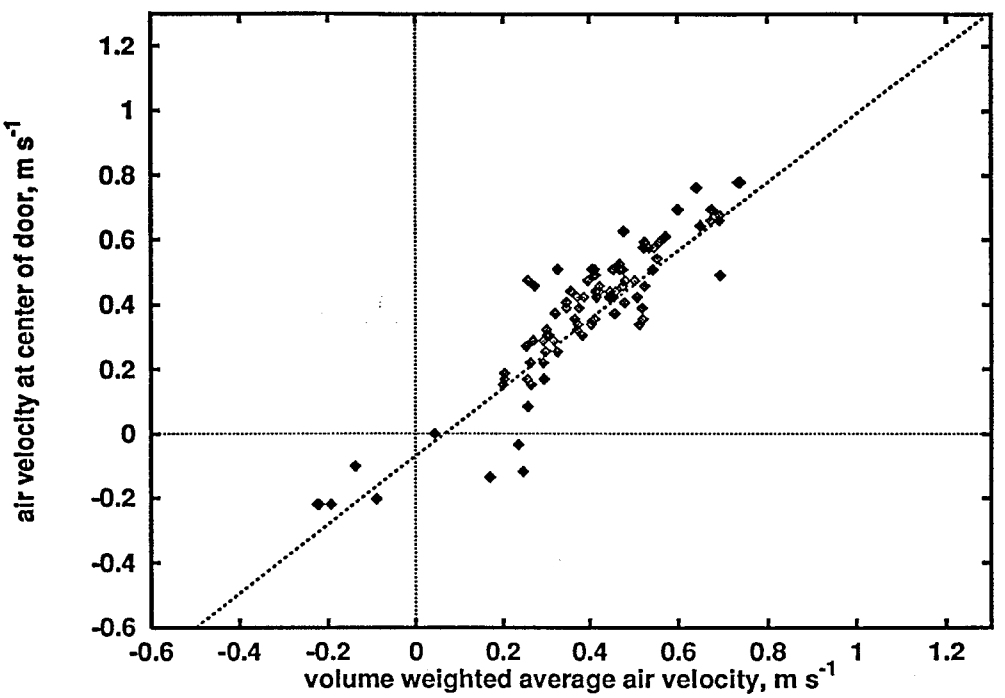

Figure 3.5 Air velocity measurements made once per hour over three 24-h periods at the center of the ground level entrance to Cave 9 compared to the volume-weighted average air velocity through that entrance computed from measurements made at a matrix of 9 points across the entrance using the mechanical air velocity meter. Regression of air velocity at the center of the door on the volume-weighted average air velocity through the door results in a slope of 1.06 $\pm$ 0.05, an intercept of -0.07 ± 0.04 $m\ s^{-1}$ and a correlation coefficient of 0.91.

rates means that the time to achieve one complete air exchange inside Cave 6 is approximately 4 times longer than Cave 9. This factor of four difference in air exchange times occurred under the condition where several of the door panels present in the upper stories of the wooden temple structure in front of Cave 6 typically were in their open position, providing less resistance to air exchange than would be the case if those doors were tightly closed (we did not seek to alter the settings of those doors; Cave 6 was examined exactly as it was operated by the Grottoes staff).

The wind speed and direction outside the caves were also recorded during April 1991. Figure 3.6a shows the wind speed component parallel to the cliff face that contains the cave entrances, with a positive wind speed taken when wind blows from west to east across the cave entrances. Figure 3.6b shows the wind speed component perpendicular to the cave entrances, with a positive component designating flow from south to north toward the front of the cliff face. Earlier, it was seen that air flow into and out of Cave 9 closely tracked changes in the air temperature data. When the outdoor wind speed data of Figures 3.6a and b are compared to the bulk air exchange through Cave 9 that is shown in Figure 3.4b, it is seen that there is little obvious effect of outdoor wind speed changes on air exchange rate changes: high wind speed days like April 28-30 show air exchange rates comparable to most other days examined, as do low wind speed days like April 18. It is concluded that air exchange through these caves is driven largely by a thermally-induced natural convection flow with outdoor wind speed changes contributing at most a secondary effect.

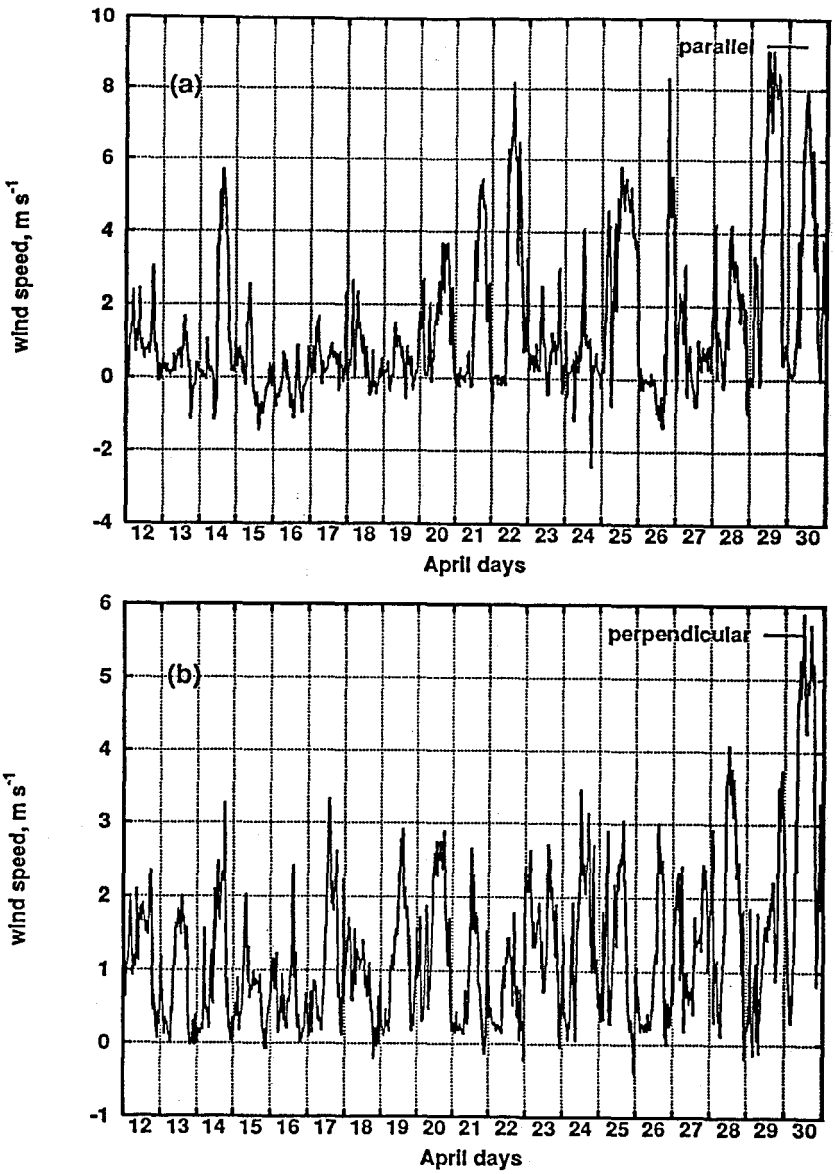

Figure 3.6 Outdoor wind speed at Yungang, April, 1991: (a) Wind speed component parallel to the front of the cliff into which the caves are carved. Positive values indicate flow from the west to the east in front of the entrance to Cave 9, while negative numbers indicate flow from east to west. (b) Wind speed component perpendicular to the cliff face. Positive values indicate flow from south to north toward the entrances to Cave 9.

3.4 Theoretical model

3.4.1 Cave 9

A theoretical model is now presented that accounts for the bulk air exchange between outdoors and the inside of Cave 9 as seen in the filtered air velocity data. Consider first the case where warm air flows into Cave 9 through the upper level entrance shown at position 2 in Figure 3.1a. The air is cooled by contact with the cave walls; cool air accumulates within the core of the cave and next exits through the ground level opening in the cave wall at position 1 in Figure 3.1a. The following three equations are used:

$$\frac{d}{dt}(\rho_a V) = \rho_o U_2 A_2 - \rho_a U_1 A_1 \tag{3.1}$$

$$\frac{d}{dt}(\rho_a V c_v T_a) = \rho_o U_2 A_2 c_p T_o - \rho_a U_1 A_1 c_p T_a - \sum_{i=1}^{3} h_i S_i (T_a - T_w) \tag{3.2}$$

$$\frac{1}{2}\rho_o U_2^2 C_L + \frac{1}{2}\rho_a U_1^2 C_L = gH(\rho_a - \rho_o) \tag{3.3}$$

where ρ_a is the bulk density of the air mass inside the cave, ρ_o is the density of air outside the cave, T_a is the absolute temperature of the air inside the central core of the cave, T_o is the absolute temperature of the air outside the cave, T_w is the absolute temperature of the cave rock walls, V is the volume of the cave, H is the elevation difference between the air entering the cave and the air leaving the cave, A_1 is the cross sectional area of the cave entrance at ground level, A_2 is the cross sectional area of the opening in the cave rock wall at the third floor level, c_p is the specific heat of air at constant pressure (1006 $J\ kg^{-1}\ {}^oC^{-1}$), c_v is the specific heat of air at constant volume (719 $J\ kg^{-1}\ {}^oC^{-1}$), g is the acceleration due to gravity (9.81 $m\ s^{-2}$), C_L is the loss coefficient for air flow through the openings in the rock walls of the cave

(taken to be 1.5 as for induction of air into a building from outdoors (Jennings and Lewis, 1965), and for flow through a square edged orifice (Sabersky et al., 1989)), and h_i is the heat transfer coefficient for natural convection boundary layer flow over the i^{th} cave surface. Three different heat transfer coefficients are used: one for the heat transfer that takes place over the vertical walls, h_1, one for heat transfer across the cave floor, h_2, and one for heat transfer that takes place at the cave ceiling, h_3. The heat transfer surface areas of the cave walls, floor, and ceiling are given by S_1, S_2, and S_3 respectively. U_2 is the air velocity entering the cave at the opening through the rock wall at the third floor level and U_1 is the air velocity exiting the cave at the ground floor level, with both velocities taken as positive in the direction of flow. The numerical values for geometric parameters H, A_1, A_2, V, S_1, S_2 and S_3 for Cave 9 are given in Table 3.1.

Equations (3.1), (3.2), and (3.3) above are essentially the continuity equation, an equation stating that the change in internal energy of the air inside the cave over time depends on energy convected in and heat transfer at the cave walls less energy convected out, and an equation that balances the pressure drops in the air path against the density differences between the indoor vs outdoor air acting on the height of the air column between the entering and exiting air paths, respectively. In writing the set of equations, the following approximations were made: (a) air inside the cave is well mixed, (b) flow through the openings between outdoors and the cave interior is plug flow, (c) flow starts due to a pressure difference due to air density differences between the interior of the cave and the outdoors, and (d) there is a natural convection boundary layer flow along the cave walls that is due to wall/air temperature differences that leads to heat transfer between the cave walls and the air in the caves.

Table 3.1 Geometric parameters of Caves 6 and 9

Parameter	Description	Cave 6	Cave 9
Z	physical height of the cave	15 m	10.35 m
H	elevation difference between entering and exiting critical fluid streamline	9.25 m	2.39 m
V	volume of cave	2222 m^3	528 m^3
S_1	nominal wall surface area based on major outline of walls[a]	1370 m^2	346.6 m^2
S_2	nominal ceiling surface area of cave	163 m^2	43.7 m^2
S_3	floor surface area of cave	179 m^2	43.7 m^2
A_1	cross-sectional area of entrance through rock wall at ground level, Cave 9		7.4 m^2
A_2	cross-sectional area of opening in rock wall at 3rd and 4th floor level, Cave 9		5.6 m^2
A_{1a}	cross-sectional area of openings in building shell downstairs, Cave 6, front door open	4.8 m^2	-
A_{1b}	cross-sectional area of openings in building shell downstairs, Cave 6, front door closed	0.46 m^2	-
A_2	cross-sectional area of entrance through rock walls at ground level, Cave 6	11.82 m^2	-
A_3	cross-sectional area of opening in rock wall at 3rd plus 4th, floor level, Cave 6	21.12 m^2	-
A_4	cross-sectional area of openings in building shell upstairs, Cave 6	4.09 m^2	-

a. The walls are covered with Buddhist sculptures in high relief; we estimate the actual surface are of the carvings to be about twice the nominal area defined by the major outline of the cave walls.

In the system of equations (3.1)-(3.3), the velocities at the entrances (U_1 and U_2), the temperature and density of the air inside the core of the cave, T_a and ρ_a respectively, are the unknowns. To solve the system, the following approximations are made: (a) $\rho_a \approx \rho_o \approx \rho$ except that $\frac{\rho_a - \rho_o}{\rho_o} \neq 0$, and also $\frac{\rho_a - \rho_o}{\rho_o} \approx \frac{T_o - T_a}{T_o}$. The equations then can be written:

$$U_1 A_1 = U_2 A_2 \tag{3.4}$$

$$\rho c_v V \frac{d}{dt}(T_a) = \rho c_p (U_2 A_2 T_o - U_1 A_1 T_a) - \sum_{i=1}^{3} h_i S_i (T_a - T_w) \tag{3.5}$$

$$U_1^2 + U_2^2 = \frac{2gH}{C_L} \frac{|T_o - T_a|}{T_o} \tag{3.6}$$

Equations (3.4), (3.5), and (3.6) may be solved for U_1, U_2, and T_a.

The solution for the velocity at the cave entrance, U_1 is

$$U_1 = \left(\frac{2gH A_2^2 |T_o - T_a|}{C_L (A_1^2 + A_2^2) T_o} \right)^{0.5} \tag{3.7}$$

The equation for the time rate of change of the air temperature in the core of the cave then becomes

$$\frac{d}{dt}(T_a) = \frac{1}{V \rho c_v} \left(\sum_{i=1}^{3} h_i S_i (T_w - T_a) + A_1 A_2 \rho c_p \left(\frac{2gH |T_o - T_a|}{C_L (A_1^2 + A_2^2) T_o} \right)^{0.5} (T_o - T_a) \right) \tag{3.8}$$

Given a continuous series of data on cave wall temperatures and outdoor air temperature and density, plus an initial value for the indoor air temperature in the core of the cave, equation (3.8) may be solved to predict air temperatures inside the core of the cave over time provided that the heat transfer coefficients can be estimated. Equation (3.7) may then be used to calculate the air velocity at the entrance of the cave from the outdoor temperatures

and the predicted cave air temperature. An analogous set of equations can be written to describe the condition where cold air enters the ground floor entrance to the cave and is warmed by contact with the warmer cave walls. A model for predicting air exchange through the cave based on the difference between the outdoor air temperature and the cave wall temperature thus results.

To use this system of equations, the heat transfer coefficient at the surface of the cave walls first must be specified. A relationship for the Nusselt number for natural convection flow over a vertical flat plate is provided by Churchill and Chu (1973):

$$\overline{Nu}_Z = \left(0.825 + \frac{0.387 Ra_Z^{\frac{1}{6}}}{[1 + (0.492/Pr)^{9/16}]^{8/27}}\right)^2 \tag{3.9}$$

$$\overline{Nu}_Z = \frac{Z h_1}{k} \tag{3.10}$$

$$Ra_Z = Pr \frac{g(T_w - T_a)Z^3}{T_a \nu^2} \tag{3.11}$$

where $\overline{Nu}_Z$ is the Nusselt number averaged over the length of the plate (in this case the height, Z, of the cave walls), Ra_Z is the Rayleigh number based on the height of the cave walls, Pr is the Prandtl number for air, k is the thermal conductivity of air, and ν is the kinematic viscosity of air. Heat transfer rates from the cave floor and ceiling vary depending on whether the heating or cooling there favors atmospheric stability or instability. A heated upward facing surface (the floor) or a cooled downward facing surface (the ceiling) creates instability. This situation will be represented as if the floors and ceilings were independent heated or cooled flat plates, for which Incropera and DeWitt (1984) provide the heat transfer estimates:

$$\overline{Nu}_L = 0.54 Ra_L^{\frac{1}{4}} \qquad 10^4 < Ra_L < 10^7 \qquad (3.12)$$

$$\overline{Nu}_L = 0.15 Ra_L^{\frac{1}{3}} \qquad 10^7 < Ra_L < 10^{11} \qquad (3.13)$$

In equations (3.12) and (3.13), both the Rayleigh number and the Nusselt number are based on the characteristic length L that is computed as the area of the surface divided by the perimeter of the surface. Equations (3.12) and (3.13) will be used to estimate the heat transfer coefficient, h_2, for the cave floor when $T_w > T_a$ and the heat transfer coefficient, h_3, for the cave ceiling when $T_a > T_w$, where the floor and ceiling temperatures are taken to be at the measured temperature of the cave rock walls. When the floor is colder than the air in the cave or when the ceiling is warmer than the cave air the expression

$$\overline{Nu}_L = 0.27 Ra_L^{\frac{1}{4}} \qquad (3.14)$$

is used to estimate h_2 for the cave floor when $T_a > T_w$ and h_3 for the cave ceiling when $T_w > T_a$ over the range $10^5 < Ra_L < 10^{10}$ (Incropera and DeWitt, 1984).

While natural convection flow over a flat vertical plate is analogous to the natural convection flow observed along the walls of the caves at Yungang, the analogy cannot be exact. This is because the cave walls are not actually flat. Instead they are covered with Buddhist carvings in high relief that both add to the actual surface area and that may interrupt the boundary layer air flow. Both of these factors would be expected to enhance heat transfer beyond that seen over a flat plate having the nominal height of the cave

walls. For that reason, a semi-empirical adjustment to the model is used: the product of the heat transfer coefficient times the nominal area of the cave walls is multiplied by a surface area correction factor to account for the fact that the cave walls are covered with Buddhist carvings and that the surface area of the walls is therefore much larger and rougher than that apparent from a superficial analysis of the available drawings of the caves. Having examined detailed photographs of the cave walls, we estimate that the actual surface area of the carvings is about 2 times larger than the nominal surface area of the major outline of the cave walls. Therefore the value of the product $h_i S_i$ appearing in equation (3.8) applied during the calculations for Cave 9 is taken to be twice as large as would be the case for a vertical flat plate having the nominal surface area of the major outline of the cave walls.

Equation (3.8) may be solved for T_a given T_o and T_w. The differential equation (3.8) is integrated for 60 s given fixed values for T_o and T_w. At the end of 60 s the values of T_o and T_w are updated from the experimental data base, the value of T_a predicted at the end of the previous 60 s is used as the initial value for the next calculation cycle and thus the solution is continued. From the resultant time series of predicted values for T_a, the air velocity through the ground level entrance to Cave 9 as a function of time is obtained from equation (3.7), with the direction of flow specified according to the sign of the temperature difference $(T_o - T_a)$. The results of this simulation for Cave 9 are shown in Figures 3.7a and b. Figure 3.7a shows the near-wall air temperature, $T_{air,nw}$, predicted at a distance 5.1 cm from the wall and 1.98 m from the floor inside Cave 9, together with the measured indoor near-wall air temperature at that location compared to the outdoor air temperatures and cave wall temperatures supplied to the model. The predicted value of $T_{air,nw}$

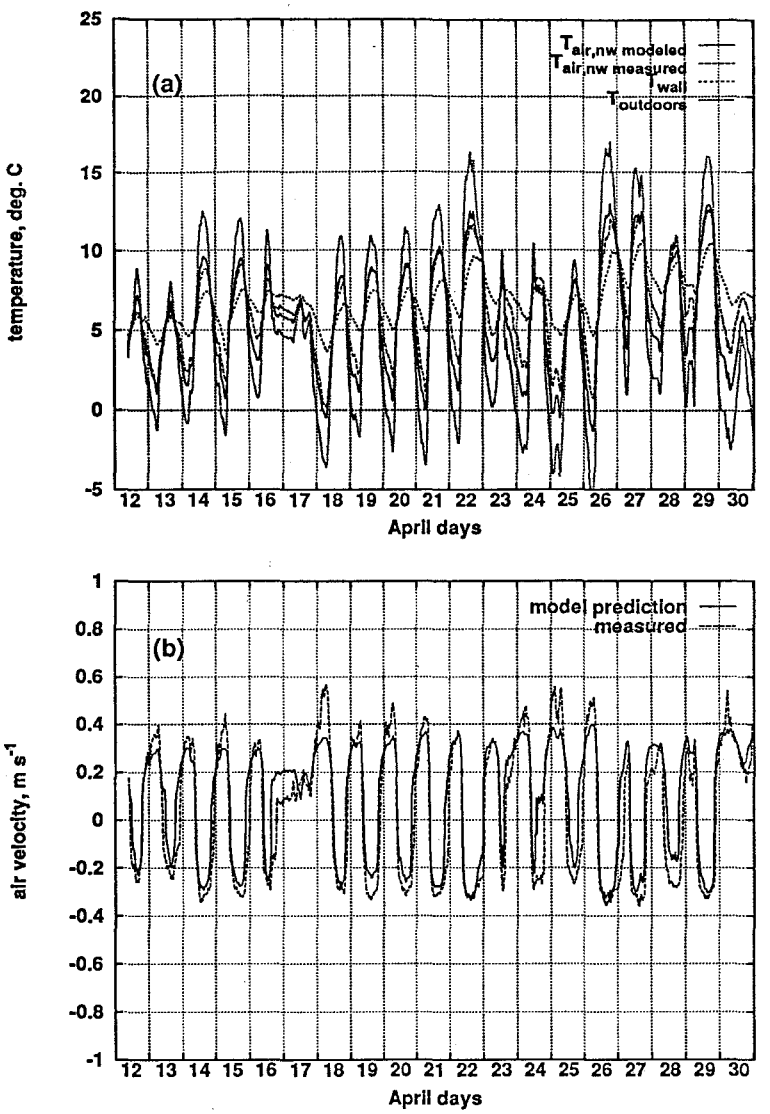

Figure 3.7 Results of the cave air exchange model at Cave 9: (a) measurements and model predictions of near-wall air temperatures inside Cave 9, compared to measured outdoor air temperatures and measured cave wall temperatures supplied to the model. Model predictions of $T_{air,nw}$ are almost coincident with measured $T_{air,nw}$, (b) measurements and model predictions of air velocity through the ground level entrance to Cave 9. A positive velocity value indicates flow into the ground level entrance to Cave 9, while a negative velocity value indicates flow out of the ground level entrance at position 1 in Figure 3.1a.

is obtained from values of T_a predicted by the model by noting that the shape of the thermal boundary layer for turbulent natural convection flow along a vertical flat plate (see Eckert and Jackson, 1951) is approximately given by

$$T_{air,nw} = T_a + \left(T_w - T_a\right)\left(1 - (\frac{y}{\delta})^{\frac{1}{7}}\right) \tag{3.15}$$

where δ is the thickness of the boundary layer and y is the distance from the cave wall. The thickness of the boundary layer depends on distance, x, from the starting point of the boundary layer flow:

$$\delta = 0.565x(Gr)^{-\frac{1}{10}}(Pr)^{-\frac{8}{15}}[1 + 0.494(Pr)^{\frac{2}{3}}]^{\frac{1}{10}} \tag{3.16}$$

where Gr is the Grashof number

$$Gr = \frac{g\beta(T_w - T_a)x^3}{\nu^2} \tag{3.17}$$

and β is the expansion coefficient of the air which is estimated to equal ${T_a}^{-1}$ with T_a stated in degrees Kelvin. The distance x is taken to be the distance from the cave ceiling to the thermistor that measures $T_{air,nw}$ for flow down the wall and to be the distance from the cave floor to that thermistor for flow up the wall. Near-wall air temperatures predicted by the model based on outdoor air temperature and cave wall temperature data are graphed in Figure 3.7a. The mean of the absolute value of the paired one-minute average temperature differences between $T_{air,nw}$ predicted vs the smoothed $T_{air,nw}$ observations is 0.86^oC.

Figure 3.7b shows a comparison of measured and predicted air velocities at the ground level entrance of Cave 9. A positive air velocity indicates air flow into the cave through the ground level entrance, while a negative

velocity indicates flow out of the cave through the ground level entrance. In general, good agreement is obtained between the model predictions and the observations of the air flows through Cave 9. Peak flows are underpredicted to some degree. If either the heat transfer coefficient or the interior wall surface area were increased, almost exact agreement between predictions and observations could be achieved.

3.4.2 Cave 6

Cave 6 still retains a wooden temple building in front of the cave entrances. A model for the air flow through Cave 6 must therefore be more elaborate. The building shell is represented as a series of pressure loss terms that are added to the LHS of equation (3.3). Specifically, a pressure drop term is added to represent flow of air through the cracks around the wooden door panels that cover the temple structure at the third floor and fourth floor levels at positions 4 in Figure 3.1b. Another pressure drop term results from the flow of air through the ground floor level of the wooden building shell at position 1 in Figure 3.1b. The latter term varies depending on the time of the day: during the daytime the front doors are kept opened, while during the nighttime the doors are closed and air is forced to exit through the various cracks and openings around the doors and in the building shell. There are also small additional pressure drop terms that are due to the flow of air across the downstairs anteroom, and across the upstairs anterooms of Cave 6. The pressure drop terms due to flow across the upstairs and downstairs outer rooms were approximated as being due to flow of air in rectangular ducts that are the size of the anterooms formed by the wooden building, and were found to be at least two orders of magnitude lower than the other loss terms that occur due to the flow restrictions as air enters through cracks or openings in the building shell or as air passes through the narrow openings

in the cave rock wall. Therefore pressure drops due to flow through the anterooms will be ignored in subsequent calculations.

There are no reliable data for some of the geometric parameters for Cave 6. One such parameter is the area of the cracks and openings in the building shell on the third floor and fourth floor levels. In order to obtain a better estimate of that number, a modified version of equation (3.6) is used, written for the case of Cave 6, the equation is written for the case where the front doors at ground level are open, (i.e., during daytime):

$$C_L U_4^2 + C_L U_3^2 + C_L U_2^2 + C_L U_{1a}^2 = \frac{2gH|T_o - T_a|}{T_o} \qquad (3.18)$$

where the various subscripts are coordinated with the labels in Figure 3.1b, as follows: position 4 refers to the cracks and openings in the upstairs building shell, position 3 to the opening in the rock wall of the cave upstairs, and position 2 to the opening in the rock wall of the cave downstairs, while the subscript 1a signifies the condition at the downstairs front entrance doors to the wooden temple structure with these doors open. The cracks and openings in the upstairs building shell range from open door panels to rectangular slots between panels. Since all openings at positions 1-4 are rectangular, the same loss coefficient, C_L, as was cited previously for use with the rectangular entrance at Cave 9 will be applied to each flow restriction term. The many openings in the building shell at the third and fourth floor level at Cave 6 act in parallel and therefore experience the same pressure drop. If the loss coefficient is roughly the same for each of these openings, then the velocities through the openings in the building shell at the third and fourth floor levels will be similar, and one term will suffice in equation (3.18) to describe the product of the square of that velocity times the loss coefficient.

Using the continuity equation, all velocities in equation (3.18) can be expressed in terms of the velocity at the downstairs opening in the rock wall

of the cave, U_2, and the dimensions of the various openings in the air path where those velocities prevail. The velocity through the cracks upstairs, U_4, thus can be expressed as a function of U_2 and the as yet unknown area of the cracks upstairs, A_4. Spot measurements of the air velocity through the downstairs opening in the rock wall of Cave 6 (at position 2 in Figure 3.1b) were made periodically during these experiments using the hand-held mechanical velocity meter. Using measured values of U_2, T_a, and T_o taken at various hours during our experiments along with measured values of the size of the openings at positions 1a, 2, and 3 in Figure 3.1b, as shown in Table 3.1, equation (3.18) is used to estimate the area of the cracks and openings upstairs. Doing so gives a crossectional area of the cracks and openings upstairs $A_4 = 4.09\ m^2 \pm 2.09$, which is larger than the value of $A_4 = 1.75\ m^2$ that we estimated by visual inspection for cracks around the upper floor door panels while at Yungang. The reason for the discrepancy is simple. Our photographs show that some of the door panels at the third floor level ($A \approx 1.67\ m^2$ for each door panel) or one of the side doors ($A \approx 2.65\ m^2$) were frequently left open by persons passing through the temple structure thus increasing the effective cross sectional area of the openings at the third floor level during our month long experiments beyond the value that would be due to cracks between door panels. In the analysis above 2 occasions when so many doors were left open that A_4 exceeded 10 m^2 were not used in determining the typical value of A_4.

Another geometric parameter that has to be confirmed is the cross sectional area of the cracks in the downstairs building shell and around the downstairs door, when the door is closed. In order to examine the condition where flow is forced through the downstairs cracks in the building shell, the air flow that occurs in the throat of the lower level opening in the rock wall of Cave 6 at position 2 in Figure 3.1b, was measured first with the front doors open and

then with the front doors closed. Interpretation of the change in air flow as the doors are closed proceeds as follows. Equation (3.18) first is rewritten in a slightly modified form:

$$\Delta P = \frac{1}{2}\rho C_L Q^2 \left(\frac{1}{A_4^2} + \frac{1}{A_3^2} + \frac{1}{A_2^2} + \frac{1}{A_{1a}^2} \right) \tag{3.19}$$

where ΔP is the total pressure drop that can be supported for air flow through the building and through the cave temple's rock entrances due to density differences between air inside vs air outside of the caves, C_L is the loss coefficient, Q is the volumetric air flow rate, and ρ is the density of air. The subscript 1a refers to the condition with the downstairs wooden doors open. Equation (3.19) may be used to calculate the available pressure drop at any point in time with the front doors open if the volumetric air flow rate, Q, based on the mechanical air velocity meter readings is known along with each of the cross sectional areas. Once ΔP is determined, the last term on the RHS of equation (3.19) can be replaced by a term that is based on the crack areas in the downstairs building shell and around the front doors with the front door closed, A_{1b}, that we estimated by inspection while at Yungang and that is given in Table 3.1. Then using the previously calculated pressure drop that can be supported by the indoor versus outdoor air density differences, a new volumetric air flow rate Q (or, equivalently, the velocity at the opening in the rock wall of the cave downstairs at position 2 in Figure 3.1b) is calculated that should prevail when the downstairs doors are closed. That calculated value of the air velocity predicted to prevail through the downstairs opening in the cave rock wall then can be compared to the measured value of the velocity at that location when the doors are closed. The predicted and measured velocities compared very well over 37 separate experiments at different times during which flow measurements were made

both with the downstairs doors open and closed (regression of the measured velocity on the predicted velocity results in a slope of 1.02 $\pm$ 0.07, an intercept of $-0.03 \pm 0.01\ m\ s^{-1}$ and a correlation coefficient of 0.92). This suggests that the original estimates of the cross sectional areas of the cracks downstairs when the front door is closed (parameter A_{1b}) that we made while at Yungang were fairly accurate (the wall panels in the ground floor level of the wooden building are fixed in place and cannot be left open as is the case upstairs).

The numerical model for air flow through Cave 9 was modified to correspond to the geometric parameters given for Cave 6 in Table 3.1 and to represent the additional pressure drops present at Cave 6. Then the time series of outdoor temperatures and cave wall temperatures was supplied to the model in order to calculate the air temperature expected inside Cave 6 and the air flows through Cave 6. Again, the product of the heat transfer coefficient times the vertical wall surface area was taken to be twice as large as that estimated from examining the major outline of the cave walls, just as was done for Cave 9. From 0700 hours each morning until 2000 hours each evening, when Cave 6 is open to visitors or staff, flows were calculated with the downstairs entry doors open, while from 2000 hours each evening until 0700 hours in the morning, air flows were calculated with the downstairs doors closed.

Figure 3.8a shows the near-wall air temperature predictions inside Cave 6 together with the measured indoor near-wall air temperature in Cave 6 compared to outdoor air temperatures and cave wall temperatures supplied to the model. The same general conclusions hold true for Cave 6 as were observed for Cave 9. Reasonable agreement is evident between the measured and predicted near-wall air temperature values inside Cave 6. The mean of the absolute differences between $T_{air,nw}$ predicted and observed is 0.59 ^oC,

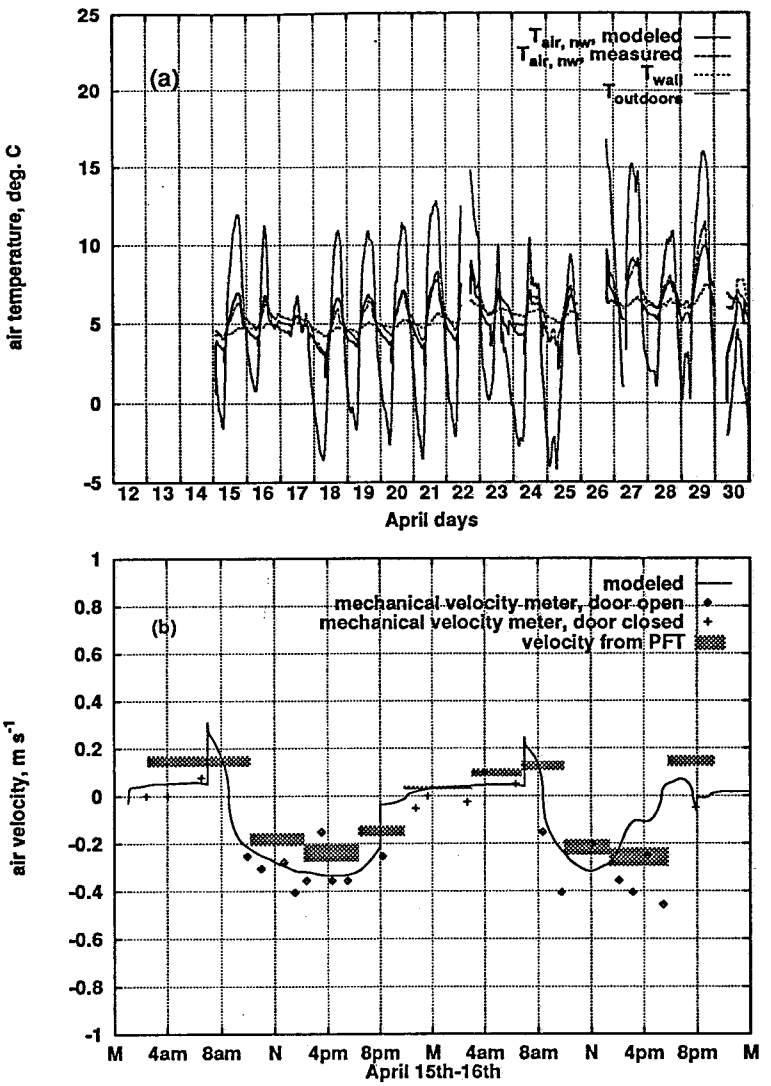

Figure 3.8 Results of the cave air exchange model at Cave 6: (a) measurements and model predictions of near-wall air temperatures inside Cave 6 compared to measured outdoor air temperatures and measured cave wall temperatures supplied to the model. Model predictions of $T_{air,nw}$ are almost coincident with measured $T_{air,nw}$, (b) measurements and model predictions of air velocity in the ground level passage through the rock wall of Cave 6 at position 2 shown in Figure 3.1b, on April 15-16, 1991. A positive velocity value indicates flow into the ground level entrance to Cave 6, while a negative velocity value indicates flow out of the ground level entrance at position 2 in Figure 3.1b. The main front doors to the temple are modeled as being open during the day and closed at night.

in spite of the fact that the strip chart recorder that recorded temperature values for the cave wall and $T_{wall} - T_{air,nw}$ can be read no more closely than $\pm 0.5^{o}C$. Figure 3.8b shows the predicted air velocity at the ground level passage through the rock wall between the antechamber and the interior chamber of Cave 6 at position 2 in Figure 3.1b, together with velocity measurements taken during April 15-16, 1991 using the mechanical air velocity meter at the same location. Velocities calculated at that location from the results of the short-term perfluorocarbon tracer tube (PFT) experiment also are shown. Again, a positive velocity is assigned for air flow into the cave at position 2, Figure 3.1b, while a negative velocity indicates air flow out of the cave at ground level. There is general agreement between the model predictions and the air flow measurements, with the model predictions falling between the results of the PFT and mechanical velocity meter readings. The model calculations find that the air flow through Cave 6 averaged 5940 $m^3\ hr^{-1}$ or 99 $m^3\ min^{-1}$ over the April 15-16, 1991 period. This corresponds to one complete air exchange at Cave 6 every 22 minutes on average during the April 15-16 period modeled in Figure 3.8b, which is a lower air exchange rate than the long-term average air exchange rate observed for the whole month as described earlier.

3.5 Conclusions

During an extensive monitoring program that took place in April, 1991, temperatures, air velocities, and air exchange rates were measured at Caves 6 and 9 at Yungang in order to establish baseline parameters necessary for modeling the air flow that carries air pollutant particles into and out of the caves.

Temperature measurements showed that in general the outdoor air is warmer

than the indoor cave wall surfaces during the day but colder during the nighttime. The temperature of the air inside the caves was found to lie between that of the outdoor air and the temperature of the surface of the cave walls.

Air exchange into and out of the caves followed a diurnal pattern based on temperature differences between the outdoor air and the cave walls. Between approximately 0930 hours in the morning until approximately 2100 hours at night, air flows into the caves through the rock opening that exists at the third floor level and out of the caves through the entrance to the caves that exists at ground level, while late at night and in the early morning hours the direction of flow reverses. This air circulation pattern indicates that the caves act as a giant thermal siphon: during the day, warm outdoor air enters the upper level entrances to the caves; that air is cooled by natural convection along the cooler cave walls; the air temperature inside the caves drops to below that outdoors; a pressure difference due to the resulting density difference between the indoor vs outdoor air develops that drives the cooler air inside the caves out of the lower level entrances to the caves. At night, the outdoor air is cooler than the cave walls, air enters the lower level entrances to the caves, is warmed by natural convection and exits through the upper level openings in the cave walls. An air velocity probe placed inside the fluid mechanical boundary layer that exists along the wall of Cave 9 showed that the magnitude of the air speed within that boundary layer tracked changes in the wall/air temperature difference, confirming that a natural convection flow exists. Measurements of outdoor wind speed and direction were compared to simultaneous measurements of air velocities through the ground level entrance of Cave 9. It appears that outdoor wind had little influence on the air velocity and direction at the entrance of that cave. The average

volumetric flow rate of air through Cave 9 during April 1991 as calculated from an air velocity probe placed at the ground level entrance to that cave agrees well with data taken using perfluorocarbon tracers (7300 $m^3\ hr^{-1}$ and 8190 $\pm$ 1240 $m^3\ hr^{-1}$ respectively). Perfluorocarbon tracers show that the volumetric air flow rate through Cave 6 during April 1991 averaged 8620 $\pm$ 1480 $m^3\ hr^{-1}$. Since the volume of Cave 6 is approximately four times larger than Cave 9, rough equality of volumetric air flow rates means that the time to achieve one complete air exchange in Cave 6 during April is about four times longer than Cave 9 on average.

Air exchange rates affect particle deposition rates by altering the number of particles entering the caves over time (Nazaroff and Cass, 1991). Air exchange rates also affect the rate at which water vapor (arising from water seepage through the cave rock surface, which damages the sculptures) can be exhausted from the caves. An ability to compute air exchange rates and how they respond to changes in meteorological conditions and to changes in the way that the structures in front of some caves are operated thus is of major importance to future efforts to conserve the Grottoes. A computer-based model has been developed that takes as input cave dimensions, outdoor air temperatures, and indoor cave wall temperatures and that predicts indoor air temperatures and air flows into and out of the caves according to the cooling of the air within the caves that is predicted to occur due to natural convection heat transfer along the cave walls. The model has the capability of accepting as further input resistances to air flow that would arise if filter material were installed in the surface of an existing or reconstructed wooden shelter in front of a cave in order to remove particulate matter from the air. Data that were gathered during the April, 1991 experiments were used for verification of the model. The results show good agreement between observed

versus predicted air flows and air temperatures, both in the case of Cave 9 (a cave without extra flow resistances), and Cave 6 (a cave that has extra flow resistances in the form of the wooden temple structure that stands over the entrances to that cave.)

3.6 References

Churchill, S.W., and Chu, H.H.S. (1975) Correlating equations for laminar and turbulent free convection from a vertical plate. *Int. J. Heat Mass Transfer* **18**, 1323-1329.

Dietz, R.N. and Cote, E.A. (1982) Air infiltration measurements in a home using a convenient perfluorocarbon tracer technique. *Environ. Int.* **8**, 419-433.

Harris, E.J. and Kingery, D.S. (1973) Ventilation, in *SME Mining Engineers Handbook* (Ed. I. A. Given), Port City Press, Baltimore, Maryland.

Incropera, F.P. and DeWitt, D.P. (1985) *Fundamentals of Heat and Mass Transfer,* Wiley, New York, Chapter 9.

Jennings, B.H. and Lewis, S.R. (1965) *Air Conditioning and Refrigeration,* 4th ed., International Textbook Company, Scranton, Pennsylvania, Chapter 12.

Nazaroff, W.W. and Cass, G.R. (1991) Protecting museum collections from soiling due to deposition of airborne particles. *Atmospheric Environment* **25A**, 841-852.

Moore, G. W. (1978) *Speleology: the study of caves*, Zephyrus Press, Teaneck, New Jersey.

Quindos, L.S., Bonet, A., Diaz-Caneja, N., Fernandez, L.P., Gutierrez, I., Solana, R.J., Soto, J., and Villar, E. (1987) Study of the environmental variables affecting the natural preservation of the Altamira cave paintings located at Santillana Del Mar, Spain. *Atmospheric Environment* **21**, 551-560.

Sabersky, R.H., Acosta, A.J., and Hauptmann, E.G. (1989) *Fluid Flow, A First Course in Fluid Mechanics*, 3rd ed., Macmillan, New York, Chapter 3.

Wigley, T.M.L. (1967) Non-steady flow through a porous medium and cave breathing. *J. Geophys. Res.* **72**, 3199-3205.

Wigley, T.M.L. and Brown, M.C. (1976) The physics of caves, in *The Science of Speleology* (Ed. T. D. Ford and C. H. D. Cullingford). Academic Press, New York.

Wilkening, H.M. and Watkins, D.E. (1976) Air exchange and ^{222}Rn concentrations in the Carlsbad caverns. *Health Physics* **31**, 139-145.

Chapter 4. Fate of Atmospheric Particles Within the Buddhist Cave Temples at Yungang, China

4.1 Introduction

From the year-long monitoring program conducted during 1991/92 described in Chapter 2 and in Salmon et al. (1994) the following background information can be provided:

(a) The outdoor airborne particle concentrations at Yungang are very high. Annual average coarse (diameter, $d_p > 2.1\ \mu m$) particle concentrations outdoors during 1991-92 averaged 378 $\mu g\ m^{-3}$, increasing to more than 1200 $\mu g\ m^{-3}$ during peak 24-hour sampling periods while fine airborne particle concentrations ($d_p \leq 2.1\ \mu m$) outdoors averaged 130 $\mu g\ m^{-3}$ (Salmon et al., 1994).

(b) The largest contributors to the coarse airborne particles include crustal dust (e.g., soil dust) accounting for over 80% of the coarse particle mass, and carbon-containing particles (10% of coarse mass). The fine particles outdoors consist of carbon-containing particles (45.5%) followed in importance by crustal dust (24%) (Salmon et al., 1994).

(c) The outdoor particles are transferred to the inside of the caves by a natural convection flow (see Chapter 3). As seen in Figure 4.1, the largest caves at Yungang contain two entrances through the stone cliff face, one at ground level and a second at about the third floor level. During the middle of the day, the outdoor air is warmer than the cave walls. As a result air enters the caves through the upper windows in the cliff face, cools as it flows down the colder interior cave walls and then exits through the ground level entrance to the cave. At night, the reverse happens: cold outdoor air flows into the caves through

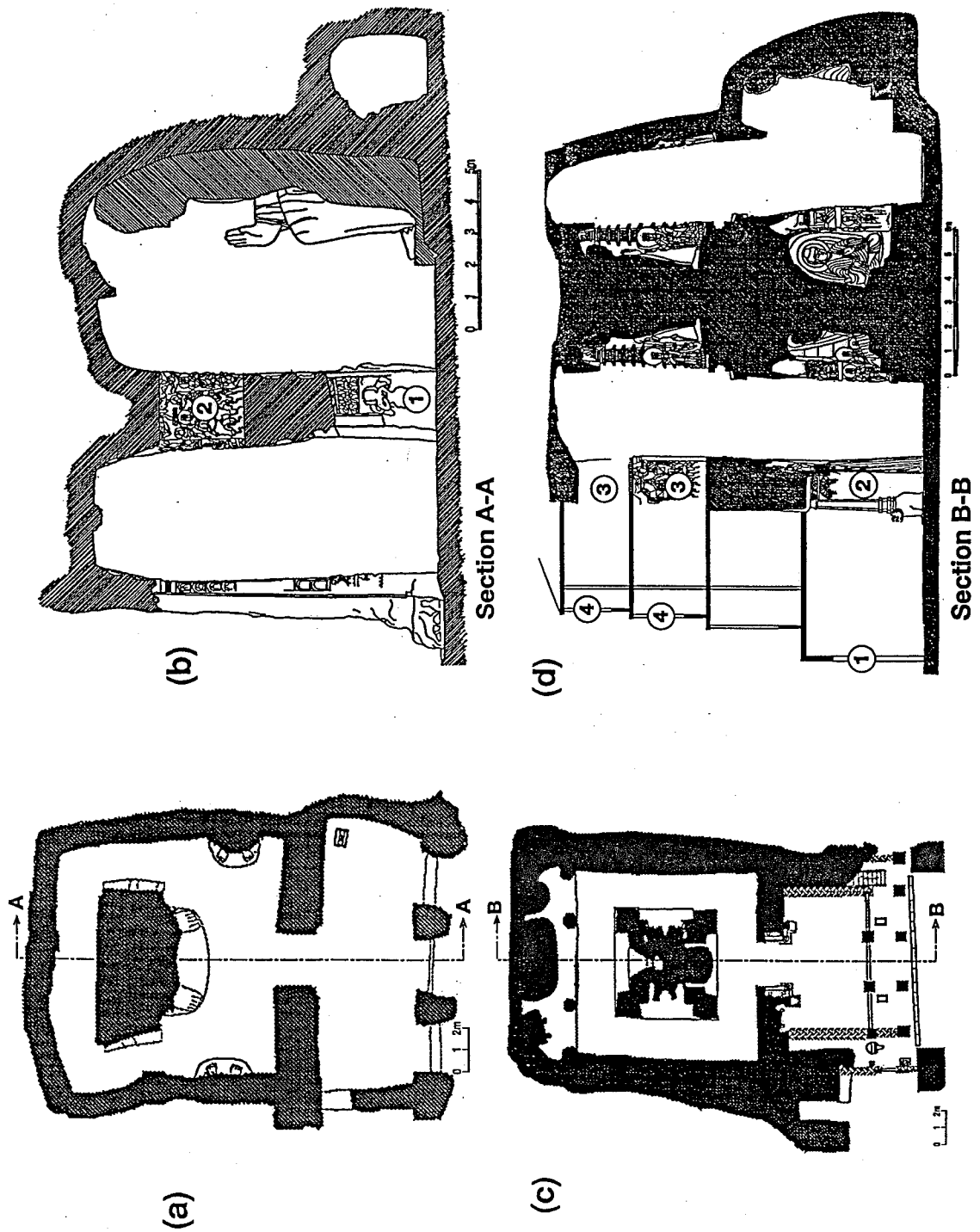

Figure 4.1 Section drawings of Cave 9 (a,b) and Cave 6 (c,d).

the ground floor entrance, flows up the warmer walls, and out of the caves through the opening in the rock face of the cliff at about the third floor level.

(d) Once inside the caves, the airborne particles deposit onto the various horizontal and vertical surfaces. For example, measurements show that over the 5 year period from 1986 to 1991, particle deposits as deep as 0.8 cm accumulated on the sculptures within Cave 9 at Yungang (Christoforou et al., 1994).

In order to test the design of systems that will control this particle deposition problem, a quantitative description of the cause and effect relationships that translate outdoor particle concentrations into the observed deposition flux is needed.

In this chapter a computer-based mathematical model will be formulated that links the outdoor particle concentration and size distribution and the air flow through the caves to the indoor particle concentration and size distribution. The particle flux to interior surfaces will be simulated along with the determination of the rate of surface coverage by depositing particles. The model will be tested using detailed measurements of the time series of outdoor particle size distributions and indoor particle concentrations and deposition fluxes within Caves 6 and 9 at Yungang during April 1991.

Once verified, this model can be used to study the effect of proposed particle filtration and control systems for the caves in advance of their adoption.

4.2 Model formulation

The airborne particle deposition model for the Yungang Grottoes is constructed by combining the features of an existing model for indoor aerosol

mechanics and particle deposition in buildings with a fluid mechanical model for the natural convection-driven air exchange between the outdoors and the cave interior.

The model for the air exchange between the interior of the caves and the outdoors is based on the description of Christoforou et al. (1995) (see Chapter 3). A natural convection flow is driven by wall and air temperature differences. When warm air flows into a cave like Cave 9 at Yungang, it enters through the upper level window in the rock wall at position 2 in Figure 4.1b. The air is cooled as it flows down the cave walls; cool air accumulates in the cave and then flows out of the ground level entrance to the cave at position 1 in Figure 4.1b. Three equations can be written that describe the simultaneous convection and heat transfer problem at Cave 9.

$$\frac{d}{dt}(\rho_a V) = \rho_o U_2 A_2 - \rho_a U_1 A_1 \tag{4.1}$$

$$\frac{d}{dt}(\rho_a V c_v T_a) = \rho_o U_2 A_2 c_p T_o - \rho_a U_1 A_1 c_p T_a - \sum_{i=1}^{3} h_i S_i (T_a - T_w) \tag{4.2}$$

$$\frac{1}{2}\rho_o U_2^2 C_L + \frac{1}{2}\rho_a U_1^2 C_L = gH(\rho_a - \rho_o) \tag{4.3}$$

where ρ_a is the mass density of air inside the cave, ρ_o is the mass density of air outside the cave, V is the volume of the cave, U_1 and U_2 are the air velocities through the openings in the rock wall between the outdoors and the inside of the cave at positions 1 and 2 in Figure 4.1b, respectively, T_a and T_o are the temperatures of the air inside the cave and the air outdoors, respectively, T_w is the temperature of the cave walls, c_p is the specific heat of air measured at constant pressure, c_v is the specific heat of air measured at constant volume, A_1 and A_2 are the cross sectional areas of the openings through the rock wall at positions 1 and 2 in Figure 4.1b, h_i is the heat transfer coefficient

for flow over the ith surface inside the cave, S_i is the surface area of the ith surface inside the cave, C_L is the loss coefficient for flow through the rectangular openings in the rock wall at positions 1 and 2 in Figure 4.1b, H is the elevation difference between the critical fluid streamline along which motion starts as air enters and leaves the cave, and g is the acceleration due to gravity. Equations (4.1), (4.2), and (4.3) above describe continuity, energy conservation, and the balance between the pressure drops in the air path versus density differences acting on the height of the air column between the entering and exiting air paths, respectively.

This system of equations is then simplified by assuming that $\rho_a \approx \rho_o \approx \rho$ except that $\frac{\rho_a - \rho_o}{\rho_o} \neq 0$, and also $\frac{\rho_a - \rho_o}{\rho_o} \approx \frac{T_o - T_a}{T_o}$, so that equations (4.1)-(4.3) become:

$$U_1 A_1 = U_2 A_2 \tag{4.4}$$

$$\rho V c_v \frac{d}{dt}(T_a) = \rho c_p \left(U_2 A_2 T_o - U_1 A_1 T_a\right) - \sum_{i=1}^{3} h_i S_i (T_a - T_w) \tag{4.5}$$

$$U_1^2 + U_2^2 = \frac{2gH}{C_L} \frac{|T_o - T_a|}{T_o} \tag{4.6}$$

An analogous set of equations can be written for the case where cold air enters at ground level and flows up the warmer walls of the cave. Equations (4.4)-(4.6) may be solved for the unknown air velocities through the openings into Cave 9, U_1 and U_2, as well as the indoor air temperature, T_a, within the cave, which are the unknown parameters in this problem. Once either U_1 or U_2 is known as a function of time, the air flow through the cave is known.

In the case of a cave like Cave 6 which still retains the wooden structure in front of the cave entrance, the additional pressure drops that occur as air flows through the doors and cracks in the wooden building must be simulated.

The incorporation of such added pressure drops to the system of equations (4.4)-(4.6) is as described in Chapter 3, section 3.4.2.

Solution of equations (4.4)-(4.6) requires that the heat transfer coefficients, for air flow over the various interior surfaces of the cave, the h_i in equation (4.5), must be estimated. Natural convection heat transfer coefficients used to represent flow over the vertical walls of the caves, the cave ceiling and the cave floor are given in Table 4.1. These heat transfer coefficients were derived for flow over flat plates, but the walls of the cave are not flat. Instead they are carved in high relief. As a result the walls contain more surface area than the superficial dimensions of the walls would indicate. The walls also contain roughness elements that will interrupt the natural convection boundary layer flow, thereby increasing heat transfer rates. To compensate for the added surface roughness and surface area, a semi-empirical adjustment to the model was developed and tested (see Chapter 3): the product $h_1 S_1$ appearing in equation (4.5) which quantifies heat transfer rates for flow over the vertical walls of the cave was taken to be twice as large as would be the case for a vertical flat plate having the nominal surface area of the major outline of the cave walls.

4.2.1 Particle deposition model

The model for particle deposition onto surfaces within the caves follows the formulation of Nazaroff and Cass (1989a). The interior of each cave is represented as a single chamber having a well-mixed core. The aerosol within the cave is represented by the multicomponent sectional formulation of Gelbard and Seinfeld (1980). The particle size distribution is divided into 22 consecutive bins that cover the range from 0.05 μm to 149.7 μm in diameter. Particles of each size may be composed of many different chemical components, but all particles of the same size have the same relative composition

Table 4.1 Natural convection heat transfer relationships used by the transport algorithm of the particle deposition model

Surface	Nusselt number[a]	Condition	Ref.
Vertical walls	$\overline{Nu_Z} = \left(0.825 + \frac{0.387 Ra_Z^{\frac{1}{6}}}{[1+(0.492/Pr)^{9/16}]^{8/27}}\right)^2$	$10^{-1} < Ra_Z < 10^{12}$	(b)
Horizontal upward facing heated or downward facing cooled surface	$\overline{Nu_L} = 0.54 Ra_L^{\frac{1}{4}}$	$10^4 < Ra_L < 10^7$	(c)
	$\overline{Nu_L} = 0.15 Ra_L^{\frac{1}{3}}$	$10^7 < Ra_L < 10^{11}$	(c)
Horizontal upward facing cooled or downward facing heated surface	$\overline{Nu_L} = 0.27 Ra_L^{0.25}$	$10^5 < Ra_L < 1.4 \times 10^{10}$	(c)

(a) $\overline{Nu_Z} = \frac{Zh_i}{k}$ is the Nusselt number based on the height of the cave walls, Z, the heat transfer coefficient, h_i, along the ith surface and the thermal conductivity of air, k.
$\overline{Nu_L} = \frac{Lh_i}{k}$ is the Nusselt number based on a characteristic dimension, L, that is computed as the area of the surface divided by the perimeter of the surface.
Ra_Z is the Rayleigh number based on the height of the cave walls. $Ra_Z = Pr\frac{g(T_w - T_a)Z^3}{T_a \nu^2}$, where Pr is the Prandtl number for air, g is the acceleration due to gravity, ν is the kinematic viscosity of air, T_w is the cave surface temperature and T_a is the air temperature in the cave.
Ra_L is the Rayleigh number based on the characteristic length, L, that is computed as the area of the surface divided by its perimeter.

(b) From Churchill and Chu (1975).

(c) From Incropera and DeWitt (1985).

(i.e. the aerosol is assumed to be internally mixed). The aerosol mass concentration within each size section is assumed to be uniformly distributed with respect to the logarithm of the diameter of the particles. The rate of change of the aerosol mass concentration for each component within each size section is governed by the following differential equation:

$$\frac{d}{dt}C_{mjk} = S_{mjk} - L_{mjk}C_{mjk} \tag{4.7}$$

where C_{mjk} represents the mass concentration of chemical component k in particle size section j within chamber m of the model; S_{mjk} is the sum of all sources of component k in particle size j within chamber m, and L_{mjk} is the sum of all losses of component k in particle size j within chamber m. Sources, S_{mjk}, include all processes that add to the particle concentration in a size section: direct emissions of particles within the cave, advection of particles into the cave from outdoors and coagulation of smaller particles to form larger particles. Particle losses, L_{mjk}, include deposition of particles onto surfaces, removal of particles from the caves by the natural convection flow that exits the cave, and loss of particles to larger sizes by coagulation. These sources and sinks vary over time.

While the model has the ability to handle coagulation calculations, that feature is not used during the present simulations because the fine particle concentrations are not high enough to cause that process to have important effects on the calculated aerosol size distribution. Therefore, when a cave is represented by a single chamber model as it is affected by advection of air through the caves, indoor sources, and particle deposition, equation (4.7) becomes

$$V\frac{d}{dt}(C_{ajk}) = C_{ojk}f_{oa} + E_{ajk} - C_{ajk}\sum_i S_i v_{d_{ijk}} - C_{ajk}f_{oa} \qquad (4.8)$$

where C_{ajk} and C_{ojk} are the concentrations of chemical component k in particles of size j in air inside (a) or outside (o) the cave, respectively, f_{oa} is the volumetric flux of air flowing from outside to inside the cave (flow in = flow out in this case), E_{ajk} is the emission of new particles of composition k and size j due to activities within the cave, S_i is the surface area of the ith surface and $v_{d_{ijk}}$ is the deposition velocity for particles containing component k in size j to the ith surface within the cave. In the present model application, particle emissions within the cave will be taken to be zero since the caves were unoccupied during the experiments related here. In the future if visitors to the caves introduce a new source of particles within the caves, then the model can be readily adapted to study that situation.

Particle deposition from the atmosphere inside the caves to horizontal and vertical surfaces in the caves is calculated for the relevant air flow regimes along the interior surfaces, including deposition of particles from the turbulent natural convection flows along the walls, as well as deposition to horizontal surfaces by both gravitational sedimentation and convective diffusion. The relationships used for computing these deposition velocities are given in Tables 4.2a and 4.2b. The deposition velocity due to gravitational sedimentation used in the present work is corrected using an appropriate shape factor to account for the irregular shape of the coarse mineral dust particles encountered (Davies, 1979).

The mean particle deposition velocity to vertical surfaces depends on particle transport in the atmospheric boundary layer near the wall. Two cases are distinguished, namely, laminar or turbulent natural convection induced by

Table 4.2a Particle deposition velocities, v_d, if induced by homogeneous turbulence in the air in the core of the cave

Surface	deposition velocity	conditions
all	$v_d = v_{CP} + v_t$	all
all	$v_t = -N_t \nu \frac{(K_e/\alpha)^{1/2}}{\tan^{-1}(\delta(K_e/\alpha)^{1/2})}$	all[a]
vertical	$v_{CP} = \frac{2}{\pi}(DK_e)^{1/2}$	b
downward facing	$v_{CP} = \frac{v_g}{exp\left(\frac{\pi v_g}{2(DK_e)^{1/2}}\right)-1}$	b
upward facing	$v_{CP} = \frac{v_g}{1-exp\left(\frac{-\pi v_g}{2(DK_e)^{1/2}}\right)}$	b

In the equations above, v_{CP} is the deposition velocity according to Corner and Pendlebury (1951), v_t is the thermophoretic velocity of particles, $N_t = K(\Delta T/T_\infty)$ is the thermophoresis parameter, ΔT is the temperature difference between the surface temperature and the temperature of air outside the boundary layer, T_∞, K_e is the turbulence intensity parameter, K is the thermophoresis coefficient (Nazaroff and Cass, 1987), D is the coefficient of Brownian diffusivity of particles, and v_g is the gravitational settling velocity.

[a] In the expression for deposition velocity, δ is the boundary layer thickness given approximately by $\delta \sim (1.2)(\nu/K_e)^{4/9} x_s^{1/9}$, where x_s is the length of the surface in the direction of flow (Nazaroff and Cass, 1989), and ν is the kinematic viscosity of air.

[b] For very small particles, v_{CP} to a surface having any orientation is more accurately given by the expression $v_{CP} = (DK_e)^{1/2}/[tan^{-1}[\delta(K_e/D)^{1/2}]]$, where δ is given in a above. For a particle to be sufficiently small for this expression to be appropriate, it must satisfy $D \geq 0.01\nu^{8/9} K_e^{1/9} x_s^{2/9}$. A typical set of conditions has $K_e = 0.1\ s^{-1}$ and $x_s = 1\ m$, for which the inequality becomes $D \geq 0.004\ cm^2\ s^{-1}$, i.e., that the particle must be smaller than 0.004 μm in diameter.

Table 4.2b Particle deposition velocities, v_d, for deposition from natural convection flows

Surface	deposition velocity	conditions
vertical	$v_d = \frac{4}{3}(g\lvert\Delta T\rvert/4\nu^2 T_\infty)^{1/4}\alpha^{1/3}D^{2/3}H^{-1/4}[\omega'(0)/Le^{1/3}]$	$Ra_H < 10^9$
	v_d = maximum of $\frac{4}{3}(g\lvert\Delta T\rvert/4\nu^2 T_\infty)^{1/4}\alpha^{1/3}D^{2/3}H^{-1/4}[\omega'(0)/Le^{1/3}]$ or $v_t + \frac{D}{H}\{0.825 + \frac{0.387 Ra_H^{\frac{1}{6}}}{[1+(0.492/Sc)^{9/16}]^{8/27}})^2\}$; where $v_t = -N_t\frac{\nu}{H}\{0.825 + \frac{0.387 Ra_H^{\frac{1}{6}}}{[1+(0.492/Pr)^{9/16}]^{8/27}})^2\}$;	$10^9 < Ra_H < 10^{12}$
horizontal upward-facing heated or downward-facing cooled surface	$v_d = s_g v_g - N_t\frac{\nu}{L}(0.54 Ra_L^{1/4}) + \frac{D}{L}(0.54 Ra_L^{1/4})$	$v_d \geq 0; 10^4 < Ra_L < 10^7$
	$v_d = s_g v_g - N_t\frac{\nu}{L}(0.15 Ra_L^{1/3}) + \frac{D}{L}(0.15 Ra_L^{1/3})$	$v_d \geq 0; 10^7 < Ra_L < 10^{11}$
horizontal upward-facing cooled or downward-facing heated surface	$v_d = s_g v_g - N_t\frac{\nu}{L}(0.27 Ra_L^{1/4}) + \frac{D}{L}(0.27 Ra_L^{1/4})$	$v_d \geq 0; 10^5 < Ra_L < 10^{10}$

In the equations above, v_d is the deposition velocity, g is the acceleration due to gravity, ΔT is the temperature difference between the surface temperature and the temperature of air outside the boundary layer, T_∞, ν is the kinematic viscosity of air, α is the thermal diffusivity of air, D is the coefficient of Brownian diffusivity of particles, H is the height of the cave, $\omega'(0)$ is the slope of normalized particle concentration at surface (Nazaroff and Cass, 1987), Le is the particle Lewis number, α/D, v_t is the thermophoretic velocity of particles, Ra is the Rayleigh number, Sc is the particle Schmidt number, ν/D, $N_t = K(\Delta T/T_\infty)$ is the thermophoresis parameter, K is the thermophoresis coefficient (Nazaroff and Cass, 1987), v_g is the gravitational settling velocity, s_g is an orientation coefficient, 1 for upward-facing and -1 for downward-facing, and L is a characteristic dimension of the surface: area divided by perimeter.

the wall-air temperature difference, and homogeneous turbulence induced by air movement in the core of the cave. The equations used for the former case arise from analogies between heat and mass transfer results and are fully described by Nazaroff and Cass (1987 and 1989ab). The equations used in the latter case are based on the work by Corner and Pendlebury (1951). Both cases are discussed more fully elsewhere (Nazaroff and Cass, 1989ab). As was the case with the natural convection heat transfer calculations to the vertical walls of the caves described earlier, a semi-empirical correction was applied to the particle deposition calculations that accounts for the added surface area of the vertical cave walls due to the carvings that are present. The product of the deposition velocity times the surface area of the vertical walls was taken to be twice that estimated for deposition to a flat surface having an area equal to that computed from the major outline of the cave walls. This increase in effective surface area is based on detailed examination of photographs of the cave walls showing the degree of surface modulation provided by the carvings.

Inputs required for use of the model defined by equations (4.4)-(4.6) and (4.8) are: (1) the particle size distribution and concentration in the outdoor air, as well as the initial particle size distribution and concentration inside the caves; (2) wall and air temperature data from which are calculated (a) the air flow into the caves by natural convection and (b) the deposition velocities of particles from natural convection flows along the walls; (3) an estimate of the turbulence intensity levels inside the caves as well as the thermophoresis coefficient for the particles (see Nazaroff and Cass, 1989ab), and (4) the geometry and size of the caves. Measured air flows into and out of the caves can be substituted for the flows predicted by equations (4.4)-(4.6) if desired. Outputs from the model include: (1) the aerosol size

distribution and concentration inside the caves, and (2) particle deposition rates as a function of particle size to walls, floors, ceilings and other horizontal or vertical surfaces inside the caves, from which mass fluxes and the rate of surface coverage by deposited particles can be calculated.

4.3 Experimental program

During April 1991, an experimental program was conducted at Yungang to gather data needed for evaluation of the present model for particle deposition in the caves. The experiment extended over two days with samples taken over consecutive four hour intensive sampling periods. The experiment began at 0200 hours on April 15, and lasted until 2200 hours on April 16. During this period the following measurements were made:

Outdoor and indoor airborne particle concentrations and size distributions. Ambient aerosol samples were taken over consecutive 4-hr sampling periods both outdoors and inside Caves 9 and 6 by drawing air at a rate of 3 $l\ min^{-1}$ through 47 mm diameter Millipore filters (0.22 μm pore size, membrane filter GSWP047 00) secured in open-faced filter holders, thus ensuring collection of both large and small particles. Subsequent automated optical microscopy analysis (Christoforou et al., 1994) yielded size distributions of the particles suspended in the air. This method was used to measure the size distribution of coarse airborne particles both inside and outside the caves over the diameter, d_p, range 2 $\mu m < d_p < 148\ \mu m$. The outdoor size distribution of fine particles over the size range 0.05 $\mu m < d_p < 2.3\ \mu m$ was obtained using a 32-channel Particle Measuring Systems model ASASP laser optical particle counter (OPC). Gravimetric determination of aerosol mass concentration, both outdoors and within the caves over each 4-hr sampling period, was obtained with the use of samples collected on Teflon membrane

filters (Gelman Teflo, 0.5 μm pore size) through which air was drawn at a rate of 10 $l\ min^{-1}$ each. Fine particle samples were collected on a Teflon filter located downstream of an AIHL-design cyclone separator that removed particles with aerodynamic diameter greater than 2.1 μm (Salmon et al., 1994), while total aerosol samples were collected simultaneously on an open-faced Teflon filter. The Teflon filters were weighed before and after sampling for gravimetric determination of aerosol mass concentration. Coarse particle concentrations were determined by difference between the total particle minus fine particle concentrations.

Indoor particle deposition flux onto both vertical and horizontal surfaces. Millipore filters (47 mm in diameter, 0.22 μm pore size, membrane filter GSWP047 00) were used as a surrogate surface for the collection of particles that deposited onto horizontal surfaces, while particles that deposited onto vertical surfaces were collected on microscope glass slides (75mm by 25mm by 1mm thick). The vertical collection plates within Caves 9 and 6 were fastened to the surface of a large aluminum plate which was then secured on the cave wall in order to achieve thermal contact with the wall surface. The horizontal deposition plates were placed on top of platforms at a height of about 1 m above ground level. A pair of horizontal collection plates were exposed for each of the consecutive 4-hour sampling periods on April 15-16, while a single set of vertical deposition plates was continuously exposed for the 19-day period from April 12 until April 30 because of the great difference in deposition rates between horizontal and vertical surfaces (Ligocki et al., 1990). Again, the deposited coarse particle size distribution was obtained by automated optical microscopy analysis by the methods of Christoforou et al., (1994).

Temperature data. Wall and air temperatures were measured by thermistor arrays that were placed inside Cave 6 and Cave 9 at Yungang. The wall thermistors (part no. 44202, Yellow Springs Instrument Co., Yellow Springs, OH) were secured in wall cracks using a thermal joint compound in order to ensure proper thermal contact with the wall. The air temperature thermistors were placed 5.1 cm away from the wall. Signal conditioning circuits transformed the thermistors' output into a voltage that was proportional to the temperature. Data were recorded every minute with the aid of a Campbell Scientific CR-10 measurement and control module (Campbell Scientific Inc., Logan, UT), with the exception of Cave 6 data, which were recorded using a strip chart recorder. The outdoor air temperature was measured at a weather station operated by the Chinese government at Yungang and the data were logged on a paper chart recorder.

Air exchange rates. In the case of Cave 9, air exchange rates were measured with the aid of an omnidirectional velocity probe (TSI model 1620) placed in the center of the ground level entrance of the cave. Data were again recorded every minute using the CR-10 data logger. A hand-held mechanical air velocity meter (vaneometer, part no. 6610A4306, Whatman Labs, Hillsboro, OR) was also used at regular intervals to measure air speed and direction in the ground level entrance to Cave 9. That information on the direction of air flow was used to assign the direction of flow to data taken continuously via the TSI omnidirectional velocity probe.

Air exchange rates through the entrance to Cave 6 were measured using the mechanical air velocity meter, and also using perfluorocarbon tracers (Dietz and Cote, 1982). Tracer sources that emitted perfluorocarbons at a slow but constant rate were placed at selected locations inside the cave. Tracer collection tubes were exposed over consecutive 4-hour periods and then were

analyzed to give the total air infiltration rate through the cave ($m^3\ hr^{-1}$) as a function of time. Analysis of the tracer samples taken was performed by the Brookhaven National Laboratory staff.

4.4 Model evaluation

The field experimental data for the April 15-16 period at Yungang were matched to the particle deposition model. Air flows and particle deposition fluxes within both Cave 6 and Cave 9 were computed starting from the cave dimensions given in Table 4.3 and the time series of measured outdoor particle size distributions plus data on the time series of the outdoor air temperatures, T_o, in equations (4.5) and (4.6), and the indoor cave wall temperatures, T_w, in equation (4.5). Air flow through Cave 6, which retains a wooden temple structure in front of its entrances, is modeled with the main ground level doors to that wooden structure open during the day but closed at night, as described in detail by Christoforou et al. (1995). The outdoor airborne coarse particle concentration ($d_p > 2\ \mu m$) and outdoor airborne fine particle concentration ($d_p < 2\ \mu m$) data supplied to the model are illustrated in Figure 4.2ab. The fine particle data of Figure 4.2b show a comparison of consecutive 4-hour average outdoor particle mass concentrations measured gravimetrically from samples collected on Teflon filters as described earlier versus the consecutive 4-hour average fine particle mass concentration computed by integrating the aerosol size distribution measured by the PMS laser optical particle counter over the size range below 2.3 μm particle diameter using an assumed fine particle density of 2.2 $g\ cm^{-3}$.

The graph of outdoor coarse particle concentrations over time (Figure 4.2a) shows data obtained by difference between gravimetric analysis of consecutive 4-hour average total particle samples collected on open-faced Teflon mem-

Table 4.3 Characteristics of Caves 6 and 9

Symbol	Description	Cave 6	Cave 9
S_1	wall area, m^2	1370	174
S_2	ceiling area, m^2	163	44
S_3	floor area, m^2	179	44
V	volume, m^3	2222	528
Z	physical height of the cave	15 m	10.35 m
H	elevation difference between entering and exiting critical fluid streamline	9.25 m	2.39 m
A_1	cross-sectional area of entrance through rock wall at ground level, Cave 9		7.4 m^2
A_2	cross-sectional area of opening in rock wall at 3rd and 4th floor level, Cave 9		5.6 m^2
A_{1a}	cross-sectional area of openings in building shell downstairs, Cave 6, front door open	4.8 m^2	-
A_{1b}	cross-sectional area of openings in building shell downstairs, Cave 6, front door closed	0.46 m^2	-
A_2	cross-sectional area of entrance through rock walls at ground level, Cave 6	11.82 m^2	-
A_3	cross-sectional area of opening in rock wall at 3rd plus 4th, floor level, Cave 6	21.12 m^2	-
A_4	cross-sectional area of openings in building shell upstairs, Cave 6	4.09 m^2	-
monitoring period			
start time, date		0200 h, 15 April, 1991	0200 h, 15 April 1991
end time, date		2200 h, 16 April, 1991	2200 h, 16 April 1991

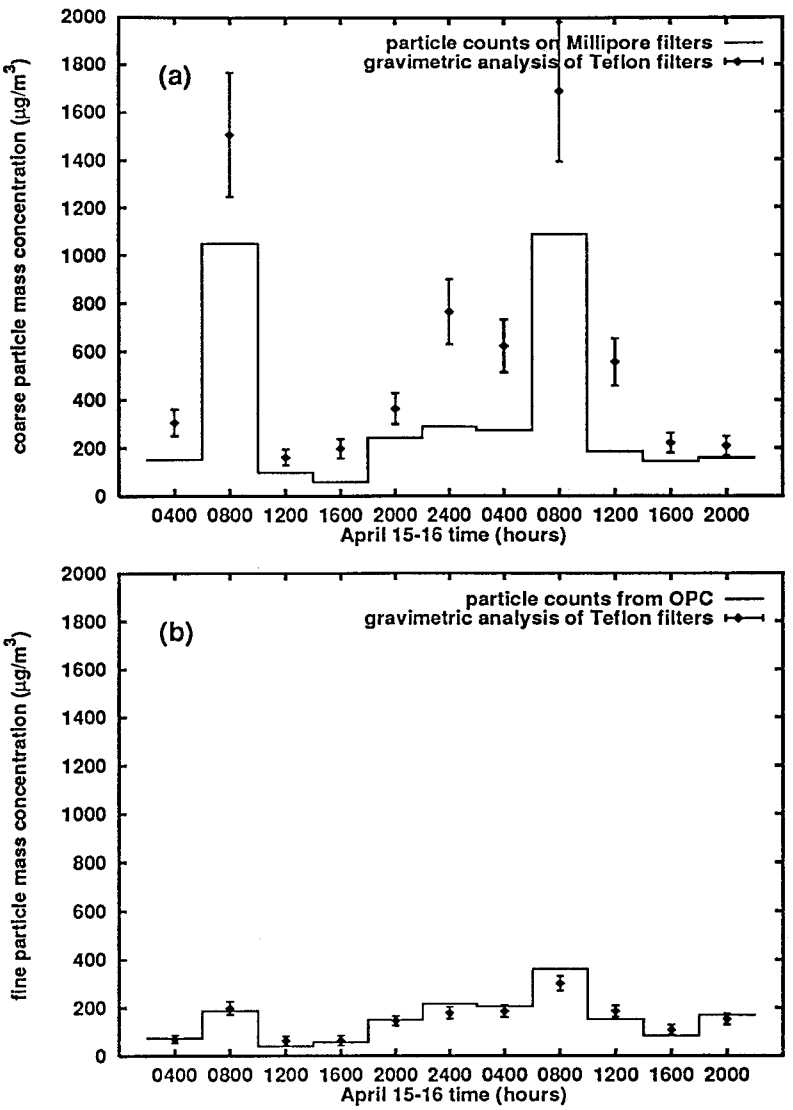

Figure 4.2 Outdoor airborne particle mass concentrations, April 15-16: (a) Coarse particle mass concentration measured gravimetrically using Teflon filters compared to mass calculated from particle counts on Millipore filters. (b) Fine particle mass concentration measured gravimetrically using Teflon filters compared to mass concentration calculated from laser optical particle counter data. Error bounds shown represent ± 1 standard deviation of the gravimetric determinations.

brane filters minus concurrent measurements of fine particle concentrations, compared to coarse particle mass concentrations estimated by automated light microscopy analysis of particles larger than 2 μm diameter collected on Millipore filters. Conversion of particle counts to mass concentrations for those coarse particle samples was accomplished using a coarse particle density of 2.2 $g\ cm^{-3}$ and a shape factor of 1.46 (Davies, 1979; Lin et al., 1994). The density values are based on examination of bulk deposits of formerly airborne material removed from surfaces in the caves at Yungang, and the shape factor is determined by examination of both airborne and deposited particle samples from Yungang. Fine particle mass concentrations measured gravimetrically are in excellent agreement with mass concentrations inferred from integration of aerosol size distribution data. Coarse particle mass concentrations measured by integrating particle size distribution data are generally lower than concentrations measured gravimetrically, but the data obtained by particle counting are still usually within ± 2 standard errors of the gravimetrically determined values.

An example of the combined outdoor airborne fine particle plus coarse particle size distribution is shown in Figure 4.3, averaged over the entire two-day experiment. That size distribution is obtained by merging the fine particle data from the laser optical particle counter with concurrent coarse particle counts taken by automated light microscopy applied to the outdoor Millipore filter samples. Similar size distribution data are available for each 4-hour period during the experiment, and those consecutive 4-hour average size distribution data form the actual inputs to the particle deposition model.

The outdoor coarse particle concentrations shown in Figure 4.2 are seen to be both much higher than the fine particle concentrations and show greater variation throughout the day. These coarse particle concentrations peak

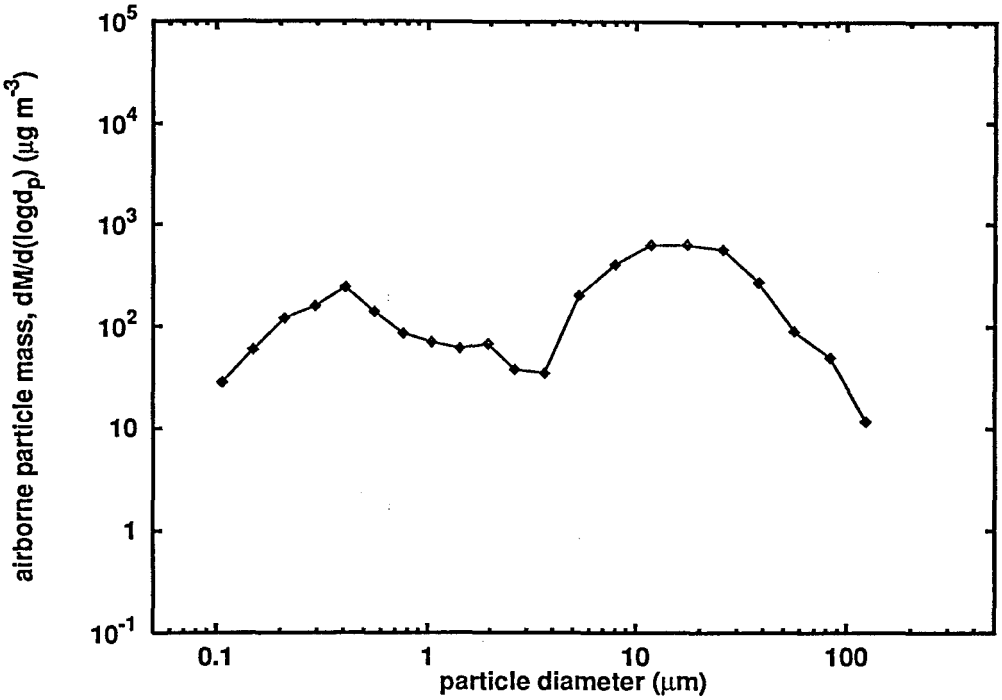

Figure 4.3 Average outdoor airborne particle mass distribution at Yungang, $dM/d(logd_p)$, averaged over the period April 15-16, 1991. Data used for the particle size range less than $2.3\mu m$ are from a laser optical particle counter. Concurrent data from automated optical microscopy analysis of samples collected on Millipore filters are used to determine the coarse particle size distribution ($d_p > 2.3\ \mu m$).

at greater than 1000 $\mu g\ m^{-3}$ over the 4-hour averaging period nominally extending from about 0600 hours to 1000 hours each morning. During the early part of this time period, activities within the small village of Yungang and along the nearby highway have begun, and broom sweeping of the dirt terrace in front of the caves is observed, but the air is generally still and mixing depths are low, leading to high outdoor particle concentrations.

In addition to the time series of outdoor aerosol size distribution data, the deposition model requires time series data on the outdoor air temperature and cave wall temperatures. From these temperature data, air flows through the caves are predicted. Figure 4.4a shows the outdoor air temperature and the cave wall temperature at Cave 9 over the two day period studied here. Also shown is the air velocity measured after having filtered the output of the thermo-electronic velocity probe located in the ground level entrance to Cave 9 at position 1 in Figure 4.1b compared to the velocity predicted by the natural convection air exchange model of equations (4.4)-(4.6) (see Figure 4.4b).

A very detailed analysis of the performance of the air exchange model over a much longer period of time is provided by Christoforou et al. (1995). From Figure 4.4 it is seen that at night when the outdoor air is colder than the cave walls, air flows into the cave at the ground level entrance (graphed as the positive flow direction in Figure 4.4b), while during the day the situation reverses. On most days during April, 1991, air flows stagnated and then reversed direction twice per day, once at about 0930 hours in the morning and again at about 2100 hours at night, as is typified by the data for April 15, with both flow reversals occurring near the time of zero temperature difference between the outdoor air and the cave walls. From Figure 4.4b, it is seen that the natural convection air flow model for Cave 9 predicts both

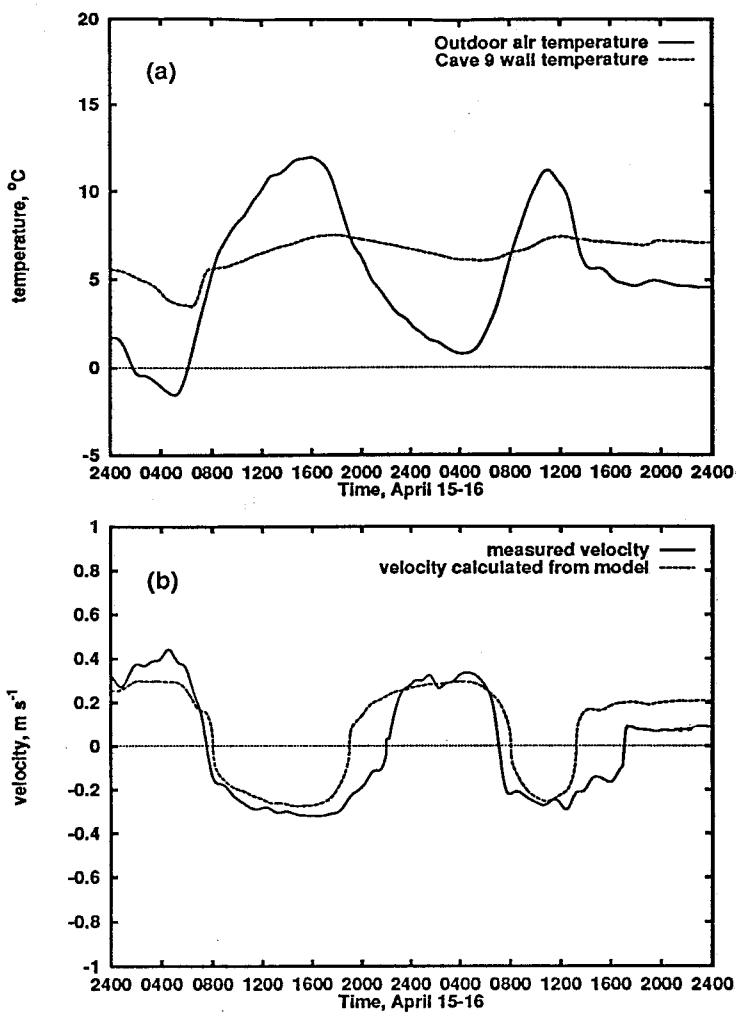

Figure 4.4 (a) Outdoor air temperature and wall surface temperature inside Cave 9, April 15-16, and (b) measured air velocity at the center of the ground level entrance to Cave 9, April 15-16, compared to velocity calculated from the model of equations (4.4)-(4.6). A positive velocity value indicates flow into the ground level entrance to Cave 9, while a negative velocity value indicates flow out of the ground level entrance at position 1 in Figure 4.1b.

the pattern and magnitude of the air flows through that cave reasonably well. Air exchange between the outdoors and the interior of Cave 6 likewise is reproduced well by the natural convection model, and these results are displayed and discussed by Christoforou et al. (1995).

Figure 4.5ab shows model predictions of the airborne particle mass size distribution inside Cave 9 averaged over the 44 hour experiment as well as the size distribution of the daily average (24 h average) mass flux of particles deposited onto horizontal surfaces within Cave 9 over that period. Model predictions in size ranges above 2 μm particle diameter are compared to particle counts obtained by automated optical microscopy analysis of airborne particle filter samples and deposited particle samples, both collected on the surfaces of Millipore filter material. Within Cave 9, excellent agreement is obtained between measured and predicted airborne particle size distributions and between the measured vs predicted size distribution of particle fluxes to horizontal surfaces.

As can be seen if Figure 4.6ab is compared in detail to Figure 4.5ab, indoor coarse particle concentrations and deposition fluxes inside Cave 6, both measured and predicted, are lower than in Cave 9. This occurs in part because the average retention time for air parcels inside Cave 6 is about 4 times longer than in Cave 9. Differences in air parcel retention time between Caves 6 and 9 vary by time of day. The wooden doors at the ground level entrance to the temple structure in front of Cave 6 are closed both at night and during the early portion of the high outdoor coarse particle concentration episodes depicted in the morning hours in Figure 4.2a. When those doors are closed, air is forced to flow through the many cracks and small openings in the wooden building shell, and the added resistance to air flow causes the indoor/outdoor air exchange rate to drop. This reduced air exchange rate in turn acts to

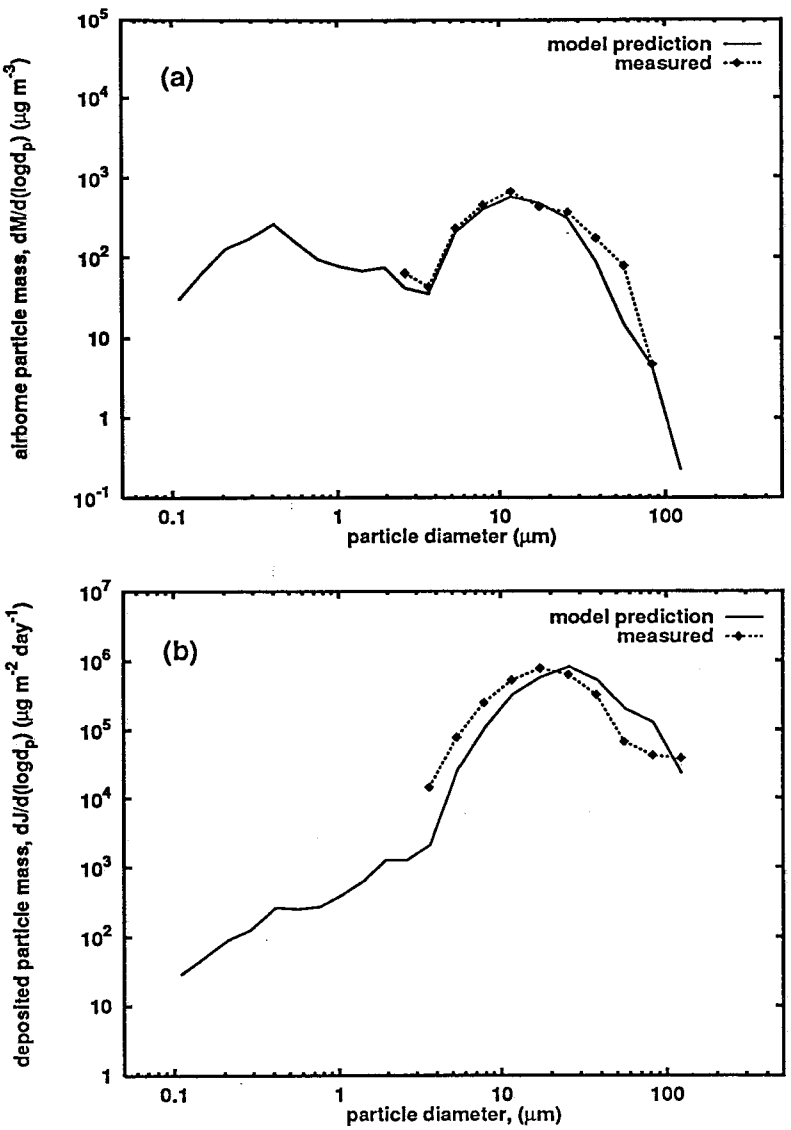

Figure 4.5 Model performance, April 15-16, Cave 9: (a) Predicted 2-day average mass distribution of airborne particles, $dM/d(logd_p)$, inside Cave 9 compared to measured values, and (b) predicted size distribution of the particle deposition rate, $dJ/d(logd_p)$, onto horizontal surfaces inside Cave 9 compared to measured values.

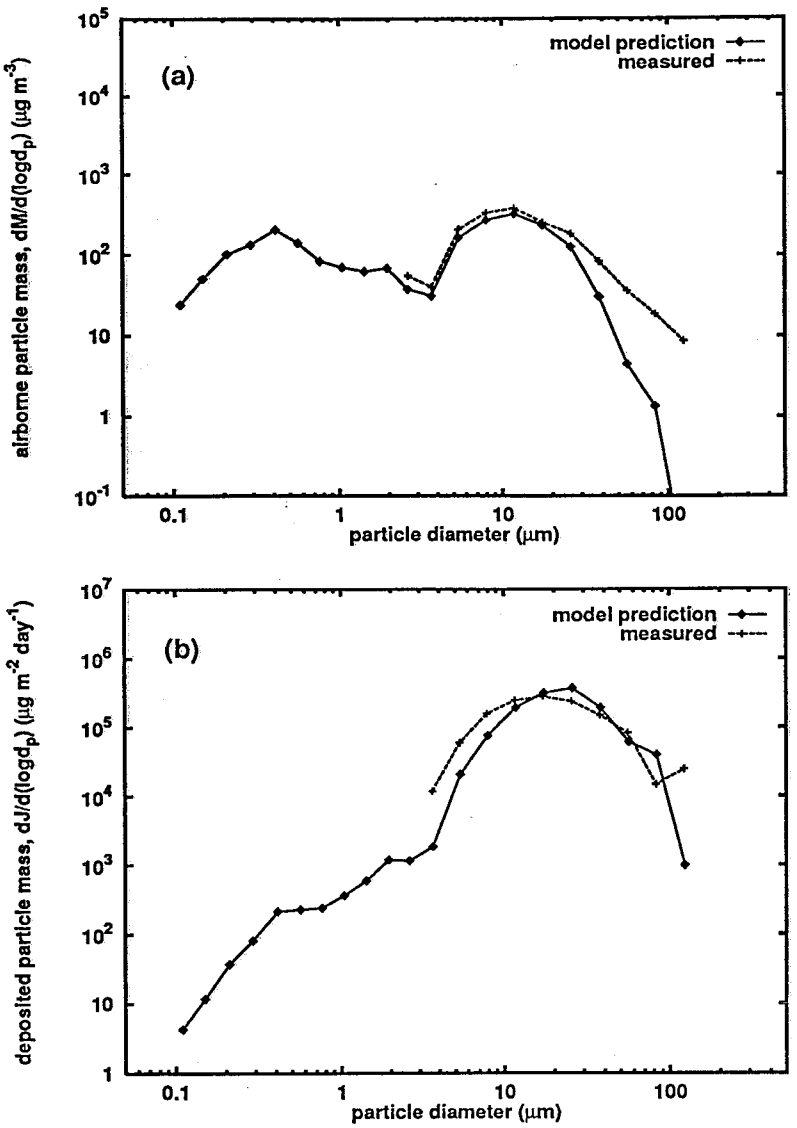

Figure 4.6 Model performance, April 15-16, Cave 6: (a) 2-day average size distribution of airborne particles, $dM/d(logd_p)$, inside Cave 6 compared to measured values, and (b) predicted size distribution of the particle deposition rate, $dJ/d(logd_p)$, onto horizontal surfaces inside Cave 6 compared to measured values.

reduce particle induction into the building in front of Cave 6 at those times, slowing the replacement of deposited particles, thus lowering both indoor airborne particle concentrations and particle deposition fluxes.

Figure 4.6ab indicates that model predictions do not match measured values in Cave 6 as closely as was the case inside Cave 9. This is due mainly to the fact that the outdoor aerosol samples used to drive predictions for both Cave 6 and Cave 9 were collected directly in front of Cave 9 (see sampler placement diagram in Figure 2.1). Coarse particle concentrations, due to their generation by fugitive dust sources and the rapid removal of very large particles by sedimentation, often vary considerably over short distances. The entrances to Cave 6 are located about 43 m away from the outdoor samplers, while the outdoor samplers are only 2 m away from the entrance to Cave 9. Airborne particle concentration and deposition fluxes inside Cave 6 also are more difficult to measure accurately because the lower concentrations and fluxes in Cave 6 compared to Cave 9 yield smaller particle counts. In spite of this, the model predictions for Cave 6 are within two standard errors of the measured value of the indoor aerosol size distribution and deposition flux data in most cases.

The time series of deposition flux predictions to horizontal surfaces inside Caves 9 and 6 are shown in Figures 4.7 and 4.8 respectively. The deposition flux predictions inside Cave 9 are in excellent agreement with measured values at most times. The deposition fluxes inside Cave 6, both measured and predicted, differ considerably from those inside Cave 9, because the early morning peak in the deposition fluxes at Cave 9 is suppressed both by the longer retention times for air exchange in Cave 6 (about 4 times longer than in Cave 9) and by the way that the wooden temple structure doors are operated at Cave 6 (the outdoor particle inputs to the models for both caves

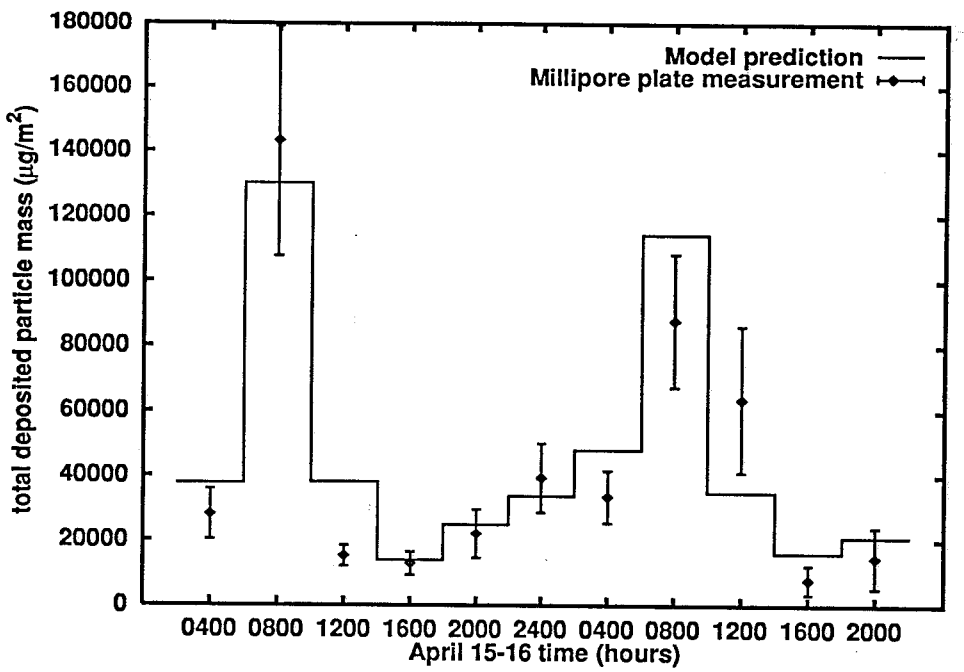

Figure 4.7 Model predictions versus measured values of the total particle mass flux per nominal 4-hour sampling period deposited onto horizontal surfaces inside Cave 9 over the period of April 15-16, 1991. Error bounds on the measured values equal one standard deviation.

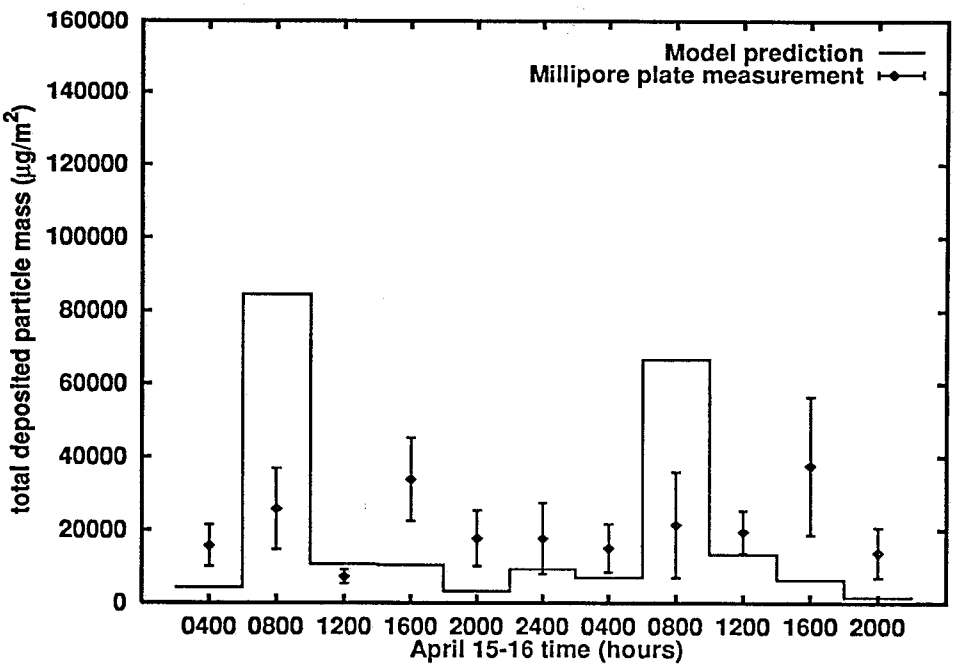

Figure 4.8 Model predictions versus measured values of the total particle mass flux per nominal 4-hour sampling period deposited onto horizontal surfaces inside Cave 6 over the period of April 15-16, 1991. Error bounds on the measured values equal one standard deviation.

are represented as being identical). Particle fluxes inside Cave 6 are generally lower than at Cave 9 at most times. The predicted particle fluxes in Figure 4.8 fall within two standard errors of the individual measurements at most times, yet there is evidence for some bias in the model or in the measurements, with model predictions falling below nominally measured values in 8 out of 11 sampling periods.

Model predictions of the integrated mass flux of particles to horizontal surfaces, to vertical surfaces, and to the ceiling of Caves 6 and 9 are given in Table 4.4. Results are stated as a deposition flux converted to a 24-hour average for the conditions that occurred on April 15-16, 1991. The horizontal fluxes can be compared to the measured values averaged over a 24-hour day. The model predictions and measured values are in good agreement. It should be noted here that deposition fluxes over longer periods of time would have been larger. Measurements made over a one year period in 1991-1992 show a deposition flux to horizontal surfaces for the year of 5.23 $\mu g\ m^{-2}\ s^{-1}$ in Cave 6, which is a factor of 4 higher than observed during April 15-16, 1991 (Christoforou et al., 1994). Differences between the two-day period examined in detail here versus the longer term annual flux are undoubtedly due to day-to-day fluctuations in outdoor particle concentrations and changes in the outdoor temperatures that drive air exchange through the caves. The model works well enough that it would probably track these changes well over long periods of time if the outdoor pollutant data and temperature data needed to exercise the model for long periods of time were acquired. While the model is fairly sophisticated, the model inputs needed are surprisingly few.

Predicted deposition fluxes to vertical surfaces and to the cave ceiling also are given in Table 4.4. Fluxes to these surfaces are orders of magnitude smaller than to horizontal surfaces. This is because deposition to horizontal surfaces

Table 4.4 Deposition fluxes to surfaces inside Caves 6 and 9 at the Buddhist Cave Temples at Yungang, April 15-16, 1991[a]

Method	Horizontal Surfaces[b] $\mu g\ m^{-2}\ s^{-1}$	Vertical Surfaces $\mu g\ m^{-2}\ s^{-1}$	Ceiling $\mu g\ m^{-2}\ s^{-1}$
Cave 9			
measured	2.9	—	—
modeled	3.0	7.12×10^{-4}	3.93×10^{-4}
Cave 6			
measured	1.4	—	—
modeled	1.4	5.41×10^{-5}	1.73×10^{-5}

[a] Note that the measured deposition fluxes over other time periods are higher. For the 21 day period April 12- May 1, 1991, the deposition fluxes averaged 13.40 $\mu g\ m^{-2}\ s^{-1}$ and 4.54 $\mu g\ m^{-2}\ s^{-1}$ to horizontal surfaces in Caves 9 and 6 respectively. Over the 1 year period 1991-92, the deposition fluxes to horizontal surfaces within Cave 6 averaged 5.23 $\mu g m^{-2}\ s^{-1}$ (Christoforou et al., 1994).

[b] Upward facing horizontal surfaces.

is dominated by gravitational sedimentation of coarse dust particles while deposition to vertical surfaces and to the ceiling is dominated by convective diffusion and thermophoresis. Deposition velocities due to gravitational settling are much higher than those due to convective diffusion and thermophoresis under the conditions at Yungang. Furthermore, coarse particle mass concentrations greatly exceed fine particle concentrations at Yungang (Salmon et al., 1994), again favoring higher deposition fluxes due to gravitational sedimentation as compared to convective deposition processes.

The size distribution of the deposited particles predicted by the model has been used to compute the time required to completely cover initially clean surfaces of various orientations with their first full monolayer of particles if particle deposition rates were to continue for long periods of time at the rates observed for April 15-16, 1991. Results are shown in Table 4.5. Cave 9 which lacks a wooden shelter in front of the cave at present is directly exposed to the outdoor atmosphere. Under April 15-16, 1991 conditions horizontal surfaces inside Cave 9 would become completely covered by a monolayer of dust in only 0.3 years, while vertical surfaces and the decorated ceiling would require 18 and 26 years, respectively, to reach the same degree of coverage. Cave 6, which is sheltered by the wooden temple front structure and which has lower air velocities along its walls and smaller wall-air temperature differences than in Cave 9 would require longer to reach the first full monolayer coverage by particles, as shown in Table 4.5. Recognizing that the deposition rate to horizontal surfaces over an annual period is about four times higher than during the April 15-16 conditions studied here, the actual average elapsed time to reach a full monolayer coverage by deposited particles is probably about one fourth as long as the values shown in Table 4.5.

Table 4.5 Predicted time (years) for 100% coverage to occur†

Surface orientation	Cave 6	Cave 9
upward-facing horizontal	0.5	0.3
vertical	260	18
ceiling	770	26

† Values shown are based on outdoor particle concentrations and air exchange rates calculated using data for the April 15-16, 1991 period (Christoforou et al., 1995). Particle fluxes over an annual averaging period inside Cave 6 are a factor of 4 higher than during the April 15-16 period of simulation, indicating that over long periods of time, the time for complete coverage to occur is probably one fourth as long as shown here.

4.5 Conclusions

A model for air circulation and particle deposition within the Buddhist Cave Temples at Yungang has been developed. The model could be applied to study the multi-story grottoes at other similar cave temple sites such as those at the Mogao Grottoes and at the Yu Lin Grottoes near Dunhuang, China, as well.

The model takes as input the temperature of the outdoor air and the cave walls, the size distribution of particles suspended in the outdoor air, the initial size distribution of particles suspended in the indoor air, as well as geometric parameters of the caves. The model then predicts the air flow rate through the caves, the indoor size distribution of particles suspended in the air as well as the size distribution of particles deposited onto various surfaces inside the caves.

A 44 hour intensive sampling experiment, conducted at Yungang during April 15 and April 16, 1991, provided the input data necessary for evaluation of model performance. Comparison of model predictions with the actual measurements shows that there is very close agreement between predictions and observations at Cave 9 at Yungang, and that predictions for Cave 6 are within the 95% confidence limits of the experimental data at most times. Calculations show that particle deposition rates within Caves 6 and 9 at Yungang are sufficiently rapid that initially clean horizontal surfaces will become completely covered by a full monolayer of deposited particles in 0.3-0.5 years if the conditions of April 15-16 studied here were to continue for long periods of time. Under annual average conditions, the soiling rate would be even faster. The present model can be used to predict the relative effectiveness of particle filtration systems and/or altered ventilation rates on the particle deposition problem at the Yungang Grottoes.

4.6 References

Christoforou, C. S., Salmon, L. G., and Cass, G. R. (1994) Deposition of atmospheric particles within the Buddhist cave temples at Yungang, China. *Atmos. Environ.* **28**, 12, 2081-2091.

Christoforou, C. S., Salmon, L. G., and Cass, G. R. (1995) Air exchange within the Buddhist cave temples at Yungang, China. *Atmos. Environ.*, to be submitted.

Churchill, S.W., and Chu, H.H.S. (1975) Correlating equations for laminar and turbulent free convection from a vertical flat plate. *Int. J. Heat Mass Transfer*, **18**, 1323-1329.

Corner, J., and Pendlebury, E. D. (1951) The coagulation and deposition of a stirred aerosol. *Proc. Phys. Soc. (London)* **B64**, 645-654.

Davies, C.N. (1979) Particle-fluid interaction. *J. Aerosol Sci.*, **10**, 477-513.

Dietz, R. N. and Cote, E. A. (1982) Air infiltration measurements in a home using a convenient perfluorocarbon tracer technique. *Environ. Int.* **8**, 419-433.

Gelbard, F., and Seinfeld, J.H. (1980) Simulation of multicomponent aerosol dynamics. *J. Colloid Int. Sci.* **78**, 485-501.

Incropera, F. P. and DeWitt, D. P. (1985) *Fundamentals of Heat and Mass Transfer*, Wiley, New York.

Ligocki, M. P., Liu, H. I. H, Cass, G. R., and John, W. (1990) Measurements of particle deposition rates inside Southern California museums. *Aerosol Sci. Technol.* **13**, 85-101.

Lin, J.J, Noll, K.E., and Holsen, T.M. (1994) Dry deposition velocities as

a function of particle size in the ambient atmosphere. *Aerosol Sci. Technol.* **20**, 239-252.

Nazaroff, W. W., and Cass, G. R. (1987) Particle deposition from a natural convection flow onto a vertical isothermal flat plate. *J. Aerosol Sci.* **18**, 445-455.

Nazaroff, W. W., and Cass, G. R. (1989a) Mathematical modeling of indoor aerosol dynamics. *Environ. Sci. Technol.* **23**, 157-166.

Nazaroff, W. W., and Cass, G. R. (1989b) Mass transport aspects of pollutant removal at indoor surfaces. *Environ. Int.* **15**, 567-584.

Salmon, L. G., Christoforou, C. S., and Cass, G. R. (1994) Airborne pollutants in the Buddhist cave temples at the Yungang Grottoes, China. *Environ. Sci. Technol.*, **28**, 805-811.

Chapter 5. Approaches to control of particle deposition and soiling within the Yungang Grottoes

5.1 Introduction

The results of experiments conducted at the Yungang Grottoes, reported previously (Christoforou et al. 1994; Salmon et al. 1994), show that the outdoor airborne particle concentrations at Yungang are very high, averaging 508 $\mu g\ m^{-3}$ over an annual period in 1991-92. Deposition of particles, typically in the size range from 10 μm to 100 μm diameter, occurs onto horizontal surfaces within the caves due largely to gravitational sedimentation. The result is that the horizontally-oriented surfaces of the more than 50,000 sculptures within the grottoes can become noticeably soiled within a matter of hours and can become covered by the first complete monolayer of deposited dust within a matter of months. Over a period of 5 years, deposits as deep as 0.8 cm and with mass loadings as high as 5 $kg\ m^{-2}$ have been measured to accumulate on the statuary within these caves (Christoforou et al., 1994).

Measurements of the chemical composition of the airborne particles and of the dust deposits on surfaces in the caves show that the deposits consist of mineral matter (e.g. soil dust) and carbon particles (e.g. unburned coal dust) (Salmon et al. 1994). This is consistent with observations of the major dust generation activities in the vicinity of Yungang which include emissions from large coal mines in the region, coal dust and road dust from trucks carrying coal (especially along a road located approximately 300 m south of the grottoes), dust from travel on unpaved roads in the village of Yungang adjacent to the grottoes, dust generated by visitors and maintenance activities on the unpaved terrace immediately in front of the caves, soil dust

generated by wind storms from the Gobi Desert, and smoke from local coal combustion.

The purpose of the present chapter is to examine alternative approaches to the control of the particle deposition problem within the Yungang Grottoes. Two general approaches are possible: (1) control of particle concentrations in the outdoor air through reduction of particle generation at the above mentioned sources, and (2) removal of particles from the air entering the caves by filtration or similar technical means. Each of these alternatives will be discussed in quantitative terms based both on field experiments conducted at Yungang and on computer-based models of the particle deposition processes within the caves.

5.2 Control of outdoor pollutant concentrations

A map of the immediate vicinity of the Yungang Grottoes is shown in Figure 5.1. The cliff face into which the cave temples are carved appears as an east-west line along the middle of the map. There is a park within the walls of the grotto grounds immediately to the south of the cliff face. The small village of Yungang lies directly to the south of the park in front of the caves. A major highway carrying thousands of coal trucks daily is located on the south and west sides of the village. A river runs past the grottoes site to the south and west of the coal-haul highway. Just south and west of the river a railroad line is situated carrying coal-fired locomotives. Coal mines are sited at the periphery of the map as well as up and down the river valley beyond the boundaries of Figure 5.1.

Over a two-day period in April, 1991, we measured the spatial distribution of the deposition of airborne particles at the center of a series of 0.5 by 0.5 km map sections laid out over the 2 km by 2 km area surrounding the caves, as is

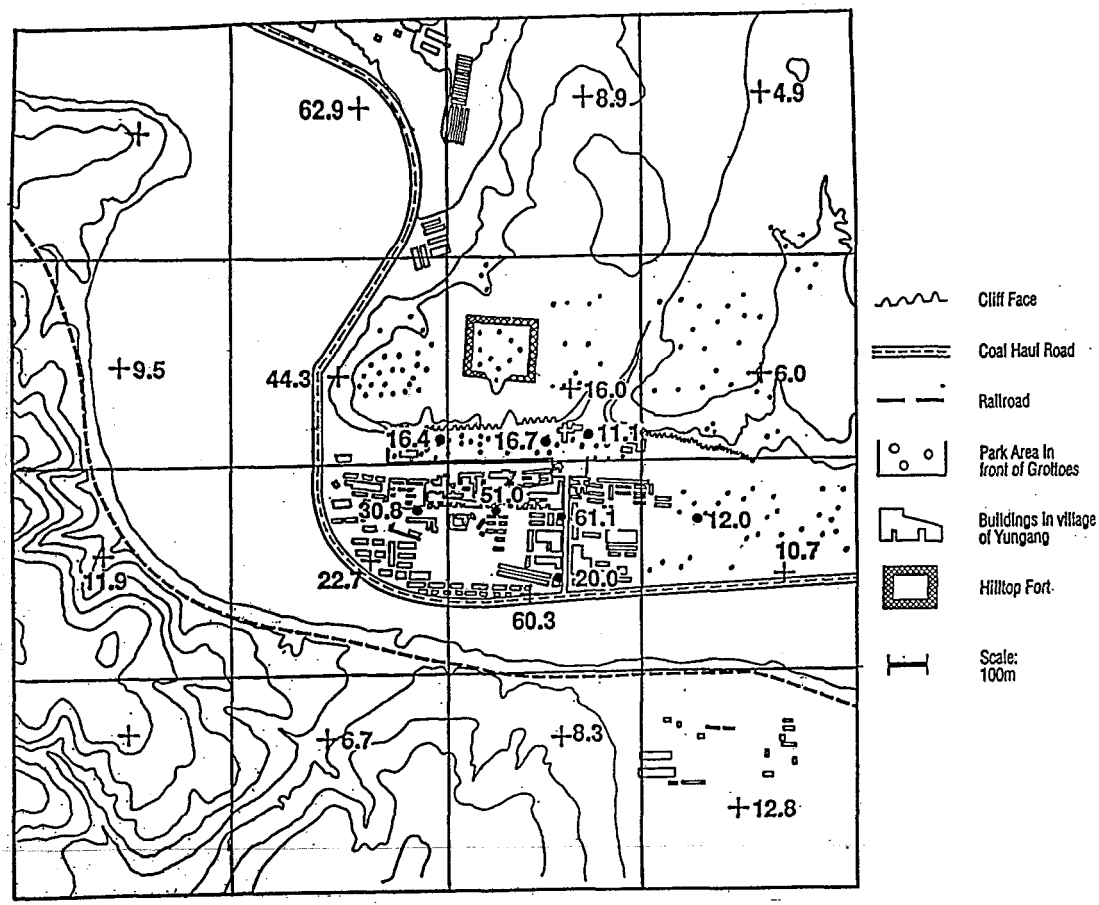

Figure 5.1 Map showing a 2 km by 2 km area surrounding the Yungang Grottoes. Numerical values shown next to the symbols + and • indicate particle deposition fluxes to horizontal surfaces over the period April 19-21, 1991, in units of $\mu g\ m^{-2} sec^{-1}$.

shown in Figure 5.1. Extra samples were collected within the village of Yungang and along the terrace in front of the caves. Measurements were made using glass microscope slides as deposition plates with the particle deposition flux to these microscope slides determined by the micro-video imaging procedure described in Chapter 2. The glass plate data are reliably translated into mass deposition rates and those results are shown in Figure 5.1. The highest deposition rates of about 60 $\mu g\ m^{-2}\ s^{-1}$ occur in the center of the map within the village of Yungang and along the coal-haul highway. Lower particle fluxes generally occur at the edges of the area mapped. This means that the sources that generate much of the airborne particulate matter are located within the high flux area, principally along the coal-haul highway and inside the village of Yungang. The caves are located between the cleaner countryside and the very dusty area along the highway and the main street of the village. As a result, the particle deposition flux at the front of the caves is lower than along the coal-haul highway or village, but higher than in the surrounding countryside.

Since the area that seems to contain this high source of particles is fairly small, it may be practical to reduce much of the local particle generation by simple means:

(a) Redirecting the coal truck traffic to roads located far from the grottoes or alternatively covering the loaded coal trucks such that coal does not fall off to be crushed and driven into the air by trucks that follow.

(b) Paving the few streets in the village of Yungang such that vehicle traffic produces much less dust there.

We have observed that the city of Xian, China, uses an excellent further measure for dust suppression. A tank truck uses water to spray-wash the

roads in the morning. At first, this may seem impractical at Yungang given the obvious general shortage of water in the area. But it should be thought about seriously. It is a measure that the grottoes staff could undertake on their own initiative with little required assistance or cooperation from others. The sections of road to be washed (e.g., the section of the highway on the map of Figure 5.1 plus the village roads) are very short. The grottoes does have its own water source, but that water may not need to be used. There is no reason to wash the roads with high quality water when a tank truck can fill up at the river (as long as the river is not dry). If necessary, a well could be drilled to increase the supply of available water locally.

A further source of possible dust creation is foot traffic and sweeping activity that occurs on the dirt terrace that is directly in front of the caves. Much of the dust deposited within the caves has a mineral composition like that of local soil dust. It is not easy to tell how much comes from the terrace in front of the caves and how much from the village. The Yungang Grottoes staff report that they plan to pave the dirt area in front of caves with stepping stones, one effect of which will be to lower dust generation at that site.

If localized particle generation from the coal-haul highway, from the village, and from the dirt area just in front of the caves could be suppressed, particle deposition rates would begin to more closely approach those in the areas of Figure 5.1 that are more distant from the caves. A reduction in particle deposition rates from about 16 $\mu g\ m^{-2}\ s^{-1}$ at present at the entrance to the caves to perhaps 10 $\mu g\ m^{-2}\ s^{-1}$ in the future on days like those measured in Figure 5.1 may be a reasonable goal. That would reduce particle deposition at the caves by about 38%. The reduction is not larger because the regional background deposition rate all over the countryside due to region-wide dust sources that include the coal mines, more distant road traffic, and other

villages, is fairly high even at sites distant from the local dust sources that can be controlled near the village of Yungang. Thus the use of local dust suppression methods at Yungang does not provide a complete solution to the particle deposition problem, but it helps. It may make an important contribution to an overall control program.

5.3 Removal of particles from the air entering the caves

Two options exist for removing particles from the air that enters the caves. First, a mechanical air filtration system powered by an electrical fan motor could be used. In antiquity, the entrance to each of the caves was sheltered by a wooden temple front building one room deep and extending several stories up the face of the cliff. Today, two of these structures still exist. A mechanical air filtration system could be concealed within the upper stories of an existing or reconstructed wooden temple front building like those that sheltered the cave entrances in antiquity. Alternatively, a passive particle filtration system could be envisioned in which the natural convection-driven air circulation within the caves is employed to remove particles as air passes through filter material placed instead of the paper that traditionally covered the many windows that exist within the door panels of a traditional Chinese temple structure.

5.3.1 Installation of a mechanical air filtration system

Figure 5.2 shows a diagram of a standard mechanical air filtration system for a building (adapted from Nazaroff and Cass, 1991). Outdoor "make-up air" containing airborne particles is fed to the ventilation system through a particle filter and then is introduced into the building (in this case a cave) interior. Previously filtered "recirculated air" is withdrawn from the building interior, filtered again, and then sent back to the building. This repeated

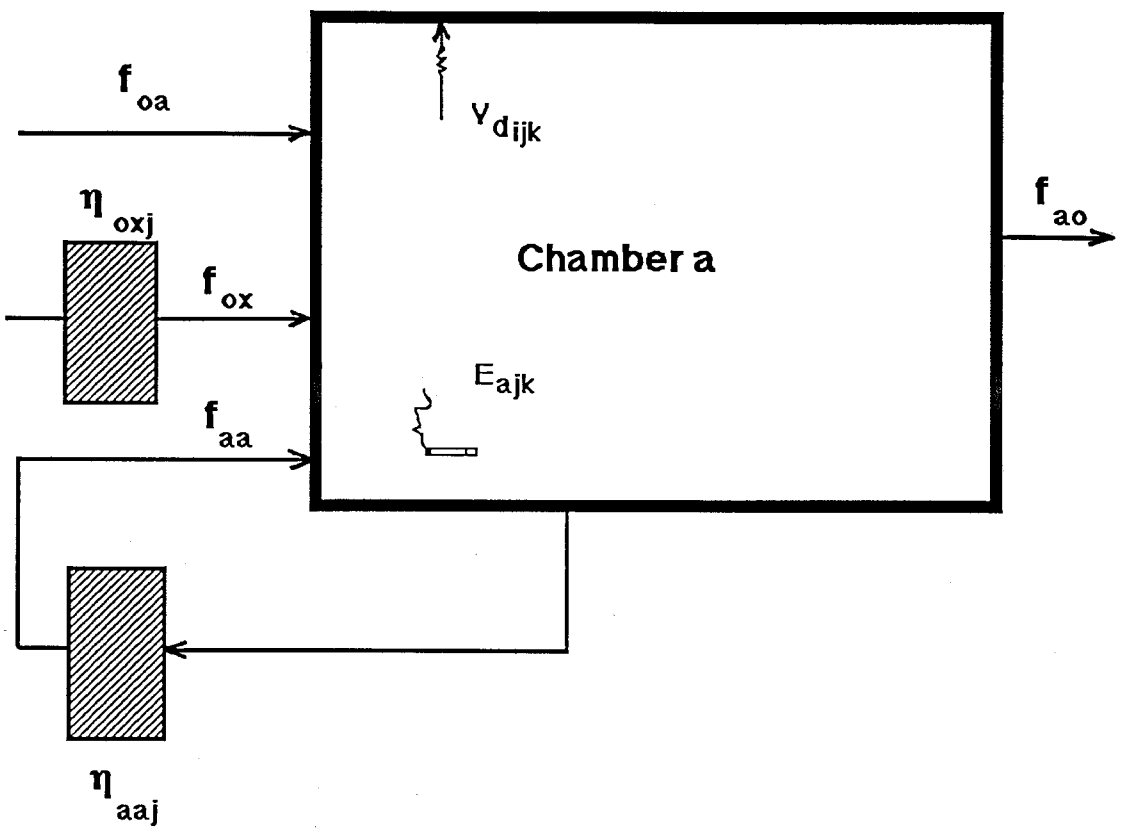

Figure 5.2 Schematic representation of the mechanical air filtration system for a building. The symbols f and η indicate air flow rates and filter efficiencies, respectively. (Figure adapted from Nazaroff and Cass, 1991.)

filtration of the indoor air means that the removal efficiency of the whole system is greater than the removal efficiency if the air made only one pass through the filters as it enters the building. A certain amount of "infiltration air" usually leaks, unfiltered, into the building through cracks in the building or when doors are opened and closed.

A filtration model for a cave that is represented as a single chamber can be written to replace equation (4.8) of the cave soiling model developed in Chapter 4:

$$V\frac{d(C_{ajk})}{dt} = C_{ojk}f_{oa} + C_{ojk}(1-\eta_{oxj})f_{ox} + C_{ajk}(1-\eta_{aaj})f_{aa} + E_{ajk} - C_{ajk}\sum_i S_i v_{d_{ijk}} - C_{ajk}(f_{oa}+f_{ox}+f_{aa}) \quad (5.1)$$

where C_{ajk} and C_{ojk} are the concentrations of chemical component k in particles of size j in air inside (a) or outside (o) the cave, respectively; f_{oa}, f_{ox}, and f_{aa} are the volumetric air flow rates associated with infiltration of untreated air, induction of outdoor air into the mechanical ventilation system, and recirculation of previously filtered air, respectively; η_{oxj} and η_{aaj} are the filtration efficiencies for particles of size j by filters placed in the outdoor make-up air and recirculated air flow lines, respectively; E_{ajk} is the emission rate of chemical component k in particles of size j within the cave, S_i is the surface area of the i^{th} surface and $v_{d_{ijk}}$ is the deposition velocity for particles containing component k in size j to the i^{th} surface within the cave. Symbols used in equation (5.1) are coordinated with the schematic diagram pictured in Figure 5.2.

A filtration system for a cave like Cave 6 at Yungang, for example, could be built by placing a mechanical fan, ductwork, and filters in an unnoticeable location in an unused area of the upper stories of the wooden structure that

shelters the front of that cave. In the cases of caves at Yungang that do not presently have a wooden shelter in front of the cave, a first step would be to gain control over air flow in and out by first reconstructing the shelter, followed by fan and filter system installation. Such a system can be operated with many possible combinations of filters, outdoor make-up air flow rates, recirculated indoor air flow rates, and untreated outdoor air infiltration. A schematic diagram showing one possible relationship between equipment location and air flow pathways for such a system located within a Buddhist cave temple front structure is given in Figure 5.3.

To begin this study, we establish a "base case" condition at Cave 6 with no temple building in front of the cave. The computer simulation begins with measured outdoor particle concentrations and particle sizes observed on April 15, 1991, and then follows particle deposition processes over a 2-day period. The air flow that occurs in this base case is that obtained using the computer model for Cave 6 described in Chapter 3, section 3.4.2, modified so that there is no temple building in front of the cave. The particle deposition rate to horizontal surfaces is calculated by coupling that base case air exchange pattern to the particle deposition model for Cave 6 that was described in Chapter 4, section 4.2.1. Under base case uncontrolled conditions, particle mass amounting to 262 $mg\ m^{-2}\ d^{-1}$ is calculated to deposit on horizontal surfaces under the conditions of the April 15-16, 1991, period of simulation, as seen in case 0 (base case) of Table 5.1.

Case 1 of Table 5.1 shows the historical case, i.e., the cave as it exists today, operated with several open door panels in the upper stories of the building and with the ground floor entrance doors open during the day but closed at night. Again, flows were calculated using the computer model described earlier, and we see that the effect of the wooden temple front as it is operated

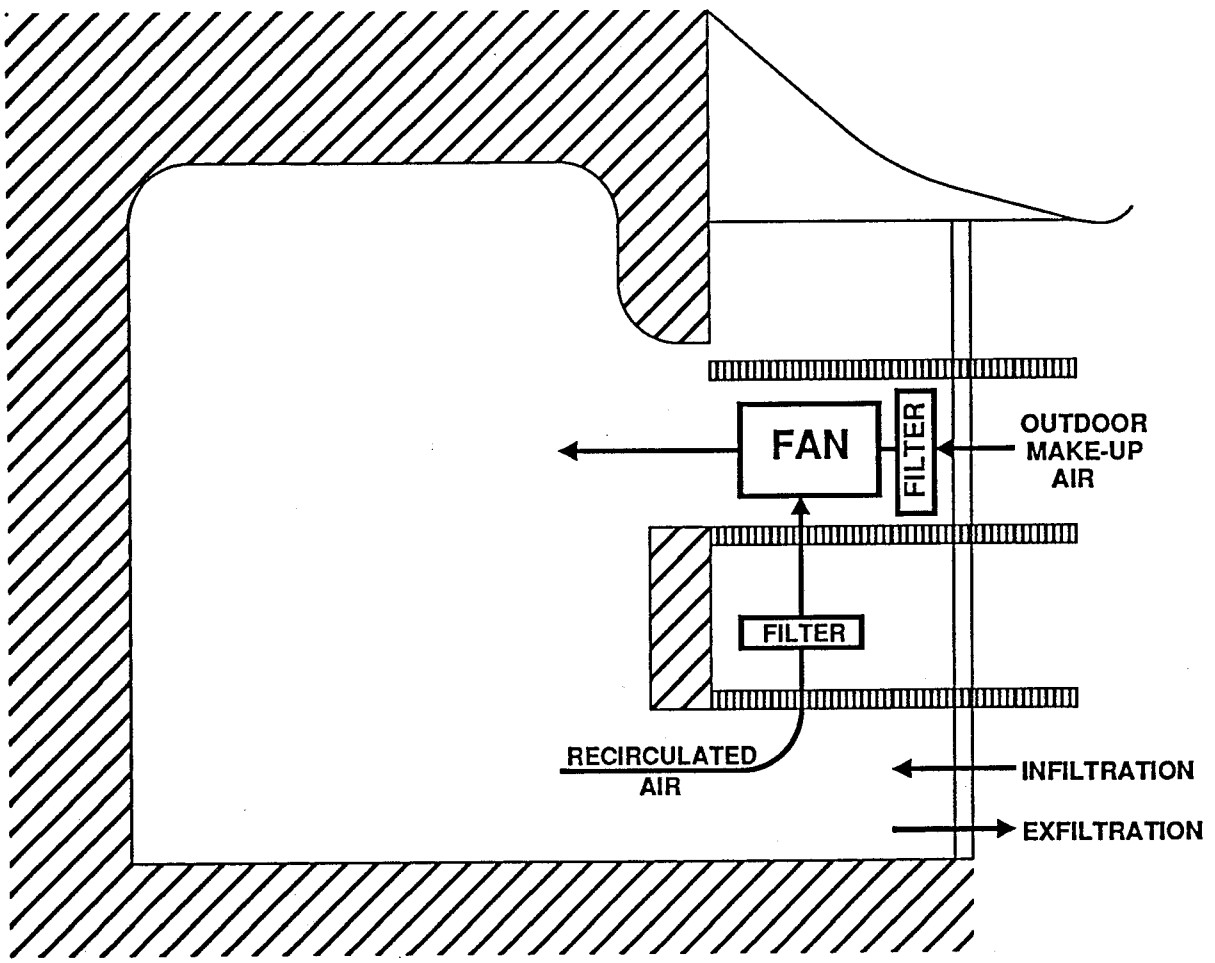

Figure 5.3 Schematic diagram showing one possible relationship between equipment location and air flow for a mechanical air filtration system concealed within the upper stories of a structure that shelters the front of a cave at Yungang.

Table 5.1 Effect of alternative mechanical filtration system designs on reducing the particle mass flux to horizontal surfaces in Cave 6 at the Yungang Grottoes[a]

	Untreated Outdoor Infiltration Air ($m^3\ min^{-1}$)	Filtered Outdoor Make-up Air ($m^3\ min^{-1}$)	Filtered Indoor Recirculated Air ($m^3\ min^{-1}$)	Filter Type	Mass Deposition to Horizontal Surfaces ($mg\ m^{-2}\ day^{-1}$)	Percent Remaining Relative to Base Case	Time to 100% Coverage by Particles (Years)
Base Case							
(0) Temple front removed[b]	317	–	–	–	262	–	0.28
(1) Historical Case	99	–	–	–	139	53	0.47
Mechanical Ventilation with low efficiency filters FB1							
(2) standard system	10	89	267	FB1	92	35	0.75
(3) reduced make-up air	10	22	334	FB1	37	14	1.8
(4) standard system with zero infiltration	0.0	89	267	FB1	82	31	0.83
(5) reduced make-up air with zero infiltration	0.0	22	334	FB1	24	9.2	2.6
Mechanical ventilation with loaded low efficiency filters FA3							
(6) standard system	10	89	267	FA3	12	4.6	5.7
(7) reduced make-up air	10	22	334	FA3	9.9	3.8	7.2
(8) standard system with zero infiltration	0.0	89	267	FA3	3.8	1.4	15
(9) reduced make-up air with zero infiltration	0.0	22	334	FA3	1.5	0.6	36
Mechanical ventilation with high efficiency filters							
(10) standard system	10	89	267	88-99%	9.9	3.8	7.5
(11) reduced make-up air	10	22	334	88-99%	9.4	3.6	8.0
(12) standard system with zero infiltration	0.0	89	267	88-99%	1.5	0.6	42
(13) reduced make-up air with zero infiltration	0.0	22	334	88-99%	0.93	0.4	72

[a] Values shown are averages of model predictions over the two day period of April 15-16, 1991, for which data are available to drive the deposition model. As discussed in Chapter 4, deposition rates under annual average conditions are about 4 times higher than under April 15-16, 1991, conditions; deposition fluxes shown above should be scaled upward proportionately and the times to reach 100% coverage by particles should be divided by a factor of 4 when considering time periods that approach a year or larger.

[b] Removal of the existing wooden temple building would expose the rock openings in the cliff face directly to the outdoor atmosphere as is the case at most of the other caves at Yungang. In that case the minimum distance between entering and exiting fluid streamlines is the distance between the top of the ground level entrance and the bottom of the upper level entrance through the rock wall, which is a distance $H = 5m$. In case 1 in this table, air must enter through the surfaces of the wooden building, and H is taken to be the average difference between the elevation of the air entering and leaving the cave: $H = 9.25m$. In all other cases air flow is generated by mechanical fans.

today compared to the base case is to reduce the particle mass deposited onto horizontal surfaces in Cave 6 by about 47%. This occurs due to reduction of air flow through the cave due to the presence of extra pressure drops in the air path caused by the structure itself; there is no particle removal by filtration in this case.

Mechanical air filtration systems in commercial buildings typically employ about a 1:3 ratio between filtered outdoor make-up air and recirculated re-filtered indoor air (see Figure 5.2). The effect of such a standard ventilation system will be approximated by setting the total air flow through such a system at 356 $m^3\ min^{-1}$, with 89 $m^3\ min^{-1}$ of outdoor make-up air and 267 $m^3\ min^{-1}$ recirculated indoor air. The infiltration of untreated air is set at 10 $m^3\ min^{-1}$ (about 10% of the make-up air flow). The total flow of outdoor air is thus set at 99 $m^3\ min^{-1}$, equal to the case 1 historically observed flow of outdoor air in the presence of natural convection on the days simulated. Maintenance of that historical flow rate of outdoor air would assure that water vapor seeping through the cave walls would be exhausted at least as effectively as has been the case historically. The infiltration air flow in reality will depend on how air-tight the building can be made to be. Initially, low efficiency filters will be tried that have a single-pass particle removal efficiency of 14% - 34% based on measurements made in a particular Southern California museum filtration system (see filter performance curve FB1 in Figure 5.4; from Nazaroff et al., 1990). The indoor particulate air quality model of Nazaroff and Cass (1989ab), which can depict particle deposition in the case of forced ventilation and filtration in a manner wholly compatible with the structure of our natural convection-driven model of Chapter 4, is used to study this and subsequent cases shown in Table 5.1. Results show that a system incorporating low efficiency filters FB1 would reduce particle

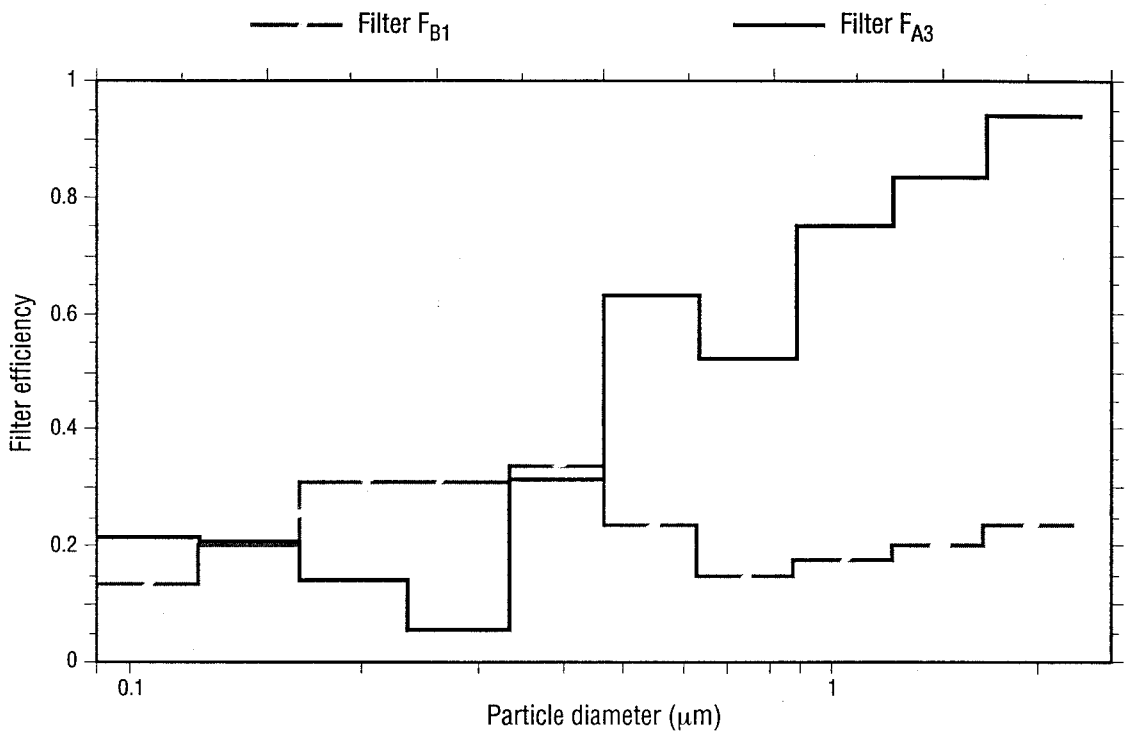

Figure 5.4 Filtration efficiency of particle filters as a function of particle size. The results are based on 21 and 4.5 hours of data for filters FA3 and FB1 respectively. The corresponding operating flow velocities across the filter faces are 0.44 and 1.7 $m\ s^{-1}$. Filter media: filter FA3 is Servodyne type SR-P1L; filter FB1 is Servodyne type Mark 80. (Figure adapted from Nazaroff et al., 1990).

deposition to 92 $mg\ m^{-2}\ d^{-1}$ or to 35% of the uncontrolled case, as seen in case 2 of Table 5.1.

Further reduction in particle deposition can be attained by reducing the outdoor make-up air from 89 $m^3\ min^{-1}$ down to 22 $m^3\ min^{-1}$ while increasing the return air flow, thus bringing fewer new particles into the cave. The result of this change is shown by case 3 of Table 5.1. Particle deposition would be reduced to 37 $mg\ m^{-2}\ d^{-1}$ or to 14% of the uncontrolled case. Particle levels are reduced, but one must be careful to determine that the reduced air exchange rate does not lead to water vapor build-up in the cave.

No matter how good the filters are, the performance of the mechanical filtration system will be limited by the amount of untreated infiltration air that leaks into the building. The above two control cases have been re-run with zero untreated infiltration air, and the results are shown in cases 4 and 5 of Table 5.1. With the higher filtered outdoor make-up air supply but no infiltration (case 4 of Table 5.1) particle mass deposited drops to 31% of the base case, and with no infiltration air plus reduced make-up air, the particle deposition flux drops to 9.2% of the base case.

Further improvements to the filtration system can be made by using more efficient filters. One air pass through filter FA3 described in Figure 5.4 removes about 96% of the very coarse dust particles that are causing much of the deposition problem in the caves. Filter FA3 has been used long enough that a "filter cake" of deposited particles has accumulated on its surface making it harder for new particles to pass through the filter uncollected. We will refer to this situation as having a low efficiency filter that is "loaded" with previously collected particles. The calculations performed in cases 2-5 of Table 5.1 are repeated for the case with the higher filtration efficiency of filter FA3. Results are shown in Table 5.1, cases 6-9. Cases 6 and 7 of Table

5.1 both approach a situation where about 4% of the particle deposition rate experienced in the uncontrolled case still remains in spite of repeated passes through filters that are 96% effective per pass at removing coarse particles. The reason for this is that unfiltered infiltration air is still entering. The purpose of cases 8 and 9 of Table 5.1 is to illustrate the importance of eliminating untreated infiltration air. It may not be practical to completely eliminate infiltration, but it is important to try to do so.

A sequence of high efficiency filters can be placed in the mechanical ventilation system that achieve 88% collection of fine particles and 99% (make-up air line) to 95% (recirculated air line) collection of coarse dust per pass. Filters of this type are based on the recommendations of a draft-ANSI standard once proposed for the air cleaning systems of archival and rare book libraries (ANSI, 1985). Such filters will cost more to operate because the pressure drop through the filters is higher, necessitating more power, a bigger fan, and more expensive filter material. In cases 10-13 of Table 5.1, the previous calculations are repeated for the case of the high efficiency filters. The principal difference with the high efficiency filters is that they reduce fine particle concentrations and thus will slow the rate of deposition onto the ceiling and onto vertical surfaces. The build-up of particles on vertical surfaces is already much slower than on horizontal surfaces. Before one can decide on the merits of the higher efficiency filters, it is important to know whether or not the horizontal surfaces of the statues (e.g., shoulders; top of heads) will be cleaned separately and more frequently than vertical surfaces (e.g., the chests of statues). If all surfaces are to be cleaned at the same time, then the horizontal surfaces will become dirty first and will trigger a round of cleaning regardless of whether filter FA3 or the more expensive high efficiency filters are used. On the other hand, if one wants to clean the vertical surfaces as

infrequently as possible, then the high efficiency filters will produce such a result.

5.3.2 Passive filtration systems

Given the large air flows through the caves at present caused by natural convection, the question arises, "Is it possible to filter the particles out of the air entering the caves without using a mechanical fan to move the air?"

The natural convection air flow model that incorporates particle deposition mechanics calculations developed in Chapters 3 and 4 of this work is ideally suited to study such passive filtration possibilities because that model is able to predict the air flow that will occur as extra pressure drops are added to the air flow path in the form of new filter material. A schematic diagram showing the relative placement of filter material in the outer wall panels of a shelter in front of a cave is shown in Figure 5.5. One possible filter material that may be used is type GSB-30, manufactured by 3M. Particle collection efficiency curves for that material, supplied by the manufacturer, are shown in Figure 5.6 and indicate high single pass filtration efficiency for the coarse particles larger than 10 μm in diameter that are the main problem at Yungang. The other major advantage of this filter material is its very low pressure drop as a function of face velocity. The pressure drop across this filter material is specified to vary linearly as a function of the air velocity through the filter for velocities under 0.5 $m\ s^{-1}$ and from the manufacturer's specifications we can infer that

$$\Delta P = \kappa\ u \tag{5.1}$$

where ΔP is the pressure drop in Pa and u is the face velocity through the

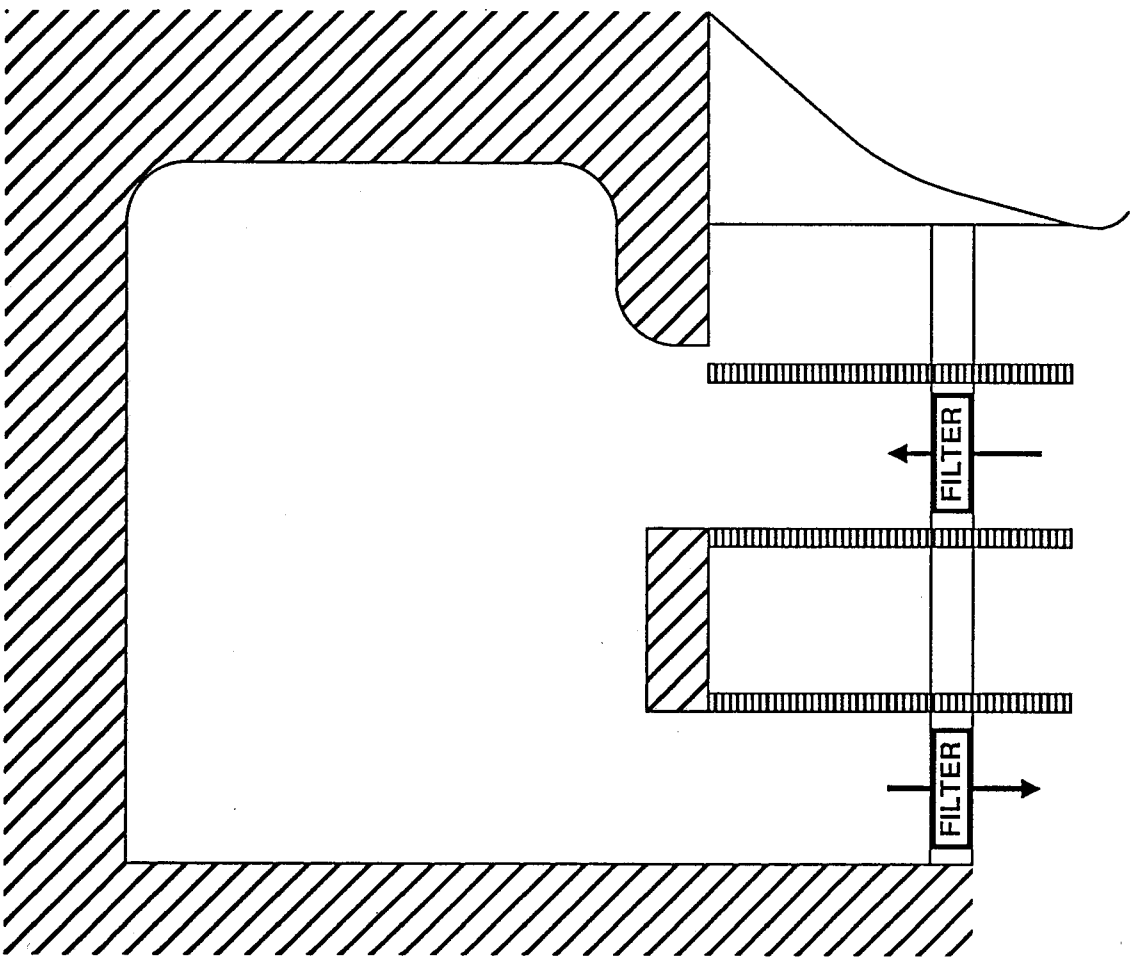

Figure 5.5 Schematic diagram of a passive air filtration system showing placement of filter material in the outer wall panels of a shelter in front of a cave at Yungang.

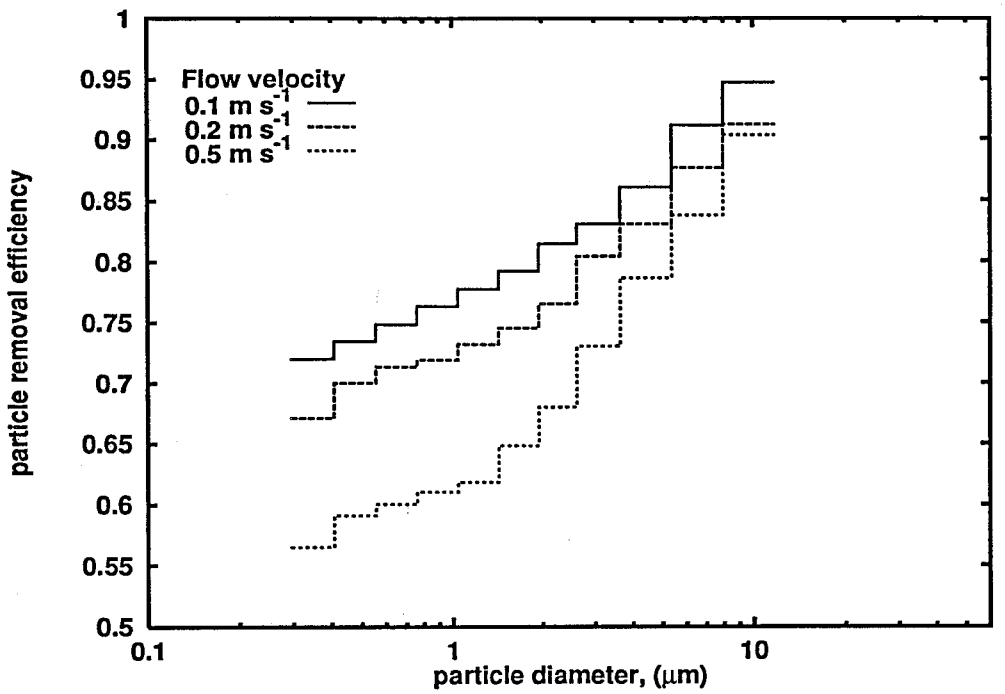

Figure 5.6 Filtration efficiency curves for 3M's GSB-30 filter material as a function of particle size and face velocity. Data are adapted from the manufacturer's specifications (3M, 1993).

the filter in $m\ s^{-1}$. κ is a constant that depends on the filter used and equals 15.1 $Pa\ m^{-1}\ s$ for filter type GSB-30 according to the manufacturer's specifications.

The system of equations presented in Chapter 3, section 3.4.1 is again used to solve for the flow of air through the caves but this time the equation that balances pressure drops in the flow path against the indoor/outdoor air density differences is changed. Additional pressure drop terms are now present in the equation that reflect losses that occur while the air passes through the filter material present in the window and door panels in the ground level as well as in the upper level surfaces of the wooden temple structure:

$$\Delta P_t = (R_1 + R_2 + R_3 + R_4)Q_t \tag{5.2}$$

where $\Delta P_t = gH(\rho_a - \rho_o)$ is the total pressure drop available to drive air through the system, $(\rho_a - \rho_o)$ is the air density difference between inside versus outside the cave, H is the elevation difference between the entering and leaving critical fluid streamline for flow through the cave, g is the acceleration due to gravity, R_1 is the resistance to the flow as air passes through the cracks and filters in the ground level surface of the building, R_2 is the resistance to the flow as air passes through the entrance in the rock wall at ground level, R_3 the resistance to the flow as air passes through the rock entrance at the third and fourth floor level, R_4 is the resistance to the flow as air passes through the cracks and filters at the third and fourth floor level surface of the wooden building, and Q_t is the total volumetric flow of air through the cave. The pressure drop as air passes through the cracks in the building shell at the ground floor level, for example, must be the same as the pressure

drop across the filter material to be located in the building wall panels at the ground floor level. By analogy to electrical circuit systems we can then write

$$R_1 = \frac{R_c R_f}{R_c + R_f} \tag{5.3}$$

where R_f is the resistance to flow due to air passage through the filter material and R_c is the resistance to flow due to air passage through the cracks in the building shell. From equation (5.1),

$$R_f = \frac{\kappa}{A_f} \tag{5.4}$$

where A_f is the surface area of the filter material used and

$$R_c = \frac{1}{2}\rho_o C_L \frac{Q_c}{A_c^2} \tag{5.5}$$

where Q_c is the air flow rate through the cracks and openings in the building shell at that level, A_c is the area of those cracks and openings, and C_L is the loss coefficient for flow through those cracks and openings (taken to be rectangular openings; $C_L = 1.5$ (see Chapter 3)). For resistances R_2 and R_3 expressions similar to equation (5.5) may be written, with the exception that now the flow would be equal to Q_t in both instances and the areas are those of the openings in the rock wall. Also, R_4, the resistance to flow through the cracks and filters at the 3rd and 4th floor level of the wooden temple structure, may be written in exactly the same way as R_1 noting that the total flow Q_t may be split in different proportions between flow through the cracks and flow through the filters there. The relationship between Q_t, Q_c and Q_f may be obtained by noting that the pressure drop across a given set

of cracks and openings in the building shell must be equal to the pressure drop across the filter material that is in parallel with those cracks:

$$\kappa \frac{Q_f}{A_f} = \frac{1}{2}\rho_o C_L \frac{Q_c^2}{A_c^2} \tag{5.6}$$

where Q_f is the volumetric air flow rate through the filter, and all other symbols are as previously defined. Also,

$$Q_t = Q_f + Q_c \tag{5.7}$$

All resistance terms can then be substituted into equation (5.2) which contains the unknown Q_t, as well as the density of the air, both outdoors and inside the cave. Also, equation (4.5) from Chapter 4, section 4.2, can be re-written as

$$\rho c_v V \frac{d}{dt}(T_a) = \rho c_p Q_t (T_o - T_a) - \sum_{i=1}^{3} h_i S_i (T_a - T_w) \tag{5.8}$$

Equation 5.8 is then solved as was described previously in Chapter 3, section 3.4.2. As seen in equation (5.2), the value of Q_t is a function of ρ_a which in turn is a function of T_a. At each time step in the solution of equation (5.8) the value of Q_t is updated by solving equation (5.2).

The case for which there are no cracks at all in the building shell is more straightforward as resistances R_1 and R_4 can then be written in a manner similar to equation (5.4) and the resulting system of equations is easier to solve.

Several alternative combinations of filter material and rates of leakage of untreated air into the shelter in front of the cave are studied in Table 5.2.

Table 5.2 Effect of alternative passive filtration system designs on reducing the particle mass flux to horizontal surfaces within a cave the size of Cave 6 at the Yungang Grottoes[†]

	Air Flow in cave $m^3\ min^{-1}$	Mass Deposition to Horizontal Surfaces $(mg\ m^{-2}\ day^{-1})$	Percent Remaining Relative to Base Case	Time to 100% Coverage by Particles (Years)
Base Case				
(0) Temple front removed	317	262	–	0.28
(1) Historical Case	99	139	53	0.47
Tightening up the wooden building				
(2) Closed doors[a]	26	50	19	1.0
Filter material installed in place of paper windows				
(3) Building still leaks[b,c]	34	45	17	1.2
(4) Building has no leaks[b,d]	6.3	3.4	1.3	9.0
Maximum amount of filter material installed				
(5) Building has no leaks[e]	86	7.5	2.9	6.3

[†] Values shown are averages of model predictions over the two day period of April 15-16, 1991, for which data are available to drive the deposition model. As discussed in Chapter 4, deposition rates under annual average conditions are about 4 times higher than under April 15-16, 1991, conditions; deposition fluxes shown above should be scaled upward proportionately and the times to reach 100% coverage by particles should be divided by a factor of 4 when considering time periods that approach a year or larger.

a. The only control measure in this case is to ensure that the doors at the ground floor level as well as balcony doors and windows on the upper floors remain closed at all times.

b. Filter material with low pressure drop characteristics is installed on the available window panels on both the ground floor and the 3rd floor in the place of the existing paper windows. The pressure drop and efficiency characteristics of 3M's filter type GSB-30 have been used in these calculations (see Figure 5.6).

c. The doors on the ground floor as well as windows and balcony doors on the upper floors are assumed to remain closed at all times, but there is infiltration of air through cracks around the doors and windows of the building shell. Calculations show that 71% of the total mass of air that enters the cave does so through the cracks. Filter area both on the ground floor and the third floor level totals 2.56 m^2 at each level.

d. In this case the cracks in the building shell have been caulked and all air entering the cave must pass through the filter material. Filter area both on the ground floor and the 3rd level totals 2.56 m^2 at each level.

e. Same as (d) except now the filter material has been increased: 55.4 m^2 filter surface area is supplied on the upper floors and 46.0 m^2 of filter surface area on the ground floor. This is consistent with the filter surface area that could be incorporated into a new shelter in front of a cave, but exceeds the amount of filter surface area that can be incorporated into the historical wooden building in front of Cave 6.

The first two lines of Table 5.2 are again the uncontrolled base case with no structure in front of the cave and the case where the cave operates as it is today, respectively. The next line in Table 5.2 shows the amount of control one would exercise if the doors at the ground level as well as the balcony doors and/or windows on the upper floors were kept closed at all times. Air flow in and out of the cave would then flow through the existing cracks around the door and window panels. Our model suggests that in this case the average flow of air into Cave 6 under April 15-16, 1991, conditions would be 26 $m^3\ min^{-1}$ as opposed to 99 $m^3\ min^{-1}$ for the cave as it is operated today with doors open during the day but closed at night and with several door panels left open on the upper floors, and 317 $m^3\ min^{-1}$ for the case if the temple front building did not exist. If all doors in the present building are kept closed at all times, particle deposition onto horizontal surfaces within the cave is reduced by about 81% relative to the situation if the cave had no wooden structure in front of it and thus were completely open to the atmosphere as is the case for the great majority of the caves at Yungang.

Next we examine the passive filtration alternative in which filter material is placed into the panels that exist around the surface of the shelter in front of Cave 6. Here we identify three sub-cases:

(a) That for which all doors in the building are kept closed but there is still leakage of unfiltered outdoor air into the cave through cracks around the doors and/or window panels. Filter material in this case will be used to replace the paper that presently covers the windows in the wooden temple structure at the ground floor and third floor levels, leaving the appearance of the existing wooden building virtually unchanged. From Table 5.2, case 3, it is seen that there is not much further improvement here, with 17% of the mass of deposited particles

relative to the base case still remaining. The reason for this is that of the 34 $m^3\ min^{-1}$ of air that enters the cave, 24 $m^3\ min^{-1}$ or about 71% of the flow into the cave still passes unfiltered through the cracks in the building shell and only the remaining 29% of the flow passes through the filter material. The available filter cross sectional area in this case was assumed to be equal to 2.56 m^2 each for both the downstairs and the upper levels of the wooden building front. This value was chosen because it is approximately equal to the cross sectional area of the paper that presently exists behind the open lattice work of the panels in the ground floor level at the temple front.

(b) Filter material is again used to replace the paper windows in two floors of the existing building as in the previous case, but particle deposition is greatly reduced by caulking all cracks in the building shell thus forcing all the flow into the cave (in this case about 6.3 $m^3\ min^{-1}$) through the GSB-30 filters. As seen in case 4 of Table 5.2, the mass of particles deposited onto horizontal surfaces within the cave would then be only about 1% of the base case. Again, 2.56 m^2 of filter material is placed in both the upstairs and ground floor surfaces of the existing temple front panels.

(c) The very low air flow rate into and out of the cave in (b) above could cause problems if air exchange rates affect the rate at which water vapor (arising from water seepage through the cave rock surface, which damages the sculptures) is exhausted from the caves. Therefore an ability to move air in and out of the caves at volumes like those observed historically may be desired. This can be achieved by increasing the cross sectional area available for placement of filter material in the surface of the building panels. This may be impractical at Cave

6 given the historical character of the present wooden temple front building, but if new shelters were constructed for other caves that presently lack any shelters, then provision for placement of greater amounts of filter material in such new structures could be considered. Preliminary design studies performed by Sedlak (1991) suggest that modified shelters can be erected in front of the caves that do not presently have a shelter that will allow a surface area for filter placement in the face of a building the size of the one in front of Cave 6 of 46 m^2 and 55.4 m^2 in the ground level and upper level floors respectively. Case 5 in Table 5.2 examines such a case using a cave with the dimensions of Cave 6 and a shelter constructed without significant air leaks between panels and with air locks at the entry doors to suppress infiltration of untreated air as doors are opened and closed. Using this greater exposed area of filter material, 86 $m^3\ min^{-1}$ of air would enter the cave. We see then that 97% of the particle mass flux can be suppressed relative to a cave with no shelter in front of it, and the time necessary to completely cover an upward-facing horizontal surface inside the cave with the first monolayer of dust would be increased to 6.3 years under conditions like those observed on April 15-16, 1991. As was mentioned in Chapter 4, actual soiling rates will be faster than this since annual average deposition fluxes are higher than during the April 15-16 events available for model calculations. Still, a 97% reduction in particle mass flux would be effected relative to annual average conditions at an unsheltered cave, which is a substantial improvement.

5.4 Conclusions

Measurements of the spatial distribution of dust deposition within a 2 km by

2 km geographical area surrounding the grottoes show that an area of high deposition flux averaging about 60 $\mu g\ m^{-2} sec^{-1}$ exists along the coal-haul highway and within the center of the village of Yungang next to the caves. This suggests that the coal truck traffic and activities within the village are major local particle sources. Examination of spatial gradients in the particle deposition flux over the area surrounding the Yungang Grottoes suggests that particle deposition at the caves could be reduced by approximately 38% if methods were applied to reduce dust generation along the nearby coal haul highway, on the dirt roads within the village of Yungang, and along the dirt terrace in front of the caves. The Grottoes staff decided prior to the present work that they will pave the dirt terrace in front of the caves with bricks. Further dust control methods could include re-routing the track traffic, covering the loads on the coal trucks, paving the streets in Yungang village, and spray-washing the highway as well as the streets in the village.

Filtration systems can be designed as shown in Tables 5.1 and 5.2 that would produce a major reduction in the rate of deposition of coarse particles inside the Yungang Grottoes. A standard mechanical ventilation system installed within either an existing or reconstructed wooden temple building in front of a cave with either high efficiency filters or low efficiency filters like filter FA3 in Figure 5.4 that are loaded with collected particles (easily achieved at Yungang) could reduce deposition rates to horizontal surfaces to about 4% of uncontrolled levels, provided that air leakage into buildings in front of the caves can be kept to no more than 10 $m^3\ min^{-1}$ (about 3% of the uncontrolled air flow). The degree of control in this case is really determined by the air infiltration rate obtained. If air infiltration could be eliminated, then reduction to less than 1% of the deposition rate that would occur at a cave that lacks a wooden shelter in front of it could be obtained, but complete

elimination of infiltration is unlikely. Alternatively, passive air filtration systems can be considered in which natural convection currents caused by indoor/outdoor air temperature (hence density) differences is used to drive air flow through filter material placed in the surfaces of a shelter in front of the cave. About the best performance that would be expected from a passive filtration system is reduction to about 3% of base case deposition rates for the case of a tightly constructed building that shelters a cave having the dimensions of Cave 6 with the air forced to pass through filter material that covers nearly the entire external surface of the shelter (case 5 of Table 5.2).

The choice between control systems for the Grottoes is not an easy one. The reason is that while the 96%-99% coarse particle deposition control efficiencies of fairly simple systems sound impressive, the outdoor air at Yungang is extremely dirty. As seen in the far right column of Tables 5.1 and 5.2, the time required to produce 100% coverage of a horizontal surface at a cave the size of Cave 6 if it lacks a wooden temple front building is only a few months at present. In the presence of the current structure in front of Cave 6, the comparable time to 100% coverage is about 0.5 years (under April 15-16, 1991, conditions). That first monolayer coverage by particles probably is sufficient to produce most of the objectionable visual character of the soiling problem. Beyond a full monolayer coverage by dust, the deposits just get deeper. Indeed, much less than a full monolayer coverage by particles is noticeable to a human observer: a 0.2% coverage by dark particles on a white surface is detectable if one looks very closely (Hancock et al. 1976) and a 1% coverage can be seen easily when examined closely. The exact point at which visitors viewing the statues from a distance would notice the soiling is not known, but it is surely less than the point at which 100% surface coverage is reached.

The time needed to accumulate the first full monolayer of deposited particles in the presence of several possible mechanical air filtration systems with some remaining air infiltration is about 6-8 years, or about 6.3-9 years with passive filtration systems like those of cases 4 and 5 of Table 5.2 under April 15-16, 1991, conditions, and about 4 times faster than this under annual average conditions. Noticeable soiling would occur in less time. Given the time and effort needed to clean and restore a cave once it gets dirty, such a high remaining particle flux may be unacceptable.

The alternative to accepting such times for recurrence of 100% coverage of the horizontal areas of the statues would involve an all-out attack on the problem, including:

(a) Careful attention to making any new buildings in front of the caves as air-tight as possible, forcing nearly all air exchange through filters. Air must still be exchanged with the outdoors through filters in order to exhaust water vapor that leaks through the rock walls of the caves; stopping air exchange completely by sealing the caves could be disastrous.

(b) Selection of the best mechanical filtration system that can be supported, and

(c) Suppression of the local outdoor dust sources as described earlier.

With zero air infiltration and a high efficiency mechanical air filtration system, Table 5.1 shows that the time to accumulation of a full monolayer of dust on horizontal surfaces could be extended to 42-72 years under April 15-16, 1991 conditions or to about 10-18 years under annual average conditions. With a further 38% reduction of particle fluxes due to suppression of outdoor dust sources, these times could be extended to 68-116 years under April 15-

16, 1991, conditions or to about 17-29 years under annual average conditions. If the interior of the caves will be open to visitors, then dust entrained by the visitors may have to be studied as those effects would become comparatively more important once the present overwhelming problems from entrainment of outdoor air pollution are solved. One could also study the effect of control of local coal smoke and regional outdoor air pollution sources other than the local road dust and soil dust.

5.5 References

ANSI (1985) *Practice for storage of paper-based library and archival documents.* American National Standards Institute standard Z39.xx-1985, draft.

Christoforou, C. S., Salmon, L. G., and Cass, G. R. (1994) Deposition of atmospheric particles within the Buddhist cave temples at Yungang, China. *Atmos. Environ.*, **28**, 2081–2091.

Hancock, R. P., Esmen, N. A., and Furber, C. P. (1976) Visual response to dustiness. *J. Air Pollut. Control Assoc.* **26**, 54-57.

Minnesota Mining and Manufacturing Co., Filtration Products (1993) Publication No. 70-0702-3443-3. St. Paul, Minnesota.

Nazaroff, W. W., and Cass, G. R. (1986) Mathematical modeling of chemically reactive pollutants in indoor air. *Environ. Sci. Technol.* **20**, 924-934.

Nazaroff, W. W., and Cass, G. R. (1989) Mathematical modeling of indoor aerosol dynamics. *Environ. Sci. Technol.* **23**, 157-166.

Nazaroff, W. W., and Cass, G. R. (1991) Protecting museum collections from soiling due to the deposition of airborne particles. *Atmos. Environ.* **25A**, 841-852.

Nazaroff, W. W., Salmon, L. G., and Cass, G. R. (1990) Concentration and fate of airborne particles in museums. *Environ. Sci. Technol.* **24**, 66-77.

Salmon, L. G., Christoforou, C. S., and Cass, G. R. (1994) Airborne pollutants in the Buddhist cave temples at the Yungang Grottoes, China.

Environ. Sci. Technol., **28**, 805-811.

Vinzenz Sedlak Proprietary Limited, (1991) *Report on a conceptual design study for a protective portico/facade for Cave 19 Yungang Grottoes, Shanxi province, PRC.*

Chapter 6. Summary and conclusions

6.1 Summary of Results

The collection the Buddhist cave temples at Yungang in Shanxi province in northern China suffers from a very high rate of deposition of airborne particles onto the more than 50,000 sculptures in those caves. In this work, analytical tools, both experimental and computational, have been formulated that advance our understanding of how to protect the sculptures inside these caves from being permanently damaged due to a continuing assault by dark-colored abrasive particles deposited from the atmosphere. In order to understand how to control the particle deposition and soiling problem at the caves, a series of investigations was undertaken during the month of April, 1991 and was continued on a less intensive pace over the ensuing year.

First, a method for measuring coarse particle size distributions, both for airborne and for deposited particles, was developed. That method is based on automated processing of video images of particles collected on deposition plates and on airborne particle filter samples. This technique was applied to samples taken inside two caves at Yungang, Cave 6 and Cave 9, as well as to samples taken in the outdoor environment. Mass deposition rates measured inside the caves using this method are approximately the same as estimates derived by removal of historically accumulated deposits from within the caves. Measurements showed that there was a marked decrease in the deposition of coarse particles inside Cave 6 when compared to Cave 9 and the outdoors due to the fact that the entrances to Cave 6 are sheltered by a wooden structure while the entrances to Cave 9 are open directly to the outdoor atmosphere. Seasonal mass deposition rates inside Cave 6 were found to be almost constant over the course of a year.

In order to identify the location and magnitude of the air pollution sources at Yungang, measurements of the spatial distribution of dust deposition within a 2 km by 2 km geographical area surrounding the grottoes were carried out during April 19-21, 1991. The results showed an area of high deposition flux averaging about 60 $\mu g\ m^{-2} sec^{-1}$ along the coal-haul highway that runs within 300 m of the caves and within the center of the village of Yungang next to the caves. This suggests that the coal truck traffic and activities on the dirt roads in the village are major local particle sources.

Once the outdoor and indoor particle characteristics have been determined, and baseline parameters have been established, the mechanisms by which these particles enter the interior of the caves were examined. It was shown that air circulation through the caves was driven by a natural convection flow that varied by time of day according to changes in outdoor temperatures and cave wall temperatures. Mathematical models were built that can predict the air flows that carry pollutants into and out of the caves based on the volume of the caves, their height, the surface area of walls, ceilings, and floors, the geometry of the entrances through which air must flow, and also thermal conditions such as cave wall temperatures and outdoor air temperatures. The models have the capability of accepting as further input resistances to air flow that would arise if filter material were installed in the surface of an existing or reconstructed wooden shelter in front of a cave in order to remove particulate matter from the air. Data that were gathered during the April, 1991, experiments were used for verification of the natural convection-based air exchange models. The results showed good agreement between observed versus predicted air flows and air temperatures, both in the case of Cave 9 (a cave without extra flow resistances), and Cave 6 (a cave that has extra flow resistances in the form of the wooden temple structure that stands over

the entrances to that cave.)

Next, a computer-based model that links outdoor airborne particle concentrations and the air circulation through the caves to the particle deposition problem within the caves was developed. This model could be applied to study other similar cave temple sites such as those at the Mogao Grottoes and at the Yu Lin Grottoes near Dunhuang, China, as well. The model takes as input the temperature of the outdoor air and the cave walls, the size distribution of particles suspended in the outdoor air, the initial size distribution of particles suspended in the indoor air, as well as geometric parameters of the caves. It then predicts the air flow rate through the caves, the indoor size distribution of particles suspended in the air within the caves as well as the size distribution of particles deposited onto various surfaces inside the caves. A 44 hour intensive sampling experiment, conducted at Yungang during April 15 and April 16, 1991, provided the input data necessary for evaluation of model performance. Comparison of model predictions to actual measurements show that there is close agreement.

Finally, the computer-based models previously described were used to evaluate alternative control strategies that could be used to achieve a major reduction in the rate of deposition of coarse airborne particles onto the sculptures inside the grottoes. Two separate cases were examined. First, a mechanical ventilation system equipped with filters of several degrees of efficiency was examined. It was found out that the degree of particle control ultimately is determined by the rate of infiltration of unfiltered air that can enter the caves through cracks and openings in the buildings that are constructed to shelter the entrances to the caves. If air infiltration could be eliminated, then reduction to less than 1% of the historical particle mass deposition rate could be obtained, but complete elimination of infiltration is unlikely. Next, pas-

sive filtration systems were examined, in which the natural convection flow present in the grottoes was used to drive air through filters without the use of a mechanical fan. It was found that if new temple front structures could be erected covering the entrances to the caves, then air flowing into the caves could be forced to pass through low pressure drop filters placed in the exterior surfaces of those structures. For the filter material examined, the results suggest that the elapsed time to achieve complete coverage of a horizontal surface by deposited particles inside a cave the size of Cave 6, for example, could be extended to about 6.3 years under the April 15-16, 1991, conditions studied, nearly a thirteen-fold improvement over historically observed values, through the use of a passive filtration system.

Given the time and effort needed to clean and restore the sculptures within a cave once they have become covered by deposited particles, even a thirteen-fold reduction in the particle deposition rate within the caves may not be sufficient. The alternative to accepting such times for recurrence of 100% coverage of the horizontal areas of the statues inside the caves would involve an all-out attack on the problem, including use of a high efficiency mechanical air filtration system, tightening of the structures that shelter the caves in order to eliminate infiltration of untreated air, and suppression of the local outdoor dust sources as described earlier.

6.2 Recommendations for future research

In order to measure coarse particle mass fluxes onto surfaces as well as coarse airborne particle size distributions, an automated micro video technique has been established. However, this method suffers from two disadvantages, inherent to microscopic determination methods of particle size and mass. First, it assumes that each collected particle has a volume equal to that of a sphere

having the same cross sectional area as is observed for that particle under the microscope, which is an approximation. Work has been done to establish more accurate approaches and generic shape correction factors can be used (as was done here) which depend on the mineralogical composition of particles. Still, more research is necessary to better characterize the shape of particles in the atmosphere and how particles of irregular shape behave, especially if the chief advantages of methods such as the automated micro video technique (economical and relatively quick) are to be preserved. Second, the density of both airborne and deposited particles must be inferred by examining deposited material from the study site before particle counts can be converted into particle mass distributions and particle mass fluxes. Better and more accurate methods for measuring the density of airborne particles would be useful.

The computer-based model developed here that predicts air exchange through the caves presently takes as one of its inputs the time series of the cave wall temperatures as well as the time series of the outdoor air temperatures. It may be possible to modify the existing model so that the time series of the cave wall temperature is not needed. Rather, only the initial temperature of the cave wall would be necessary in order to start the solution and cave wall temperatures could then be predicted over time by solving the transient heat transfer problem that occurs as changing air temperatures propagate their effects into the rock walls of the caves. The solution of the system of equations would then begin by calculating the air temperature inside the cave, given the outdoor air temperature and the initial cave wall surface temperature. Once the indoor air temperature is calculated, the cave wall surface temperature could then be calculated as the temperature of the surface of a semi-infinite solid (the cave wall) subjected to the calculated air temper-

ature inside the cave. It is thus possible to perpetuate the solution by just specifying changes in the outdoor air temperature. In this case the history of the cave air temperature, and thus the air flow in and out of the caves, could be calculated by just monitoring the outdoor air temperature.

Another aspect that presents opportunities for further improvement in the present model formulation is that of particle deposition onto rough vertical surfaces, such as are present on the interior cave walls. At present, the fact that the cave walls are not smooth vertical flat surfaces has been treated by doubling the heat and mass transfer rates relative to the solution that would be obtained for a flat surface. If detailed knowledge of the turbulent air flow boundary layer features along the actual rough surfaces in the caves could be obtained, then a more theoretically elegant model could be formulated.

More experimental work is necessary to fully understand the mechanics of atmospheric particle deposition onto vertical surfaces, smooth or otherwise. The body of experimental evidence taken from real outdoor or building interior surfaces in such cases is very sparce. The reason for this is that particle fluxes onto vertical surfaces are several orders of magnitude less than those onto horizontal surfaces. To overcome this, either experiments of long duration are needed, or an improved method of sampling and detection is necessary in order to reduce exposure times, thus making experiments more manageable.

Finally, as previously mentioned, the measurement methods and models developed here could be applied to other analogous sites. Many other similar cave temple sites exist along the Silk Road extending from Metropolitan China to Afganistan, and also in Northern India and Sri Lanka. Further, these methods may be of use in studying particle deposition onto surfaces in natural caves and in mines, including the deposition onto the sculptures in

the historical salt mine at Wieliczka in Poland.